

Classical and quantum Chaos plus RMT and some applications

ARUL LAKSHMINARAYAN

Department of Physics
IIT Madras, Chennai.
arul@iitm.ac.in

Notes for the Bangalore Summer School on Statistical Physics, 9-13, July, 2018. ICTS, Bangalore.

Contents

1 Hamiltonian Classical Chaos	5
1.1 Preliminaries	5
1.2 Welcome to 1.5 degrees of freedom	7
1.2.1 Stroboscopic Map	9
1.3 Kicked Hamiltonian Systems, Justforkix	14
1.3.1 Important Area-Preserving Maps in 2D	15
1.3.2 Poincaré Surface of Section: Hamiltonian Flows to Maps	20
1.4 Poincaré Recurrence Theorem, Ergodicity, Mixing	21
1.4.1 Recurrence theorem	21
1.4.2 Ergodicity	23
1.4.3 Mixing	25
1.5 Fully chaotic, exactly solvable, model systems	26
1.5.1 The Baker Map	26
1.5.2 The cat map	32
2 Hamiltonian Chaos: Quantum Mechanics	37
2.1 Introduction	37
2.1.1 But is there quantum chaos?	40
2.1.2 Spectrum of Chaotic systems: Eigenfunctions	40
2.1.3 Billiards	42
2.1.4 Scars of the classical	44
2.1.5 Nonlinear oscillators	46
2.2 Quantum Maps: Generalities	47
2.2.1 Comments	49
2.2.2 Quantum maps on the plane and cylinder	50
2.2.3 Standard map on the cylinder	51
2.2.4 Quantum maps on the torus	54
2.2.5 General toral quantum maps	57
2.2.6 Quantum standard map on the torus	58
2.2.7 Quantum bakers map	58
2.3 Eigenfunction of quantum maps	61
2.4 Eigenvalues and quantum chaos	64
2.4.1 The staircase function, density of states, and spectral fluctuations	66
2.4.2 Semiclassics of Eigenvalues	69

3 Random Matrix Theory and applications to quantum chaos	75
3.1 Introduction	75
3.2 Ensembles of matrices	78
3.2.1 The Gaussian Orthogonal Ensemble	79
3.2.2 Gaussian Unitary ensemble: GUE	81
3.3 More on the nearest neighbor spacing and ratio of spacings	82
3.4 Eigenfunctions of random matrices	84
3.4.1 GOE eigenvectors	85
3.4.2 GUE eigenvectors	86
3.5 Trace constrained Wishart matrices: Entanglement	87
3.5.1 The Marchenko-Pastur law	89
3.6 Applications to Quantum chaos and thermalization	90

Chapter 1

Hamiltonian Classical Chaos

1.1 Preliminaries

Hamiltonian systems are a very special class of dynamical systems that are of central concern to physics. They encompass the classical mechanics of Newton and are the starting point for quantum and statistical physics. The dynamics completely specified by specifying the values of a minimum number of coordinates of the particles involved and their conjugate momenta. This minimum number, the *number of degrees of freedom*, or DoF, is a crucial number and is determined by the number of constraints on the system. Thus a simple pendulum is a 1 DoF system although it moves in a plane. But the Kepler problem is really 6 degrees of freedom (for the two masses). The fact that it finally reduces to the motion of one particle on a plane and in fact even further, so that an effective one-dimensional potential in radial coordinates is emerges is not due to mechanical constraints but to a large number of constants of motion.

Let the number of DoF be d . Let us state at the very outset that this is a very critical number. All that we understand reasonably well today, *in detail* are utmost 2 DoF systems! Detailed structures and behaviour of say even 3 DoF systems is not yet achieved. One of the key reasons for this surprising inability is “chaos”, which is potentially present for any system whose $d > 1$; however even the complexity arises from the intricate mixtures of chaotic and regular orbits in large parts of phase space. Let the coordinates that make up the DoF be labelled (q_1, q_2, \dots, q_d) . Then the *phase-space* is the space that also includes the conjugate momenta (p_1, p_2, \dots, p_d) . Thus the phase-space has $2d$ dimensions. This is the proper space in which Hamiltonian mechanics is to be studied. Every physical system is assumed to be described by an Hamiltonian H which is a scalar function on the phase-space and completely determines the future and past of the $2d$ variables. The central equations are the Hamilton equations of motion:

$$\begin{aligned}\frac{dq_i}{dt} &= \frac{\partial H}{\partial p_i} \\ \frac{dp_i}{dt} &= -\frac{\partial H}{\partial q_i}, \quad 1 \leq i \leq d.\end{aligned}\tag{1.1}$$

These $2d$ first order ordinary differential equations are determined by the *single* phase-space function H . Note the $-$ sign in the momentum equation. Given any initial point $(q(0), p(0))$ it evolves to $(q(t), p(t))$ after a time t under the Hamiltonian equations of motion. Here $q(0)$ is written for the d position variable collectively, and similarly for momentum. Thus the Hamiltonian generates a **flow** in the phase-space and classical mechanics is all about studying this flow. The Hamiltonian H could in general depend on all the $2d$ phase space variables as well as time t . If it depends on time t , the system is said to be

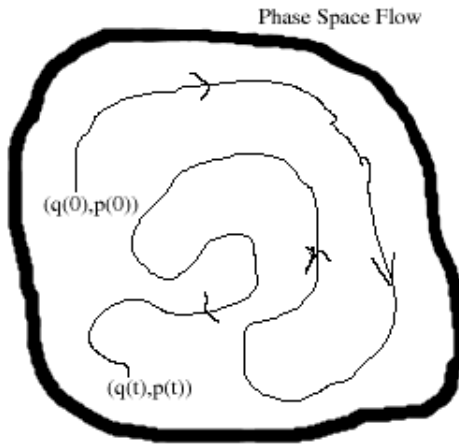


Figure 1.1: A phase space doodle

non-autonomous, otherwise it is autonomous. For autonomous Hamiltonian systems, **trajectories in phase-space do not cross**. This follows from uniqueness of solutions of the set of first order o.d.e.s in Eq. (1.1).

If the trajectories crossed, then the partial derivatives of the Hamiltonian would have to be multi-valued at a given phase-space point. In fact they can be multivalued at different times if the system is non-autonomous and therefore phase-space trajectories can cross in this case. For such systems an extended $2d + 1$ space which is phase-space plus time space is such that trajectories don't cross here. It is easy to see that the no-crossing condition places severe restriction for a flow in a plane, i.e. for $d = 1$ cases. Refer to the phase-space doodle in Fig. (1.1). It is easy to see that for spaces where the phase-space is higher than 2 there is a possibility for fairly complicated trajectories. In fact all $d = 1$ Hamiltonian systems are trivially *integrable*, $H = \text{constant}$ will give the phase space trajectories. There is no chaos.

The notion of **integrability** in the sense of Liouville and Arnold pervades the discourse on chaos. A d DoF Hamiltonian autonomous system is said to be **integrable** if there exists d independent constants of motion $F_i(q, p)$ that are said to be in **involution**, that is their mutual Poisson brackets vanish: $\{F_i, F_j\} = 0$. Notice that the fact that there is a one dimensional orbit seems to imply in general $2d - 1$ constants of motion. However these are in general so convoluted and singular that for almost all cases they do not exist. On the other hand, for integrable systems, these $F_i(q, p)$ are smooth functions of phase space and only d of them are needed. General theorems then ensure that these can be chosen as actions in an action-variable construct, restricting the orbits to lie on d -dimensional manifolds that are topologically d -dim. tori. Thus for a 2-DoF system, the existence of just one more constant of motion, apart from the energy, ensures integrability and the orbits in phase space are restricted to lie on surfaces that are topologically as 2-torus. Note that, as stated above, all 1-DoF systems are integrable as energy is a constant (if unforced), and motion takes place on "surfaces" that are topologically 1-tori or circles. If insufficient constants of motion exist, as would be the typical case, the system is said to be non-integrable. A double-pendulum, the gravitational three-body problem, actually pretty much almost all system are non-integrable. Integrable systems are very special and uncommon.

The moment we step out of $d = 1$ we see interesting physics, in particular deterministic "randomness" or "chaos" appears as a generic (meaning usual) phenomena. For instance take the class of Hamiltonians

$H(q, p, t)$, with $d = 1$, that is nonautonomous one degree of freedom systems, the extended phase-space is 3D, (q,p,t). Sometimes these systems are referred to as "one and a half" degree of freedom systems.

Exercises:

1. 1-d Harmonic oscillator: $H = p^2/2 + \omega^2 q^2/2$. Verify that the Hamiltonian equations of motion are linear and that the phase space trajectories are nested ellipses. Draw the phase space flow, paying attention to equilibrium points and direction of flow. Do the same for when the potential is a repulsive inverted parabola: $-\omega^2 q^2/2$.
2. The simple pendulum Hamiltonian is $H = p^2/(2ml^2) + mgl(1 - \cos(q))$. Show that the equations are now nonlinear. Show that there are stable equilibrium points at the origin and for every $(q = 2\pi k, p = 0)$, and there are unstable, hyperbolic points at $(q = \pi(2k + 1), p = 0)$, where k is any integer. Draw qualitatively the time period vs energy, paying attention to energies from 0 across $2mgl$ and beyond.
3. Draw the phase-space trajectories of the so-called Harper Hamiltonian $H = \cos(2\pi p) + g \cos(2\pi q)$ for some constant g . In particular analyze the cases as g crosses unity.

1.2 Welcome to 1.5 degrees of freedom

All this is autonomous so far. Lets step out of $d = 1$ into $d = 1.5$, that is nonautonomous 1 DoF systems. We will take our elementary examples and modify them slightly. We will parametrically force them, i.e. change their parameters, like the restoring force, the length of the pendulum, gravity etc., in time. The harmonic oscillator case is well-known, the solutions are the *Mathieu* functions, the oscillator can be stable or unstable depending on the forcing amplitude and frequency. The case of the pendulum and the Harper Hamiltonian leads to chaos. These are *nonlinear* systems, and it may be expected that almost all nonlinear systems that are parametrically forced, even if they have only one-degree of freedom, can be chaotic depending on the system parameters and initial conditions. We will study some examples to get a first glimpse of what it means to be chaotic.

Consider the general $d = 1.5$ Hamiltonian, for some functions f and V

$$H(q, p, t) = f(p) + g(t) V(q) \quad (1.2)$$

where $g(t)$ is some smooth function of time t . In the **case when $g(t)$ is a periodic function, of period T say, important simplifications occurs**. As an illustration consider the two Hamiltonians

$$H_{ho}(q, p, t) = \frac{1}{2}p^2 + g_0(1 + \epsilon \sin(2\pi t))\frac{1}{2}q^2, \quad (1.3)$$

$$H_{pend}(q, p, t) = \frac{1}{2}p^2 + g_0(1 + \epsilon \sin(2\pi t))(1 - \cos q). \quad (1.4)$$

of a parametrically forced harmonic oscillator and a simple pendulum. The forcing functions are identical and are determined by the amplitude ($g_0\epsilon$) and a time period that has been chosen as 1, setting a time scale in the problem. Note that the harmonic oscillator without forcing ($\epsilon = 0$) has the frequency $\sqrt{g_0}$. The pendulum has been chosen such that for small amplitudes it is identical to the harmonic oscillator just discussed, as $1 - \cos q \approx q^2/2$. The equations of motion are

$$\frac{dq}{dt} = p, \quad \frac{dp}{dt} = -g_0(1 + \epsilon \sin(2\pi t)) q, \quad \text{and} \quad (1.5)$$

$$\frac{dq}{dt} = p, \quad \frac{dp}{dt} = -g_0(1 + \epsilon \sin(2\pi t)) \sin q \quad (1.6)$$

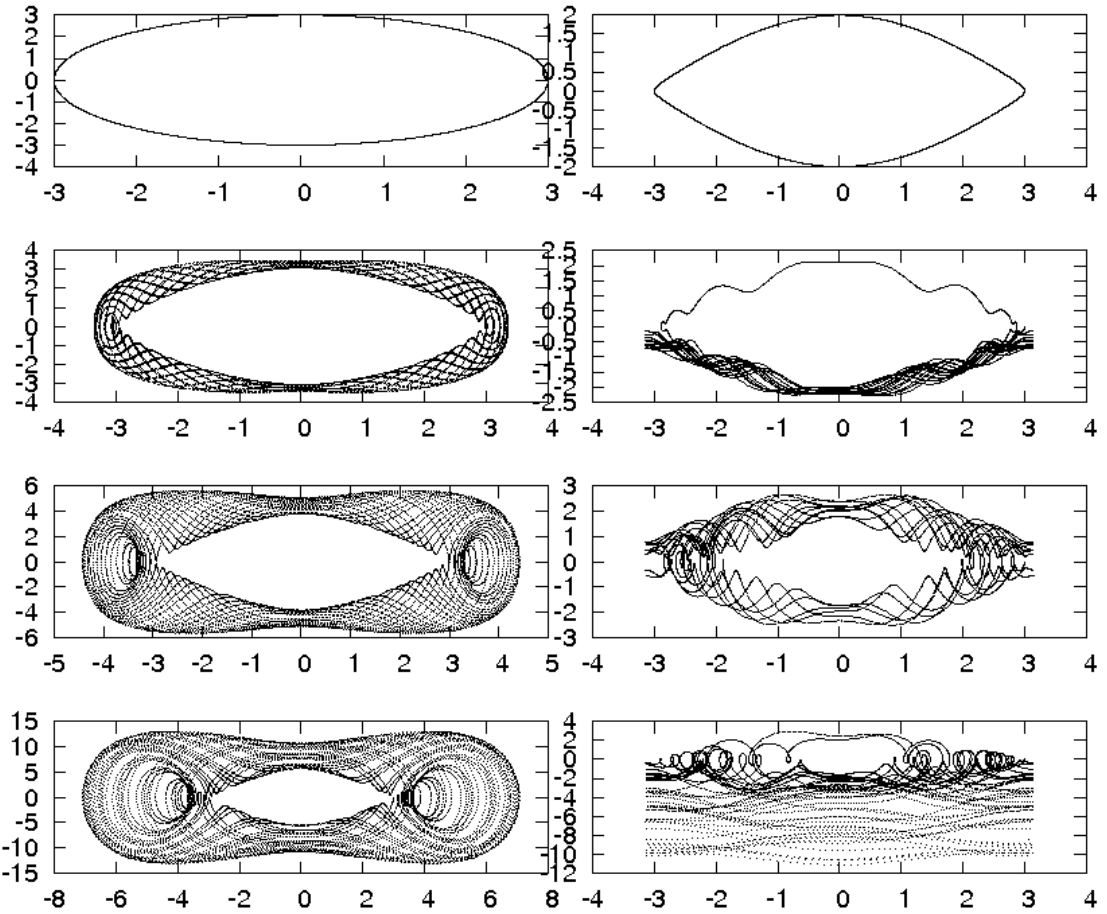


Figure 1.2: One phase-space trajectory of the parametrically forced harmonic oscillator (left) and the pendulum (right). Plotted is (q, p) as a function of time, all plots having the same initial condition $(q(0) = 3.0, p(0) = 0)$, and running for a time=100 (arb. units). The forcing function is $g_0(1+\epsilon \sin(2\pi t))$, and the parameters are $g_0 = 1.0, \epsilon = 0, 2, 5, 10$ from top to bottom.

respectively.

By numerically integrating these equations, in Fig. (1.2) we see the fate a particular initial condition for different amplitudes of forcing. Due to the non-autonomous nature of the systems, the phase-space trajectories cross, however they seem to be forming regular patterns in the case of the harmonic oscillator, while in the pendulum case the behaviour starts “looking complicated” for increasing forcing. Note that the choice of the initial condition $(q(0) = 3, p(0) = 0)$ is designed so that in the case of the unforced pendulum the energy is large and close to that of the “separatrix” that separates the rotational motions from oscillations (go back to phase-space of the simple pendulum if this is not obvious).

The forced pendulum can be used to illustrate an important feature of chaos: **sensitivity to initial conditions**. Shown in Fig. (1.3) are now the fate of *two* initial conditions that are separated initially by a small amount. We see that the parametrically forced pendulum appears unstable, in the sense that these two trajectories quickly depart from each other, while the harmonic oscillator looks stable. There is at best a statistical resemblance between the two initially nearby trajectories in the case of

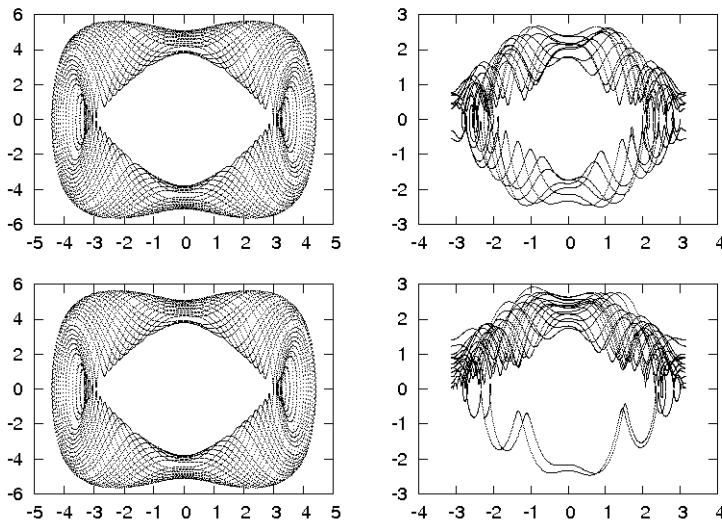


Figure 1.3: Tale of two initial conditions. On the left is the harmonic oscillator and the right is the pendulum. The initial conditions were $(q(0) = 3, p(0) = 0)$ (top) and $(q(0) = 3.0, p(0) = 0.001)$ (bottom). In both cases $\epsilon = 5$ and $g_0 = 1$. The forcing function is same as that in Fig (1.2).

the pendulum, while the eye can discern no difference in the case of the harmonic oscillator. The harmonic oscillator can also be driven to instability, but the instability in the pendulum is of a very different nature. The instability that may arise in the harmonic oscillator is like the instability of a hill-top, anything dropped at the top runs away to infinity, while the pendulum instability can be there in *bounded* space.

While the pictures above are instructive, they are not terribly so. We have inferred that the harmonic oscillator is allegedly simpler, the pendulum is more complicated and perhaps sensitive to initial conditions. The pictures above have a disadvantage: this is only one trajectory, if we went ahead and plotted say 100 of them, so as to get a global understanding of phase-space behaviour, we will get some picture that looks worse than the Tamil Nadu Assembly in an excited state (anachronistic reference, used many years back when these notes were first written, now the Assembly looks like in an equilibrium point, with nothing moving) This difficulty is overcome if we study the return maps and now described.

1.2.1 Stroboscopic Map

We are helped, crucially, by the fact that the forcing is periodic. **We will choose to monitor the phase-space only at times separated by a period of the forcing.** This will give us a discrete set of points, and the **dynamics is specified by where any point maps into after one time period of the forcing, – the stroboscopic map.** Although the equations of motion are invariant under a time translation by T , the solutions are in general not periodic, let alone periodic with period T (see the pendulum pictures! Also *more generally the system's symmetries need not be shared by the solutions*).

Let $f_{t_0}^t$ map evolve phase-space points at time t_0 by time t , i.e.

$$f_{t_0}^t(q(t_0), p(t_0)) = (q(t_0 + t), p(t_0 + t)) \quad (1.7)$$

$f_{t_0}^t$ does not have have the continuous semigroup structure seen for autonomous systems, in the sense that $f_{t_0}^t \circ f_{t_0}^t \neq f_{t_0}^{2t}$. We cannot use the same map to propagate further by the same time t , as the map will depend on the base time, so that it is true that $f_{t_0+t}^t \circ f_{t_0}^t = f_{t_0}^{2t}$. However due to the time-periodicity of the Hamiltonian, the map over a time T will possess a discrete simple Abelian group structure.

$$f_{t_0}^T \circ f_{t_0}^T = f_{t_0}^{2T} \quad (1.8)$$

The map $f_{t_0}^T$ propagates phase-space at time t_0 by T and repeated applications n times gives us $(q(t_0 + nT), p(t_0 + nT))$. Also clearly we have $f_{t_0}^T = f_{t_0+T}^T$, so that we have to only consider stroboscopic maps with base points between any two periods, say $[0, T]$. There is still an *infinity* of such stroboscopic mappings, however all of these are equivalent in a strong mathematical sense, they are *topologically conjugate* to each other. This means that the maps produce qualitatively identical structures, if there is a periodic orbit in one, there will be a corresponding periodic orbit in the other. This is a generalization of what we study as a property of homogeneous potentials. The stroboscopic 2 dim map has *all* the information present in the extended phase-space, in a faithful manner. If there are periodic orbits in the phase-space, it will show up as a finite periodic collection of points on the map.

In Fig. (1.4) we see how the map looks for the forced harmonic oscillator, and the forced pendulum. In the case of the parametrically forced harmonic oscillator, the phase space looks filled with orbits that look elliptic. Remarkably these are indeed ellipses independent of what forcing function is used (discussed in more detail presently). The simplicity of the forced harmonic oscillator is lost in the case of the forced pendulum in many ways. Firstly, as is clear from the figures we are talking of qualitatively different behaviour. The simple elliptic orbits are replaced by a mixture of random splatter of points and regular looking curves. These are intermixed in an intricate manner that is not readily visible to our eye. This is in fact the generic phase-space of $d = 2$ (or $d = 1.5$) Hamiltonian systems: there is a mixture of chaos and regularity, what is called (naturally) a “mixed phase-space” (not to be confused with mixing *in* phase space). Complete chaos, and complete regularity are exceptional.

Linear maps

Of Floquet and the Harmonic Oscillator.

The *simplicity of the map for the parametrically forced harmonic oscillator is due to the fact that whatever may be the type of forcing function, $g(t)$, the stroboscopic map is a linear one. This follows because if $(q(t), p(t))$ is a solution then so is $q(t+T), p(t+T)$* , but from the linearity of the differential equation the latter solution cannot be new, but must be a linear combination of the former. Thus we must have:

$$\begin{aligned} q(n+1) &= a(t_0, T) q(n) + b(t_0, T) p(n) \\ p(n+1) &= c(t_0, T) q(n) + d(t_0, T) p(n), \end{aligned} \quad (1.9)$$

where $q(n) \equiv q(t_0 + nT)$ etc. This is an **autonomous linear map**, in the sense that the coefficients (a, b, c, d) do not depend on the iterate n , but they can depend on the base point t_0 , and the period T . Also a very general property of Hamiltonian systems is reflected in the area-preserving condition that $ad - bc = 1$.

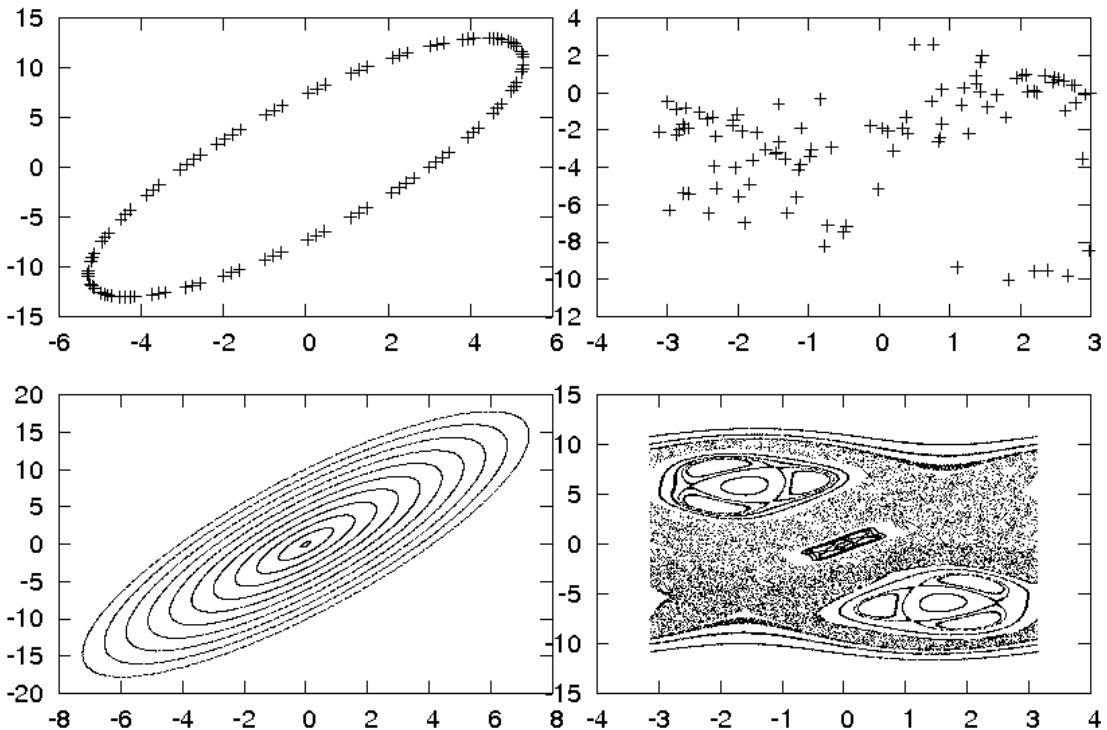


Figure 1.4: On the left is the harmonic oscillator and the right is the pendulum, stroboscopic maps. The top panel is for one hundred iterations with the initial conditions were $(q(0) = 3, p(0) = 0)$, while the bottom one features about 10000 iterations and many more initial conditions. In both cases $\epsilon = 10$ and $g_0 = 1$. The forcing function is same as that in Fig. (1.2)

Floquet theory of linear differential equations with periodic coefficients, which predates a similar theorem due to Bloch which is applied for spatially periodic potentials in the Schrödinger equation and determines electronic band structure in solids, can be applied here, and the Floquet exponents are the eigenvalues of the matrix $\{(a, b), (c, d)\}$. If the eigenvalues are complex and lie on the unit circle, the system is stable and gives rise to elliptic orbits as illustrated above. Otherwise they will appear as pairs of real numbers whose product is unity and in this case the orbits will generically be hyperbolas. The exact expression (a, b, c, d) depend on the forcing function $g(t)$ and are in general quite hard to find. For instance if $g(t)$ is a cosine function, the solutions are not elementary functions, but special ones, the Mathieu functions. However there are important cases where we can write down analytically the stroboscopic map. As a warm up ...

Exercises

4. Consider the “Jekyll and Hyde” Hamiltonian:

$$H = \frac{1}{2}p^2 + \frac{1}{2}s_T(t)\omega^2q^2, \quad (1.10)$$

where $s_T(t)$ is the periodic function:

$$s_T(t) = \begin{cases} 1 & 0 < t \leq T/2 \\ -1 & T/2 < t \leq T \end{cases}. \quad s_T(t) = s_T(t+T).$$

That is dynamics is that of a stable harmonic oscillator for half the time and then suddenly the potential becomes unstable and inverted and the particle tries to run off to infinity, only to find that stability is restored and so on. Whether the dynamics will be effectively unstable or not depends on the frequency of the harmonic oscillator ω and the period of switching T . Show that if $\tau = \omega T/2$, then the linear stroboscopic map, starting from the “base point” $t_0 = 0$ is given by

$$\begin{pmatrix} q_{n+1} \\ p_{n+1} \end{pmatrix} = \begin{pmatrix} a & b \\ c & d \end{pmatrix} \begin{pmatrix} q_n \\ p_n \end{pmatrix} \quad (1.11)$$

where $q_n = q(nT)$ etc. and

$$a = \cosh \tau \cos \tau - \sinh \tau \sin \tau, \quad b = (\cosh \tau \sin \tau + \sinh \tau \cos \tau)/\omega, \quad (1.12)$$

$$c = \omega(-\cosh \tau \sin \tau + \sinh \tau \cos \tau), \quad d = \cosh \tau \cos \tau + \sinh \tau \sin \tau \quad (1.13)$$

A linear map such as in Eq. (1.29), is easy to analyse and completely solve. After all, if we denote it as $X_{n+1} = MX_n$, where X_n is a column vector with d entries for a d -dimensional map and M a constant $d \times d$ matrix, then $X_n = M^n X_0$, and the crucial task is taking a matrix power. If $M = P\Lambda P^{-1}$ is the diagonalization of M with P containing its eigenvectors and Λ a diagonal matrix with its eigenvalues, then $M^n = P\Lambda^n P^{-1}$. Therefore the stability is completely determined by the eigenvalues λ_i . If any of them has a modulus larger than 1, it will lead to exponential growth and instability.

For the two-dimensional map, such as in Eq. (1.29), we have that $\det M = 1$ (hopefully, verify it), and therefore only the trace $\text{tr}M$ matters. The two eigenvalues are given by

$$\lambda_{\pm} = \frac{1}{2}(\text{tr}M \pm \sqrt{(\text{tr}M)^2 - 4}). \quad (1.14)$$

Notice that there are only two possibilities:

- (a) $|\text{tr}M| \leq 2$: The pair of eigenvalues are complex conjugates of each other, and lie on the unit circle. That is they come in pairs as λ, λ^* (or as $e^{\pm i\theta}$.)
- (b) $|\text{tr}M| > 2$, the pair of eigenvalues are real and identified best as $(\lambda > 1, 1/\lambda < 1)$. This situation is unstable as the eigenvector of a λ defines direction along which there is exponential growth.

Note that in linear maps only $(0, 0)$ is a fixed or equilibrium point. These eigenvalues determine then the stability of this equilibrium point, **if $|\text{tr}M| < 2$ the fixed point is elliptic and stable while if $|\text{tr}M| > 2$ it is hyperbolic and unstable.** The marginal case $|\text{tr}M| = 2$ is neutrally stable and is the case at points of **bifurcations** when the orbit is changing stability as a function of some parameter.

Exercise

5. Analyze the “Jekyll-Hyde” Hamiltonian for stability. Will a very rapid switching from stable to unstable ($T \ll 1/\omega$) be conducive for overall stability? Show (numerically, unless you know a better way) that around $T \approx 3.75/\omega$ there is a change of overall stability and find the next. This solvable example shows the same phenomenology as sinusoidal forcing with the stability occurring in parameter windows. You can generalize the problem by switching at times other than at half the period.

Nonlinear maps

A general nonlinear map in two dimensional phase space is given by

$$q_{n+1} = f_1(q_n, p_n), \quad p_{n+1} = f_2(q_n, p_n), \quad (1.15)$$

where f_1 and f_2 are arbitrary functions. However for Hamiltonian systems as time evolution is always symplectic it has to preserve the area. Thus the simplest models of Hamiltonian chaos are **area-preserving maps** (in higher dimensions it has to be truly symplectic). Thus there is the restriction that $\det J = 1$, where J is the Jacobian matrix

$$J(q_n, p_n) = \begin{pmatrix} \frac{\partial f_1}{\partial q_n} & \frac{\partial f_1}{\partial p_n} \\ \frac{\partial f_2}{\partial q_n} & \frac{\partial f_2}{\partial p_n} \end{pmatrix}. \quad (1.16)$$

The Jacobian matrix depends on the phase space location (and not really on n , as long as the map is autonomous). This matrix also determines stability properties, for say we consider two initially nearby points: $(q_0 + \delta q_0, p_0 + \delta p_0)$ and (q_0, p_0) . Then

$$\begin{pmatrix} \delta q_n \\ \delta p_n \end{pmatrix} = J(q_{n-1}, p_{n-1}) \cdots J(q_0, p_0) \begin{pmatrix} \delta q_0 \\ \delta p_0 \end{pmatrix} \equiv J_n \begin{pmatrix} \delta q_0 \\ \delta p_0 \end{pmatrix}, \quad (1.17)$$

J_n defined as the product of n Jacobians (order is important as they do not commute in general). If X_n is the difference vector $(\delta q_0, \delta p_0)^T$ at time n , then

$$\|X_n\|^2 = X_n^T X_n = X_0^T J_n^T J_n X_0, \quad (1.18)$$

is the (square) of the Euclidean distance between the two orbits. The growth of this is completely determined by the matrix $J_n^T J_n$. Note that this is a positive matrix, with eigenvalues $\mu_i(n) \geq 0$. The **Lyapunov exponents** of the orbit are given by

$$\lambda_i(q_0, p_0) = \lim_{n \rightarrow \infty} \frac{1}{2n} \ln \mu_i(n). \quad (1.19)$$

These are rates of growth of the square of the distance $\mu_i(n) \sim e^{2n\lambda_i}$ and the distance between the orbit and its neighbours grow at the rate λ_i . If all $\lambda_i < 0$, the orbit is attracting nearby orbits, else it is repelling them in some direction. For a 2-dimensional map, J_n is a 2×2 matrix that satisfies $\det J_n = 1$. Hence $\det(J_n^T J_n) = 1$ as well, and the two eigenvalues μ_1 and μ_2 must be inverses of each other. As the matrix is positive these have to be real and positive. Hence **the two Lyapunov exponents for an area preserving map add to zero.**

Exercise

6. The generalization of 2– dimensional area preserving maps is to $2d$ dimensional symplectic maps, corresponding to periodically driving a d DoF system. The Jacobians J then satisfy

$$J^T \Omega J = \Omega, \quad \Omega = \begin{pmatrix} 0 & I_d \\ -I_d & 0 \end{pmatrix}, \quad (1.20)$$

where I_d is the $d \times d$ identity matrix. Show that this implies that the $2d$ Lyapunov exponents come in pairs $\pm \lambda_i$ and hence satisfy

$$\sum_{i=1}^{2d} \lambda_i = 0. \quad (1.21)$$

Thus either there is no exponential separation of trajectories along some directions, or if there is separation in some direction there is a contraction in another to exactly compensate this. This is consistent with the fact that the phase space volume remains unchanged, also stated as Liouville’s theorem, however for higher dimensional (> 2) maps, the symplectic condition is much more restrictive, not only do the Lyapunov exponents sum to zero, they actually come in pairs that sum to zero.

Even writing down the stroboscopic map, that is finding explicit forms for $f(q, p)$ and $f_2(q, p)$ is difficult in general, for example I have no idea how to do this for the parametrically forced pendulum. We know that it exists, but not much else. This is because we need to be able to integrate the equations of motion over one time period (as you probably did for the Jekyll-Hyde Hamiltonian). If you attempt the same “Jekyll-Hyde” protocol for the pendulum (the acceleration due to gravity switching directions abruptly, half the time we are pulled up, half down – tough life), you will learn a lot about Jacobian elliptic functions, and yet the map will not be simple enough. For the record, I still have no idea what it is. The map will be of course *nonlinear* in general. However we can in fact write down nonlinear stroboscopic maps for one kind of forcing function, which is essentially the derivative of the step function s_T , namely a train of *delta* functions. This amounts to impulses at regular intervals of time. This case is often referred to as the ”kicked” Hamiltonians and form a very important and well-studied genre of low-dimensional Hamiltonian chaos problems. In recent literature on many-body systems and quantum chaos, it continues to find favour due to its simplicity.

1.3 Kicked Hamiltonian Systems, Justforkix.

Consider Hamiltonians of the form

$$H = f(p) + \sum_{n=-\infty}^{\infty} \delta(t/T - n) V(q). \quad (1.22)$$

The Dirac delta function train is denoted in short as $\delta_T(t)$. The Hamiltonian equations of motion are:

$$\frac{dq}{dt} = \frac{\partial H}{\partial p} = f'(p) \quad (1.23)$$

$$\frac{dp}{dt} = -\frac{\partial H}{\partial q} = -\delta_T(t)V'(q) \quad (1.24)$$

We need to now integrate these equations over one period. Let us choose as $t_0 = 0^+$, so that we are going to consider the stroboscopic map just *after* each kick. The variables just after the n^{th} kick (q_n^+, p_n^+) are to be evolved to the next kicked. Just after the kick, there is no force till just before the next kick. Therefore we can write:

$$p_{n+1}^- = p_n^+, \quad q_{n+1}^- = q_n^+ + Tf'(p_n^+) \quad (1.25)$$

We have to now integrate over the kick number $n + 1$ to arrive at q_{n+1}^+, p_{n+1}^+ . Assuming that $f(p)$ is some smooth function of p , which does not itself have delta function dependencies, integrating the first of the equations of motion over the infinitesimal interval about the $n + 1$ kick implies that the position of the particle is frozen. Integrating the second (force) equation gives us the impulse that is imparted, thus we can write:

$$q_{n+1}^+ = q_{n+1}^-, \quad p_{n+1}^+ = p_n^- - TV(q_{n+1}^+). \quad (1.26)$$

Finally combining the two sets of equations we get the stroboscopic map as:

$$\begin{aligned} q_{n+1} &= q_n + Tf'(p_n) \\ p_{n+1} &= p_n - TV'(q_{n+1}). \end{aligned} \quad (1.27)$$

We have dropped the + superscript, as now every variable is defined as just after the respective kicks. Note that the second equation has the force ($-V'(q)$) evaluated at the *new* time. This follows from the equations of motion and make the above class of maps **area-preserving for any functions f and V** .

Exercises.

7. Prove that map given in Eq. (1.27) is area-preserving. That is find the Jacobian of the transformation:

$$J = \begin{pmatrix} \partial q_{n+1}/\partial q_n & \partial q_{n+1}/\partial p_n \\ \partial p_{n+1}/\partial q_n & \partial p_{n+1}/\partial p_n \end{pmatrix}, \quad (1.28)$$

and show that $\det J = 1$.

8. Find the stroboscopic maps in the case where the variables are monitored from just before the kicks, and in the case where they are monitored midway between kicks.

1.3.1 Important Area-Preserving Maps in 2D

We now point out some of the important cases:

- 1. Linear Map.** This case is when $V(q) = \omega^2 q^2/2$ and $f(p) = p^2/2$. We have already seen how *any* forced harmonic oscillator leads to linear maps, the kicked harmonic oscillator is no exception, but now the stroboscopic map is absolutely straightforward to write down:

$$q_{n+1} = q_n + T p_n \quad (1.29)$$

$$p_{n+1} = p_n - T \omega^2 q_{n+1} = p_n(1 - \omega^2 T^2) - T \omega^2 q_n.$$

The trace of the Jacobian, $\text{tr}J = 2 - T^2\omega^2$, recall that it is an important quantity in this case and depending on whether $|\text{tr}J| <$ or > 2 we have either stability (ellipses) or instability (hyperbolae). The phase space is the plane. This implies that motion is stable if $0 < \omega T < 2$. Thus like the Jekyll-Hyde (JH) case, if T is sufficiently small, $T < 2/\omega$, stability occurs. This is a general feature as if the forcing frequency is very rapid compared to the natural frequency, it is as if the forcing was always present. In other words as $T \rightarrow 0$, the map is approximated by a differential equation which is precisely Newton's laws for a unforced particle in the potential $V(q)$. However unlike the JH case, there are no windows of stability, if T is larger than $2/\omega$ there is only increasing instability.

2. The Standard Map. This is the case of the kicked pendulum, $f(p) = p^2/2$ and $V(q) = -g \cos(2\pi q)/(2\pi)^2$. The stroboscopic map becomes:

$$\begin{aligned} q_{n+1} &= q_n + p_n \pmod{1} \\ p_{n+1} &= p_n - \frac{K}{2\pi} \sin(2\pi q_{n+1}). \end{aligned} \tag{1.30}$$

Here we have rescaled momentum: $T p \rightarrow p$, and $K = T^2 g$ is a rescaled effective parameter. This is the only parameter the kicked pendulum depends on. This map is one of the most widely studied of simple chaotic systems, called variously as the “standard map”, the “Chirikov map” or the “Chirikov-Taylor” map, after those who pioneered its study. The modulo operation is necessary as the coordinate is cyclic, an angle, that has been scaled to lie in $[0, 1)$. Thus the natural phase space is a cylinder, cyclic along q and infinitely extended along the p or the angular momentum direction.

See Fig. (1.5) for the dynamics at various K values. Rotational invariant curves, extending smoothly along the angular coordinate prohibits transport across it and they remain despite the perturbation, as a consequence of the KAM theorem. The last of them, corresponding to a winding number of the most irrational number – the golden mean, breaks around a critical value of $K_c \approx 0.971635$. The map is called “standard” as most typical systems display locally such behaviours. There are few analytical results possible, but for the standard map at least nontrivial results exist such as the statement due to Goroff that for $K > 2\sqrt{1 + \pi^2} \approx 6.59$ the map is hyperbolic (chaotic) in a finite subset.

3. The Harper Map. This is the case of the kicked Harper Hamiltonian, $f(p) = \cos(2\pi p)/(2\pi)$ and $V(q) = g \cos(2\pi q)/(2\pi)$. The stroboscopic map becomes:

$$\begin{aligned} q_{n+1} &= q_n - T \sin(2\pi p_n) \pmod{1} \\ p_{n+1} &= p_n + gT \sin(2\pi q_{n+1}) \pmod{1}. \end{aligned} \tag{1.31}$$

Thus this is a two parameter map (T and gT), defined on a *torus* which is a square which has its opposite sides identified, the topology is that of a south-Indian “medu vada”, the only popular type of vada north of the Vindhyas. This map also has been used in many studies.

As you may imagine, choosing any $f(p)$ and $V(q)$ and possibly imposing different boundary conditions, such as above, will lead to a plethora of maps. In fact it is quite a challenge finding any, apart from of course the harmonic oscillator, that are *not* chaotic in some parameter range. Naturally you are encouraged to try it. One needs to also watch out for cases where the phase-space points go out to infinity. There do exist nonlinear but nonchaotic maps, but they are rare, and we state the following as an example.

4. An Integrable, nonlinear map.

$$\begin{aligned} q_{n+1} &= q_n + p_n \\ p_{n+1} &= p_n + q_{n+1}(A - 2q_{n+1}^2)/(B + q_{n+1}^2). \end{aligned} \tag{1.32}$$

Here A and $B > 0$ are real, but otherwise arbitrary, constants. You can find the corresponding kicking potential easily and it represents an exact discretization of the quartic double-well potential. This map is special, in that there exists a constant of motion, that is a function $F(q, p)$, such that $F(q_n, p_n) = F(q_{n+1}, p_{n+1})$. The integrability of this map is intimately connected to very special properties of Jacobian elliptic functions. But such maps are very rare and even less understood. It is not clear how to check whether a given map is *not* chaotic, i.e. integrable. This forms an active area of research in Mathematical Physics.

Exercises.

8. Find the fixed points (q^0, p^0) of all the maps stated above, and analyse their stability as function of system parameters. Fixed points are those that do not move, that is $q_{n+1}^0 = q_n^0, p_{n+1}^0 = p_n^0$. The stability is checked by find the Jacobian at these points and evaluating their eigenvalues or trace.
9. Plot all of the maps above for various parameters and initial conditions. Get a feel for how easy it is to get pretty pictures. It is quite difficult though to make sense of them.
10. Show that translation along p by one unit $S = (p \rightarrow p + 1, q \rightarrow q)$ is a symmetry of the standard map. An operation S is a symmetry if it commutes with the map itself, if we call the map M then $M \circ S = S \circ M$. Show that the reflection about the center of the unit square: $(q \rightarrow 1 - q, p \rightarrow 1 - p)$ is also a discrete symmetry of the standard map. What effect do these symmetries have on the way the phase space looks?

In Fig. (1.5) is shown many orbits for the standard map for a few parameter values. The standard map is plotted as if the phase-space was a torus, that is the modulo condition is applied on the momentum as well. This gives us a true picture of what is happening on the cylinder as this unit cell repeats indefinitely along the cylinder. This follows from the fact that translation along p by one unit is a *symmetry* of the standard map (see exercise above).

Exercise: Classical Transport in the Standard Map:

11. Iterate the standard map on the cylinder (no mod 1 on the momentum), and plot p as a function of time for various initial conditions for $K \gg 6$, say $K = 10$. Notice the similarities between this graph and a 1-d random walker.
12. Then find $\langle p^2(t) \rangle$, where you first square the momentum and the average is over many initial conditions at a given time. The initial conditions could be for instance chosen to be uniformly spread along $p = 0, 0 \leq q < 1$. This is the “ensemble” averaging. Similarly find $\langle p(t) \rangle$ and hence plot the variance $\langle p^2(t) \rangle - \langle p(t) \rangle^2$ as a function of time t .

You should observe a straight line with a slope approximately proportional to K^2 , which can be predicted with simple arguments. However the exact value of the slope (the “diffusion” coefficient) is a very important quantity whose evaluation is a challenging and open problem in general. In particular there are K values where diffusion is violated, due to the presence of small islands, like

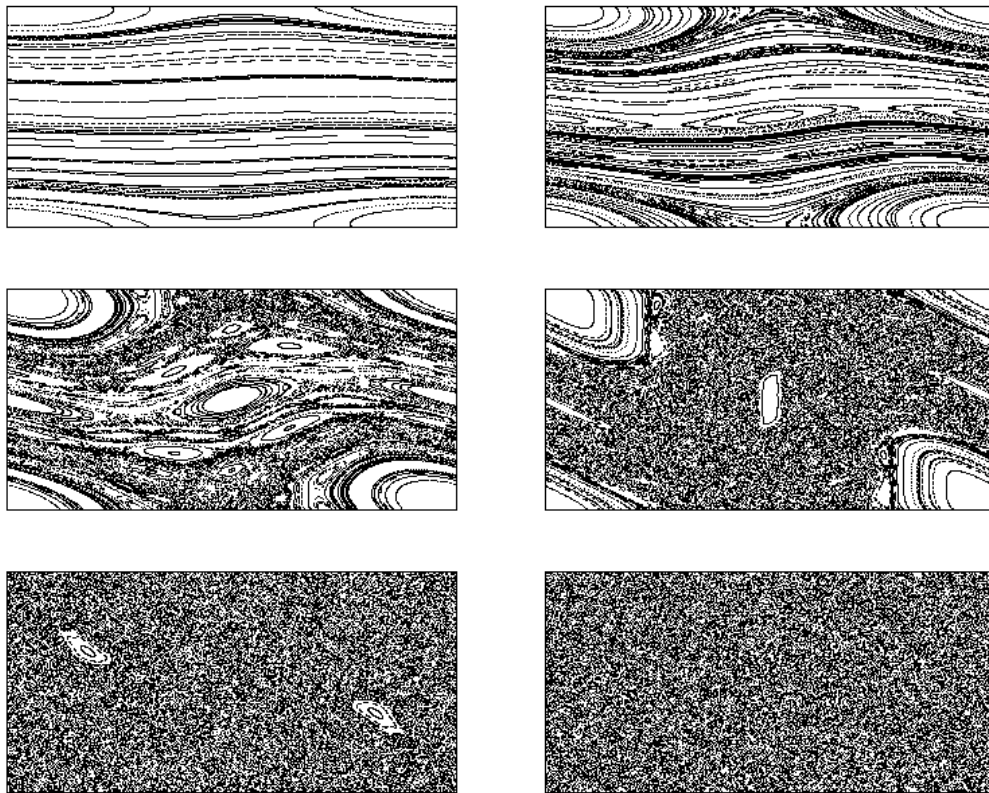


Figure 1.5: The standard map ($q - p$) plot for parameter values $K = 0.1, 0.5, 1.0, 2.0, 5.0, 7.0$, increasing top left to bottom right for a random collection of 100 initial conditions followed 500 times. In all figures both the q and p directions go from 0 to 1.

those seen in the figure for $K = 5$, which don't fully disappear and lead to so-called "anomalous" diffusion, with diffusion mixed with purposeful marching, along so-called "accelerator modes". For further details "google".

The Fig. (1.5) shows how Hamiltonian chaos develops in typical low-dimensional systems. The standard map is one of the earliest models to have their *quantum mechanics* studied. The classical momentum diffusion leads to increasing energy to the pendulum indefinitely. It was found that quantizing the system lead to a suppression of this diffusion, which lead to the phrase "dynamical localization", and energy of a quantum kicked pendulum even for large kicking strengths does not absorb energy indefinitely. This phenomenon has been linked to Anderson localization that is responsible for metal-insulator transitions. Apparently very dissimilar systems, but having a lot in common.

The standard map is so-called because it has a typical transition to chaos as the parameter is increased. As this happens orbits that were stable lose their stability through bifurcations (a well-studied theory exists in dynamical systems), but many new orbits are "born" as well and these could be stable for a while before changing over. The scenario involves two well known theorems: one to **Kolmogorov Arnold and Moser (KAM)**, and the other called the **Poincare-Birkhoff theorem**. As these will take us into details of dynamical systems, we refrain from doing so and sort of jump straight into the arms of chaos. We wish to understand the large K regime where almost every initial condition wanders all over the phase space (torus), visiting every neighborhood in an apparently random manner. In this regime there is the **sensitivity to initial conditions** that was mentioned in the forced pendulum. Only here we do not need to use an integration routine. We can estimate the **Lyapunov exponent of orbits in the standard map** as follows.

The Jacobian after n time steps is

$$J_n = \prod_{j=1}^n \begin{pmatrix} 1 & 1 \\ -K \cos[2\pi q_j] & 1 - K \cos[2\pi q_j] \end{pmatrix}. \quad (1.33)$$

The larger eigenvalues at each individual step are

$$\mu = \frac{1}{2}(\text{tr}M + \sqrt{(\text{tr}M)^2 - 4}), \quad (1.34)$$

where $\text{tr}M = 2 - K \cos(2\pi q)$. Assuming that $|\text{tr}M| \gg 2$ when there is instability and chaos we approximate $|\mu| \approx |\text{tr}M| = |2 - K \cos(2\pi q)|$. This is approximately the factor with which phase space areas are being stretched along unstable manifolds. After n steps the stretching is $\mu_n = \prod_{j=1}^n |2 - K \cos(2\pi q_j)|$, and if the Lyapunov exponent is λ , then $\mu_n \sim e^{n\lambda}$. (Note: this μ is approximately the square-root of the μ as the eigenvalues of $J^T J$ discussed earlier. Therefore finally,

$$\lambda \sim \lim_{n \rightarrow \infty} \frac{1}{n} \sum_{j=1}^n \ln |2 - K \cos(2\pi q_j)| = \int_0^1 \ln |2 - K \cos(2\pi q)| dq = \ln(K/2). \quad (1.35)$$

When the sum has been replaced by an integral there is the assumption that q_j "goes all over" $[0, 1]$ uniformly, we are assuming ergodicity. This is an estimate made by Chirikov and is extremely accurate as can be checked by following the methodology outlines earlier. It is valid for $K > 5$ or so. Corrections to this formula have been found to go as $1/(K^2 - 4)$. Note that there is no initial condition information left: **all orbits** have this Lyapunov exponent (LE), to be precise almost all orbits have this LE. We just speak of The LE of the map, as if there is just one, with this caveat. The LE is used as a measure of chaos: it is really a measure of instability: unstable linear systems have a positive LE. However it is understood that **if the orbit is bounded, and has a positive LE, it is chaotic**.

1.3.2 Poincaré Surface of Section: Hamiltonian Flows to Maps

The stroboscopic maps in the family Eq. (1.27) present a very rich source of dynamical systems. Also while we have derived them from 1.5 dimensional systems, that is one-degree of freedom nonautonomous systems, it is important to note that they share the same phenomenology as the **Poincaré surface of section (PSOS)** for two-degree of freedom autonomous Hamiltonian systems. The phase space is now **4 dimensional**, say (q_1, p_1, q_2, p_2) . The PSOS of such systems are also area-preserving transformation of the same kind. PSOS are obtained by restricting ourselves to a given energy shell $H = E$, in the case of $d = 2$ a 3-dimensional surface, and observing the orbits as they cross a given section. Traditionally the section can be $q_1 = 0$ in the positive ($p_1 > 0$) sense of the flow. The only difference between the PSOS and the stroboscopic maps is that the time of return to the PSOS is in general not the same and itself is a very complex, and ill-understood, function of phase-space. The popularity of maps such as in Eq. (1.27) is the simplicity of numerical work: we only have to iterate now and in principle there are no errors introduced due to truncation in integration schemes. Also certainly more analytical work is feasible in this approach. However, obviously Hamiltonian flows are very important due to their centrality.

Many 2–DoF systems have been analyzed, the include a large class of Billiard problems two dimensional enclosures with hard walls that specularly reflect a particle trapped inside. For example a rectangular enclosure is integrable: it conserves the magnitude of the two momentum components, so is a circular billiard as it conserves energy and angular momentum. Both these cases are quite obvious. Somewhat surprisingly the *elliptic billiard* is also integrable, conserving in addition to energy, the product of the angular momentum about the two foci. (Exercise: prove this). Almost any other shape leads to nonintegrability and chaos, as they only conserve energy.

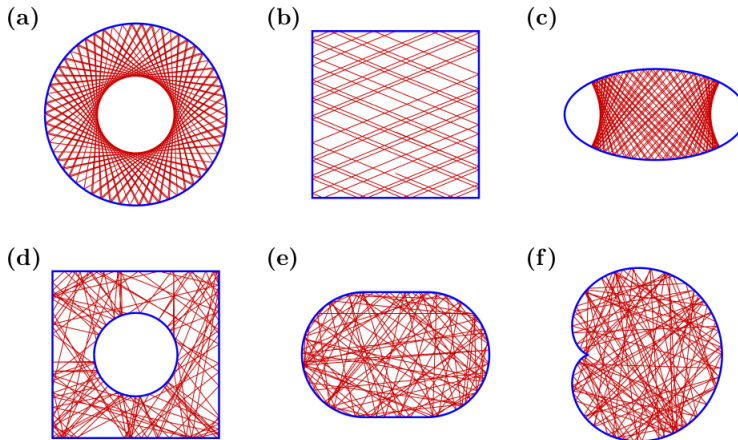


Figure 1: For different billiards 100 successive reflections of one orbit are shown. The regular dynamics for the billiard in the (a) circle, (b) square and (c) ellipse is in contrast to chaotic dynamics for the (d) Sinai billiard, (e) stadium billiard and (f) cardioid billiard.

The figure above illustrates typical trajectories for the integrable (above) row and some nonintegrable ones below. This picture and most of the billiard figures that will appear are taken (as of now without permission) from the **Habilitation thesis of Prof. Arnd Bäcker of TU Dresden**. The Sinai billiard (circle cut out of a square), the stadium or Bunimovitch billiard, and the cardioid billiard are all **fully chaotic**: all trajectories are unstable and exponentially separate from their neighbours, they have a positive Lyapunov exponent. The deformation of the circle: $\rho(\phi) = 1 + \epsilon \cos(\phi)$ is known as the

Limacon billiard, when $\epsilon = 0$, it is the integrable circle billiard, and when $\epsilon = 1$ it is the fully chaotic cardioid. However for intermediate values, it has a mixed phase space, with both regular as chaotic orbits as we saw for the standard map. This is shown in the figure below for the case of $\epsilon = 0.3$.

What is shown is the PSOS, where the section is the boundary of the billiard. The coordinate is the arclength along the billiard and the conjugate variable is the projection of the (unit) velocity vector along the tangent to the billiard. This is also called a Birkhoff map after the great mathematician and physicist. It is remarkable that for a shape that looks like a very small distortion of the circle, the measure of chaotic orbits is very large. (Exercise: How does the PSOS look for a circular billiard? For a rectangular billiard?).

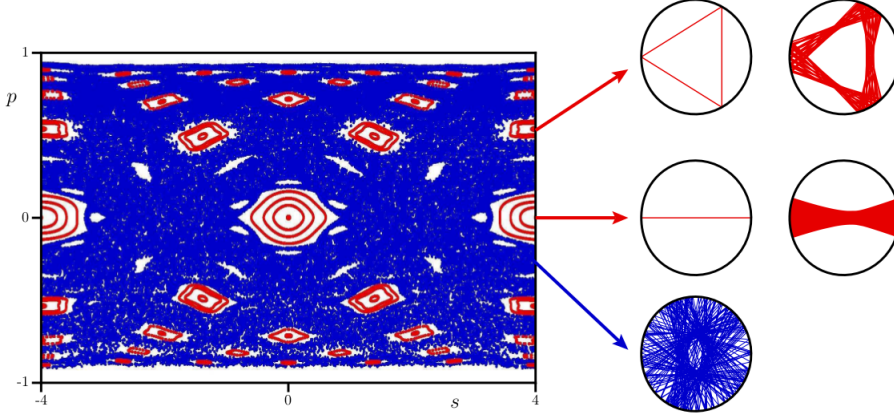


Figure 6: Example of a system with a mixed phase space. Shown are several regular orbits and one chaotic orbit in the Poincaré section of the limaçon billiard at $\epsilon = 0.3$. To the right two regular orbits and trajectories in the surrounding are displayed in position space in comparison with a chaotic trajectory.

Another widely used class of $d = 2\text{DoF}$ flows are nonlinear oscillators, such as the Hénon-Heiles system or coupled quartic oscillators. For example consider the family

$$H = \frac{1}{2}(p_1^2 + p_2^2) + \frac{1}{4}\alpha(q_1^4 + q_2^4) + \frac{1}{2}\gamma q_1^2 q_2^2, \quad (1.36)$$

parametrized by two parameters α and γ . Clearly when $\gamma = 0$ it is separable and integrable (as an exercise find another case of an integrable set). The Fig. (1.3.2) (from an early and excellent review article “Quantum Mechanics of Classically Non-Integrable Systems by Bruno Eckhardt, Physics Reports, 163, No. 4 (1988) 205-297), is a PSOS of this system for a fixed value of $\gamma = 1$. As α decreases we see a transition to chaos no unlike what we saw for the standard map. In fact the case $\alpha = 0$ is very interesting for several reasons. It is the pure x^2y^2 potential that was thought to be fully chaotic for some time, till it was shown that there are tiny islands of stability lurking in the chaos. Its quantum mechanics is interesting and challenging as well.

1.4 Poincaré Recurrence Theorem, Ergodicity, Mixing

1.4.1 Recurrence theorem

One of the general results in dynamics is Poincaré’s recurrence theorem. Simply stated: almost every initial phase space point comes back to its neighbourhood eventually. This is true for *all* Hamiltonian

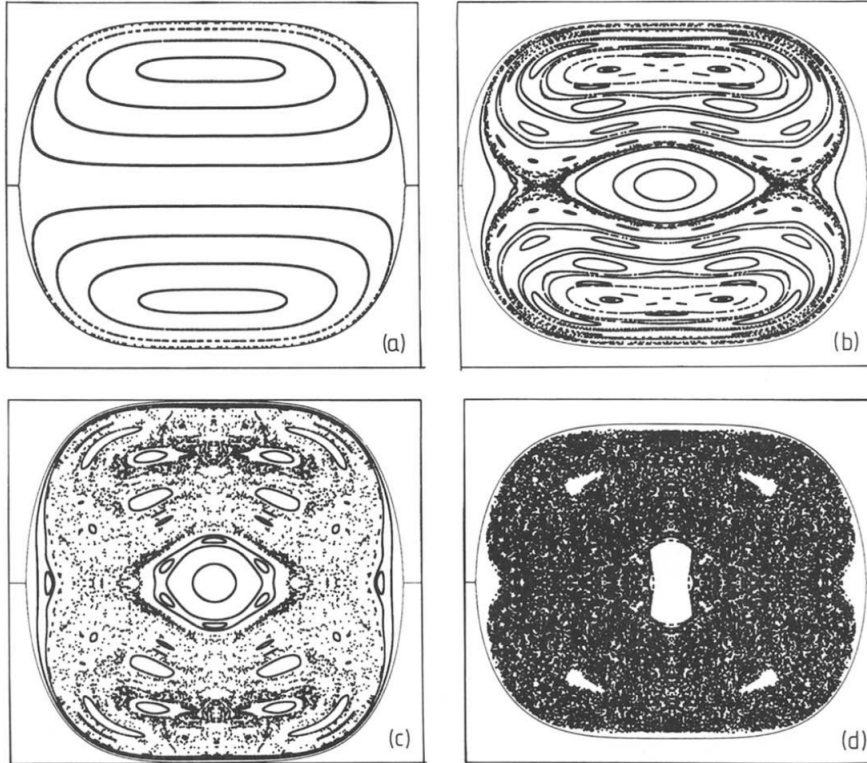


Figure 1.6: Poincaré surfaces of section for the Hamiltonian of Eq. (1.36). The section condition is ($q_2 = 0, p_2 > 0$) and the parameters are $\gamma = 1$ and (a) $\alpha = 0.333$, (b) $\alpha = 0.28$, (c) $\alpha = 0.25$ and (d) $\alpha = 0.166$. Panel (d) was obtained by plotting 4×10000 iterates of one trajectory in the chaotic region.

system, irrespective of whether it is chaotic or not. It holds for a more general class of systems that preserves some measure. A transformation T preserves measure μ if $\mu(T^{-1}A) = \mu(A)$, where A is some set on the phase space and $\mu(A)$ is its measure. We can simply think of the “volume” of the set as a measure, and it is the case for Hamiltonian systems, which are measure preserving as volumes in phase space do not change: Liouville’s theorem. For a 2D area-preserving map, the measure is simply the area.

Let Ω be a finite phase space $\mu(\Omega) < \infty$ and T be a measure μ preserving transformation on Ω . For almost all $x \in A$, and $\mu(A) > 0$, the recurrence theorem is that the orbit $\{T^n(x)\}$ returns infinitely often to A . The “almost all” implies that the set of exceptional points are of measure 0 ($\mu(\text{exceptions}) = 0$). The proof is standard, and I reproduce it here: Let

$$E = \{x \in A | T^n(x) \in A \text{ for infinitely many } n\},$$

we have to show that $\mu(A \setminus E) = 0$. Define the set

$$F = \{x \in A | T^n(x) \notin A \text{ for } n \geq 1\}$$

Observe that F is not $A \setminus E$ as F only contains points that will leave A in one iteration and never return.

$$A \setminus E = \bigcup_{k=0}^{\infty} T^{-k}F \cap A$$

$T^{-1}F \cap A$ contains *all* points of A that remain in A after one iteration to then never return. $T^{-2}F \cap A$ contains *all* points of A that are found in A after two iteration and then never return. These could contain points that leave A after one iteration and then comes back or that remains in A for two consecutive iterations and then leaves it. And so on. Then we have

$$\mu(A \setminus E) = \mu\left(\bigcup_{k=0}^{\infty} T^{-k}F \cap A\right) \leq \mu\left(\bigcup_{k=0}^{\infty} T^{-k}F\right) \leq \sum_{k=0}^{\infty} \mu(T^{-k}F).$$

We now observe that $T^{-k}F$ constitute non-overlapping sets. For let $y \in T^{-n}F \cap T^{-m}F$ and $m > n$, then $T^ny \in F$ and $T^my \in F$. However $T^my = T^{m-n}(T^ny)$. The last must leave the set A to never return, therefore there is no such y and the sets are independent. Therefore

$$\sum_{k=0}^{\infty} \mu(T^{-k}F) = \sum_{k=0}^{\infty} \mu(F) < \mu(\Omega),$$

which is possible iff $\mu(F) = 0$ and this in turn implies that $\mu(A \setminus E) = 0$, as a countable union of measure 0 sets has measure 0.

There are two important aspects of chaotic systems that are conventionally stated as the basis of statistical physics: ergodicity and mixing. We briefly discuss these notion before discussing area-preserving maps that illustrate very simply these concepts.

1.4.2 Ergodicity

Let $y \in \Omega$ and $\epsilon >$ be an arbitrary number. The transformation T , which preserves measure μ is said to be ergodic on Ω if for almost all $x \in \Omega$, there exists some $n > 0$ such that $|T^n x - y| < \epsilon$. In words,

almost all points visit any neighbourhood of another point eventually. It is a statement of “wandering”. Importantly it is equivalent to a statement of **time average = phase space average** as (Birkhoff) for almost all $x \in \Omega$, and for a smooth function f

$$\lim_{n \rightarrow \infty} \frac{1}{n} \sum_{j=1}^n f(T^j x) = \int_{\Omega} f d\mu. \quad (1.37)$$

Note that the LHS is dependent (apparently) on the initial condition, but this information is washed out in the infinite time limit.

Examples

1. 1-D harmonic oscillator: motion is ergodic on the energy shell, this being just the corresponding ellipse. In fact any periodic 1-D motion is trivially ergodic as the orbit and the shell are identical.
2. 2-D harmonic oscillators, coupled or otherwise are not chaotic on the full energy shell. This is because E_i the energies of the two normal modes are conserved. Not all points on the total energy shell $E = E_1 + E_2$ can be accessed. Dynamics could be ergodic on lower dimensional subsets.
3. Any separable system is not ergodic for the similar reasons as the case above. In fact any dynamics that has more than one conserved quantity (energy being assumed to be constant) is not ergodic on the energy shell. If there are as many independent constants of motion as number of degrees of freedom, it is said to be **integrable**.
4. Any system without any constants of motion apart from energy could be ergodic on the energy shell or on subsets of it. These are **non-integrable** systems. For example a sufficiently energetic double pendulum could be ergodic.
5. Consider $\theta_{n+1} = \theta_n + 2\pi\alpha \bmod 2\pi$, a simple rotation map on a circle. If α is a rational number p/q show that the dynamics is exactly periodic, all points coming back after q iterations, having performed p full rotations. This is not of course ergodic. However, if α is irrational, then it is not hard to show that it is ergodic and that any point eventually comes arbitrarily close to any other.

In the above examples we have avoided talking about the invariant measure, which is needed if we are to find time averages. In the case of the irrational rotation, the invariant measure is the uniform (Lebesgue if you are so inclined) or simply the arc length on the circle. That is the points $\{\theta_n\}$ get uniformly distributed on the circle. In the case of area-preserving maps such as the standard map, it is simply the area. For Hamiltonian systems that are autonomous there is a detail that is often glossed over, namely that the Liouville volume measure is on the $2d$ dimensional phase space, whereas the ergodicity (word originating from energy surface) is restricted to a constant energy (hyper)surface of dimension $2d - 1$. On this hypersurface the $2d - 1$ -dimensional volume element is not conserved, but there is an invariant measure. To find it we visualize two energy shells that are separated by a small amount dE and a phase space volume element dV_1 trapped there in the vicinity of (q_1, p_1) . Then

$$E + dE = H(q_1 + \delta q_1, p_1 + \delta p_1) = E + \nabla H \cdot (\delta q_1, \delta p_1)$$

If $(\delta q_1, \delta p_1)$ is taken along the gradient, then we get the “width” of the energy shell at (q_1, p_1) as $\sqrt{(\delta q)^2 + (\delta p)^2}$, which is then $dE/|\nabla H|_1$. Therefore $dV_1 = dA_1 dE/|\nabla H|_1$, where dA_1 is the “area”

element on the energy shell, which is really a $2d - 1$ dimensional volume. As the volume element evolves under the flow, dE and dV_1 remain constant, therefore the invariant measure on the energy shell is

$$\frac{dA}{|\nabla H|}.$$

For example for 1-DoF systems, the orbit in general does not uniformly fill the shell and the area element is a line-element, while for 2-DoF systems, the energy shell is 3-dimensional and dA is a 3-volume.

Ergodicity is a property of “indecomposability”, T is ergodic on M iff every invariant set is either of measure 0 or measure 1 ($\mu(\Omega) = 1$).

Exercise

13. Show that the irrational rotation is ergodic with the invariant measure being the uniform one. That is show that

$$\lim_{n \rightarrow \infty} \frac{1}{n} \sum_{j=1}^n f(\theta_j) = \frac{1}{2\pi} \int_0^{2\pi} f(\theta) d\theta,$$

where $f(\theta)$ is any smooth function on the circle. Suggestion: Express $f(\theta)$ as a Fourier series and show that only the zero mode survives the time average.

14. Do the same as the previous exercise but now for the “doubling map”, $x_{n+1} = 2x_n \bmod 1$.

1.4.3 Mixing

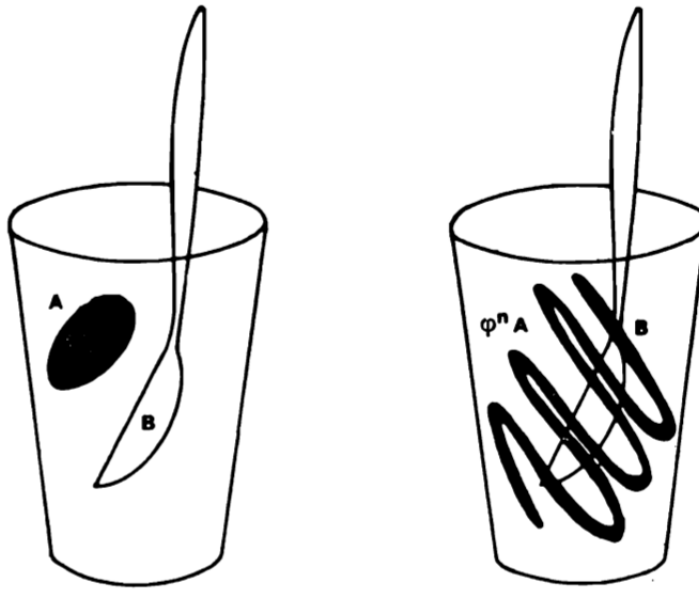
The following is from the (classic) book by Arnold and Avez, “Ergodic problems of classical mechanics”. They use ϕ^t for T^n , the transformation after time n . Also they normalize the measure of their phase space to 1.

§8. Mixing

Let M be a shaker full of an incompressible fluid, which consists of 20% rum and 80% Coca Cola (see Figure 8.1). If A is the region originally occupied by the rum, then, for any part B of the shaker, the percentage of rum in B , after n repetitions of the act of stirring, is

$$\frac{\mu(\phi^n A \cap B)}{\mu(A)}$$

In such a situation, physicists expect that, after the liquid has been stirred sufficiently often ($n \rightarrow \infty$), every part B of the shaker will contain approximately 20% rum. This leads to the following definition.



T is mixing if

$$\mu(T^n A \cap B) \rightarrow \mu(A)\mu(B) \text{ as } n \rightarrow \infty.$$

This requires every region A to become striated and contort itself so that its volume does not change, but it is spread everywhere in phase space. Imagine for example dropping ink in water (Rum and coke have same color), the volume of the ink (and alas rum) does not change, but it is “spread” in water democratically. Ergodicity does not require this, in fact the irrational rotation which is ergodic, merely rotates arcs by the same angle and therefore remains intact, like a metal pellet in water, it moves all around but does not mix.

However **mixing implies ergodicity**. To see this, take A to be an invariant set (that is $T^{-1}A = A$) and $B = A$, then mixing implies that $\mu(A \cap A) = \mu(A) = \mu(A)^2$, and hence $\mu(A) = 0$ or 1 , as required for an ergodic transformation. Thus mixing is a stronger condition than ergodicity.

1.5 Fully chaotic, exactly solvable, model systems

1.5.1 The Baker Map

“The baker’s map is the harmonic oscillator of chaos”
—Predrag Cvitanovic.

On the lightly floured surface, flatten the dough slightly into a disk-shape. Use the heels of your hands to PUSH the dough away. Pick up the edge furthest away from you and FOLD it toward you, sliding the dough back to its original spot on the counter. TURN the dough a quarter-turn. Vigorously repeat “push, fold, and turn” steps.

— From www.baking911.com. (without permission).

So what's all this fuss about? The baker does it every day, and while making chappathis we adopt similar strategy to mix thoroughly the *atta* with the water. Looking at the instructions for baking we see two crucial ingredients, PUSH, and FOLD. Pushing provides the instability, while folding provides the confinement, the classic “stretch and fold” mantra of chaos. (For the moment we ignore the instruction

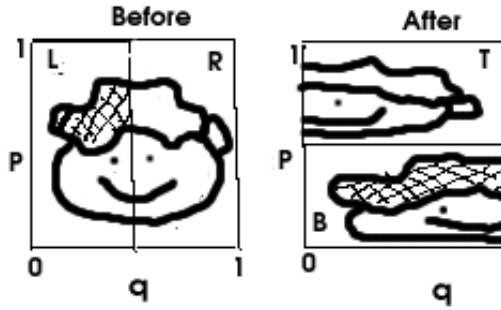


Figure 1.7: The dough before and after. Notice how the baker’s smile becomes a bit wane, as his face is stretched in the q direction and compressed in the p , both by a factor of 2, cut in the center and stacked with the right half on top of the left, so that $L \rightarrow B$ and $R \rightarrow T$. It is a wonder that the baker is still smiling at all.

of the baker to “turn”). We also assume that the dough is 2D and a perfect square!

BAKER MAP.

$$\begin{aligned} q_{n+1} &= 2q_n \\ p_{n+1} &= p_n/2 \end{aligned} \quad \left\{ \begin{array}{l} 0 \leq q_n < 1/2; \\ p_{n+1} = (p_n + 1)/2 \end{array} \right\} \quad \begin{aligned} q_{n+1} &= 2q_n - 1 \\ p_{n+1} &= (p_n + 1)/2 \end{aligned} \quad \left\{ \begin{array}{l} 1/2 \leq q_n < 1. \end{array} \right. \quad (1.38)$$

The baker map is area preserving, its Jacobian is simply $\text{diag}(2, 1/2) = \{(2, 0), (0, 1/2)\}$ everywhere, the eigenvalues are 2 and $1/2$. The map is **uniformly hyperbolic**, the stretching is the same throughout phase space. The lyapunov exponents for the baker map are $\ln(2)$ and $-\ln(2)$, recall that for area-preserving maps the sum of the LE must be 0. Thus with a positive nonzero Lyapunov exponent the map is a candidate for chaos. It is in fact a paradigm of chaos, and this becomes clear if we work in the binary representation of numbers.

Let (q_0, p_0) be an initial phase space point that is evolved by the baker map in Eq. (1.38). How is the phase space point after n iterations (q_n, p_n) related to the initial conditions? In short can we *solve* the baker map? If you look more closely at the baker map, you realize that the evolution of q has nothing to do with p , while the evolution of p is dependent on q . Thus we could solve for q_n for instance, and in fact **the q map is known as the doubling or the sawtooth map**. It is simply $q_{n+1} = 2q_n \pmod{1}$, whose solution is $q_n = 2^n q_0 \pmod{1}$. Although we have “solved” for q_n the solution does not leave us much wiser. This is a good illustration that **chaos is not about the lack of analytical solutions**, but is a statement about dynamics.

To “understand” the baker any further, we need to do something more than solve it. Let the phase space points be specified in the binary representation, say as $q_0 = 0.a_0a_1a_2\dots$ and $p_0 = 0.a_{-1}a_{-2}a_3\dots$, where $a_i = 0, 1$. Recall that this means

$$q_0 = \frac{a_0}{2} + \frac{a_1}{2^2} + \frac{a_2}{2^3} + \dots; \quad p_0 = \frac{a_{-1}}{2} + \frac{a_{-2}}{2^2} + \frac{a_{-3}}{2^3} + \dots \quad (1.39)$$

Note that $a_0 = 0$ if q_0 lies in left half L and it is 1 otherwise. Thus $q_1 = 2q_0 - a_0$ whether $a_0 = 0$ or 1. Similarly $p_1 = (p_0 + a_0)/2$ in either case. We get

$$q_1 = \frac{a_1}{2} + \frac{a_2}{2^2} + \frac{a_3}{2^3} + \dots; \quad p_1 = \frac{a_0}{2} + \frac{a_{-1}}{2^2} + \frac{a_{-2}}{2^3} + \dots \quad (1.40)$$

If we write Eq. (1.39) as a *bi-infinite* sequence of the following form

$$(p_0|q_0) = \dots a_{-3}a_{-2}a_{-1} \circ a_0a_1a_2 \dots \quad (1.41)$$

then

$$(p_1|q_1) = \dots a_{-2}a_{-1}a_0 \circ a_1a_2a_3 \dots \quad (1.42)$$

The notation $(p|q)$ is to indicate a phase space point, the right side is to be thought of symbolically, with the small circle separating the p in the left from the q on the right. Thus given the right side, we can read off q and p . Thus the action of the baker dynamics is transparent. It shifts the entire sequence of a_i to the left by one place. Iterating the map simply shifts it further and futher. Thus the small circle, dividing q from p , also acquires the significance of the *present moment*. This dynamics is known as a **left shift**. Although this appears to be very special it is some form of left shit on possibly infinite symbols (not just 0 and 1) that underlies chaos, including that found in many body problems. The left shift is in many senses the heart of chaos, Hamiltonian or otherwise.

This representation then reveals many features of the baker map:

1. Proliferation of errors. The left shift reveals the alarming nature of chaos and eventually the limitations of mathematical modelling for prediction. We would know the initial conditions only up to some precision, say we have an accuracy of $10^{-20} \approx 2^{-67}$, that is we know $(a_0, a_{\pm 1}, \dots, a_{\pm 66})$ and a_{-67} . The rest of the binary expansion coefficients are inaccessible to us. On iterating the baker map, we lose one bit of information every time, and after 66 times the following is the case:

$$\begin{aligned} (p_0|q_0) &= [u] a_{-67} \dots a_{-1} \circ a_0 \dots a_{66} [u] \longrightarrow \\ (p_{66}|q_{66}) &= [u] a_{-67} \dots a_0 \dots a_{65} \circ a_{66} [u]. \end{aligned} \quad (1.43)$$

We have indicated the any unknown bit strings uniformly as $[u]$. The initial area of ignorance is a square of size $2^{-67} \times 2^{-67}$, whose left-bottom corner is at $(q = 0.a_0 \dots a_{66}, p = 0.a_{-1}a_{-2} \dots a_{-67})$.

What do know about $(p_{66}|q_{66})$? About q_{66} we only know the first significant bit which is a_{66} , we are at the edge of our knowledge. Thus all we can say about q_{66} is whether it is in the left half ($a_{66} = 0$), or the right half ($a_{66} = 1$) of the square. We seem to have compensated for our q losses in p , we now know it to a *greater(!)* accuracy of about 10^{-40} now. After one more iteration we have no clue where q_{67} is, we can only make the trivial, but consoling, statement that it is somewhere in the square, we are not losing any dough, and the accuracy of p is at its best. The area of ignorance is now the rectangle of size (1×2^{-134}) , with the left-bottom corner being at $(q = 0, p = 0.a_{66}a_{65} \dots a_0a_{-1} \dots a_{-67})$.

What next? Only *now* does chaos rear its head. The situation described in the previous paragraph is really only a consequence of instability, the PUSHING action of the baker. It is true for unstable nonchaotic systems, like a ball rolling down a hill, as well. the unknown bits of q now become the *most significant* bits of p due to FOLDING. Now we have a peculiar situation that we know some of the less significant bits of p , but the most significant ones are being lost, or rather are being taken over by the unknown bits of q . What is the error in p ? Remember that the error in q is now the maximum possible, namely 1.

Lets take stock after $n = 68$ steps.

$$(p_{68}|q_{68}) = [u] a_{-67} \dots a_{66} u_1 \circ [u], \quad (1.44)$$

where we denote by u_k , one of the 2^k unknown bit strings of length k , u_1 could be 0 or 1. Thus the area of ignorance is now *two* rectangles, each of area 1×2^{-68} , one whose left-bottom corner is at

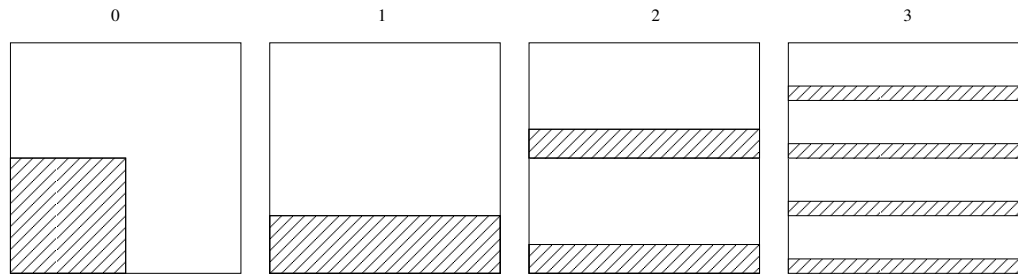


Figure 1.8: Evolution of an area in the baker map

$(q = 0, p = 0.0a_{66} \dots a_{-67})$ and the other at $(q = 0, p = 0.1a_{66} \dots a_{-67})$. After one more time step there are *four* areas of ignorance of size 1×2^{-69} etc. Thus it is clear that the area of ignorance remains a constant, after this *is* an area preserving transformation! However the area of ignorance after a critical time, which depends on the original area, starts taking on such complex and proliferating branches, typically exponentially large in number, that it loses the typical meaning of “error bars” anymore.

Naturally a picture is in order here. See Fig. (1.8) for an illustration where the initial area of ignorance is pretty large, being one quarter of the square (some really bad equipment here!), this size meaning we don’t wait inordinately long for things to happen. The evolution of this area is $[u]0 \circ 0[u] \rightarrow [u]00 \circ [u] \rightarrow [u]00u_1 \circ [u] \rightarrow [u]00u_2 \circ [u]$. The two possibilities for u_1 is reflected as the two horizontal strips at $n = 2$ (the one at the top is $u_1 = 1$, while the one below is $U_1 = 0$); similarly the four possibilities for u_2 results in four strips at $n = 3$.

On the other hand, the baker map is very special in that it singles out q and p axes, in general the error will increase along a direction that itself changes in a complex way along the orbit, this infact being the unstable manifold, and the error will decrease along the stable manifold. We have seen that the geometry of these is so complicated that all practical observables will experience an increase in the error and it is quite right to say that *errors proliferate, typically exponentially, in the case of chaotic systems*.

Sensitivity to Initial Conditions. Closely related to the proliferation of errors is this property that is often taken to be synonymous with chaos. Two initially close points will share a very long common number of bits in both p and q , but the differences will come to the fore, exponentially fast, they will fly farther apart along q , while coming together along p till they separate also on p .

Mixing. The evolution of areas shown above also illustrates the important property of mixing, the shaded region has the same area but tends to get thoroughly mixed in the background. This is of course why the baker was interested in this transformation in the first place. Mixing was properly described mathematically by Hopf, who also invented the baker map. It is characterized by certain numbers that describe how fast it occurs, the so called Ruelle-Pollicot resonances, something we will not expand upon here.

Periodic Orbits Everywhere. From pictures such as we saw for the kicked pendulum and the standard map, we may think that chaos is some formless mess. This is not necessarily the case, in this mess there is a backbone of periodicity, a periodicity that is more prolific than even for regular systems. Consider the fate of points such as

$$(p_0|q_0) = \dots u_k u_k \circ u_k u_k \dots \quad (1.45)$$

where u_k is any binary string of length k . It is then clear from the left shift dynamics that $(p_k|q_k) = (p_0|q_0)$, that is this initial point comes back to itself after k steps. It also immediately follows that after any multiple of k the point recurs, in short we have a *periodic point* of period k . As there are 2^k possible u_k strings for any k , there are exactly 2^k possible periodic points for the baker map of period k . The repeating string is often denoted by an overbar, thus $(p_0|q_0) = \overline{u_k} \circ \overline{u_k}$.

For example the point $\overline{01} \circ \overline{01}$ is a periodic point of period 2, and in usual decimal representation it is $(q_0 = 1/3, p_0 = 2/3)$.

Exercise.

15. Enumerate all periodic points of period 1, 2, 3 and 4, writing them out in binary and decimal forms. Note how period 4 points include period 2 points and how all of them include period 1 (fixed) points.

16. Prove that the decimal representation of $(p_0|q_0) = \overline{u_k} \circ \overline{u_k}$, is

$$q_0 = d(u_k)/(2^k - 1), p_0 = Rd(u_k)/(2^k - 1). \quad (1.46)$$

If the string $u_k = a_0a_1\dots a_{k-1}$ then $d(u_k) = 2^{k-1}a_0 + 2^{k-2}a_1 + 2^{k-2}a_2 + \dots + a_{k-1}$ is the value of the binary string u_k , and $Rd(u_k) = 2^{k-1}a_{k-1} + 2^{k-2}a_{k-2} + \dots + a_0$ is the value of the string that is obtained by reversing the string u_k , with the least significant bit becoming the most significant bit etc. Note that this is different from the bit-reversal operation that interchanges the 0 and 1 bits. Getting Rd from d is quite a nontrivial, nonlocal, operation that has in it an element of the complexity of the baker map. In an (apparently) totally unrelated event, this operation is central to the Fast Fourier Transform (FFT) and occurs as the scrambling of the output frequencies.

The exercise shows how to find the periodic orbits. Where are they? The *periodic orbits are dense*, that is *arbitrarily close to any phase space point there is some periodic orbit*. The proof is also easy from the left shift dynamics. If we take as the random point $(p_0|q_0) = \dots a_{-1} \circ a_0a_1 \dots$, and we want to find a periodic point within a radius $\epsilon < 2^{-K}$ for some large and positive K , we will consider the periodic point with the repeating string $u_{2K} = a_0a_1\dots a_Ka_{-K}a_{-K+1}\dots a_{-1}$. At $n = 0$ this will be within 2^{-K} distance from the chosen random point, but it will be an periodic orbit of period $2K$. Thus it is clear that periodic orbits are dense.

A number if said to be **normal** in some base if all possible strings of a given length occur with equal frequency. For example in the binary representation, a normal number will have an equal fraction of 0 and 1 ($1/2-1/2$), an equal fraction of 00, 01, 10, 11 each occurring with a frequency $1/4$ etc.. It is fascinating that while it is proved that almost all numbers are normal, to prove that a given number is normal is extremely hard. For our purposes, existence and measure 1, implies that there is a *dense orbit* in the baker map. This is an orbit such that it comes arbitrarily close to any other phase space point. In fact dense orbits are dense in phase space. Dense orbits imply and are implied by *ergodicity*.

In Fig. (1.9) we see all the periodic orbits of periods 5, 10 and 15, there are 32, 1024 and 32768 points in each respectively. It is also clear that the periodic orbits are *isolated*, they do not form continuous families. This distinguishes chaotic systems from most regular ones. The stability of periodic orbits is of course of central importance. In the baker map all the isolated periodic orbits are *unstable*. If the baker map were not exactly solvable in terms of an explicit left shift, we would not have a ghost of a

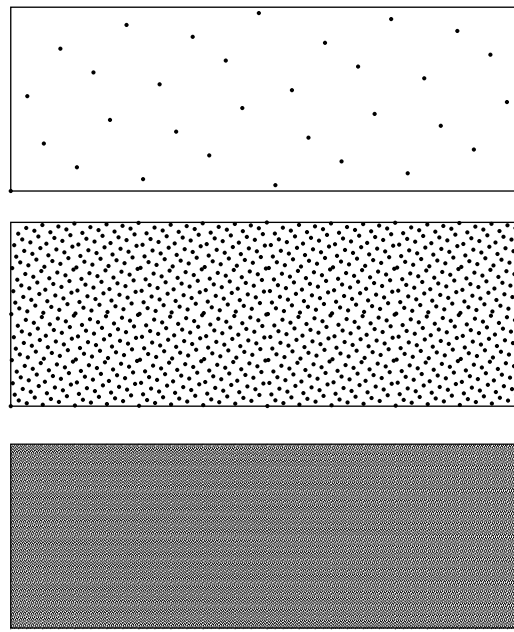


Figure 1.9: All periodic points of the baker map of periods 5, 10 and 15 from top to bottom. The plots are all on unit (q, p) squares.

chance finding “long” periodic orbits even of length as small as 15. Numerical errors of deviation from the periodic orbit will take us far afield.

The arrangement of periodic orbits in the phase space is important, and for area preserving maps and for PSOS of $d = 2$ Hamiltonian systems it is believed that they are uniformly spread over the phase space. The periodic orbits of the baker map hold out intriguing patterns, as yet unexplored, of course to the best of the authors’ knowledge.

Exercise.

17. Prove that all the periodic orbits of the baker map are uniformly unstable with a Lyapunov exponent of $\ln(2)$.
18. Devise an algorithm to find all the periodic orbits of a given period in the baker map.

As can be seen from above the baker map has many features of chaotic systems in a completely transparent manner and helps us understand features of what is called “hard chaos”. In particular the dense set of unstable periodic orbits plays a very important role in both classical as well as semiclassical mechanics. The fact that they exponentially proliferate $P(T) \sim \exp(hT)/T$ and are uniformly spread in phase space are also of crucial import.

While there are more aspects of this map that can be usefully studied, we turn to another system which is better suited for our purposes now, the so called “cat map”. We wish to turn attention away from individual orbits to collections of orbits, or densities. The relevant classical mechanics equation will then be the Liouville equation rather than Hamiltonian equations. These two formulations, while

mathematically distinct, are of equal importance, and are complementary descriptions of the same dynamical system.

Statistical mechanics deals with collections of orbits, or ensembles, and during the early days of statistical physics, ergodicity was discussed extensively. During the momentous developments of the last century, these questions were relegated to relatively dark corners, as important models of equilibrium statistical physics, such as the Ising model, took the centerstage. There is now renewed interest in the foundations of nonequilibrium statistical physics and its relationship, if any, with dynamical chaos. For instance one issue that comes up with regularity is whether chaos can explain the lack of time-reversibility in the macroscopic world, despite the fundamental equations of motion possessing this property.

Let us recall Liouville's equation for a density in phase space. Hamiltonian flow is incompressible as the divergence of the vector field of the flow is zero. The flow velocity in phase space is $\vec{v} = (\dot{q}, \dot{p}) = (\partial H / \partial p, -\partial H / \partial q)$ and its divergence is

$$\nabla \cdot \vec{v} = \frac{\partial}{\partial q} \left(\frac{\partial H}{\partial p} \right) + \frac{\partial}{\partial p} \left(-\frac{\partial H}{\partial q} \right) = 0. \quad (1.47)$$

A phase space density $\rho(q, p, t)$ obeys from conservation of “mass” (no phase space points get created or destroyed)

$$\frac{\partial \rho}{\partial t} + \nabla \cdot (\rho \vec{v}) = 0$$

Which implies on using the vanishing divergence that

$$\frac{\partial \rho}{\partial t} + \{\rho, H\} = 0 \quad (1.48)$$

or $d\rho/dt = 0$, that is the density remains constant as we flow along with the phase space points. This is the classical Liouville equation. Note that all the content of Hamiltonian dynamics is present in the Liouville equation and that it is a **linear partial differential equation**. If we define the linear operator \mathcal{L} as $\mathcal{L}\rho = \{H, \rho\}$ get formally

$$\rho(q, p, t) = \exp(t\mathcal{L})\rho(q, p, 0). \quad (1.49)$$

The operator $\exp(t\mathcal{L})$ is the **Perron-Frobenius** operator and it is **unitary**. The analogies with quantum mechanics is obvious and we will return to this later, for now it is time we evolved some densities.

1.5.2 The cat map

The cat map was introduced by Arnold and Avez (1967) in their study of ergodicity in classical mechanics. It is also a 2D area preserving map defined on the unit square or torus. Unlike the baker map it is a smooth system, no discontinuity exists. It is linear, the nontriviality of the map arises solely from the re-injection of trajectories thanks to the periodic boundary conditions. It is given by the map:

$$\begin{aligned} q_{n+1} &= aq_n + bp_n \pmod{1} \\ p_{n+1} &= cq_n + dp_n \pmod{1} \end{aligned} \quad (1.50)$$

There are four parameters (a, b, c, d) and the map will be continuous if these are integers, in fact they are smooth dynamical systems in this case. We also assume that $ad - bc = 1$, which makes them area preserving and if $|tr| = |a + d| > 2$ then the map is also hyperbolic and completely chaotic. The

map with $(a = 2, b = c = d = 1)$ is usually referred to as the cat map, or the Arnold cat map, but we will call this generalization as the family of cat maps. The two eigenvalues of the matrix $\{(a, b), (c, d)\}$, $\lambda_{\pm} = (\text{tr} \pm \sqrt{\text{tr}^2 - 4})/2$ provide the expansion and contraction rates, and the positive Lyapunov exponent is $\ln(\lambda_+)$.

The cat map is so called, because its inventors illustrated its action on a set of points by displaying what happens to its image as the map is iterated. However since the cat should hardly be credited for the development of chaos in this world, we illustrate it with another picture instead. See Fig. (1.10).

Consider what happens to a collection of initial conditions described by the density function $\rho(q, p; 0)$. This means that $\rho(q, p; 0) dq dp$ is the fraction of initial conditions in the area $dq dp$ around (q, p) at time 0. After a time n the initial condition is at say (q_n, p_n) and the area is now $dq_n dp_n = dq dp$, due to area preservation. Thus we have that

$$\rho(q_n, p_n; n) = \rho(q, p; 0). \quad (1.51)$$

Symbolically if we write $(q_n, p_n) = f^n(q, p)$ as the time evolution we get

$$\rho(q, p; n) = \rho(f^{-n}(q, p); 0), \quad (1.52)$$

the Liouville condition of phase space incompressibility expressed in discrete language. Thus for evolving densities forward in time we need to evolve phase space points backward in time.

From the Liouville equation it is clear that if the initial density was uniform then it would remain uniform. That is the *uniform density is an invariant density or measure for all area preserving maps*. However if the map was not chaotic there exist other smooth invariant densities, and in general any initial density (that is not uniform) does not march on toward the uniform density as time goes by. Put in more technical language, in the space of densities, the uniform one is not an attractor, and there is general no attractor. However for chaotic systems it is almost as good as an attractor, and we illustrate this, not only by making use of Dubya but also by the following analysis.

The Dubya picture shows how complicated the outcome of the Liouville equation could be if the underlying dynamics f is chaotic. It appears from the picture that Dubya is uniformly spread all over the phase space. It is as if a “macroscopic” equilibrium has been reached after an initial scrambling. It is widely believed that this is the way in which thermodynamic equilibrium is reached, due to the mixing behaviour of the underlying dynamics. The evolution of densities such as Dubya’s is in general difficult to track, as indeed it is tantamount to solving the equations of motion. However for the cat map this is possible, despite the presence of hard chaos. Since any density on the torus is doubly periodic we can write:

$$\rho(q, p; 0) = \sum_{kl} a_{k_1 k_2}(0) \exp(2\pi i k^T v), \quad (1.53)$$

where we have introduced the integer vector $k \equiv (k_1, k_2)^T$ and phase space $v \equiv (q, p)^T$. Here T in the superscript stands for the transpose. We note that from normalization of the density $a_{00}(0) = 1$. For a typical smooth function ρ the Fourier coefficients $a_{k_1 k_2}(0)$ will decrease with wavenumbers sufficiently fast for the series to converge.

The solution of the cat map is: $v_n = M^n v \pmod{1}$, where M is the 2×2 matrix $\{(a, b), (c, d)\}$. Note that this is only possible because M is an *integer* matrix, otherwise the act of taking powers of M do not commute with the modulo operation: the fact that the cat is a “diffeomorphism” is important here. Thus we have from Liouville equation Eq. (1.52) that:

$$\rho(q, p; n) = \sum_{kl} a_{k_1 k_2}(0) \exp(2\pi i k^T M^{-n} v) = \sum_{kl} a_{k_1 k_2}(n) \exp(2\pi i k^T v), \quad (1.54)$$

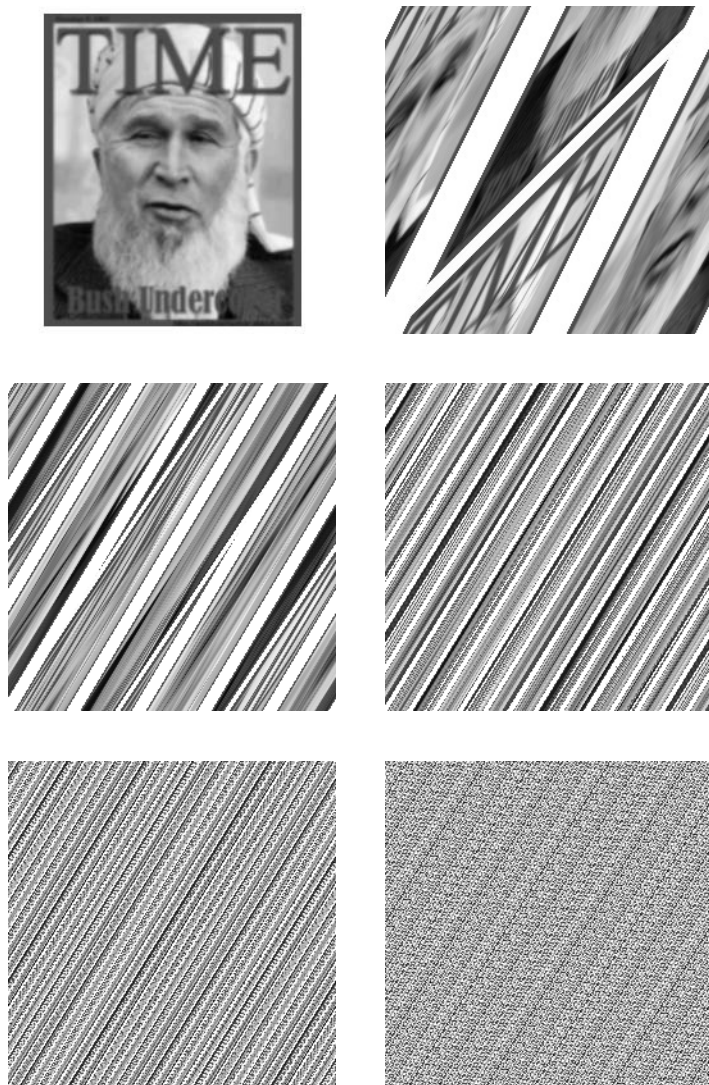


Figure 1.10: Dubya subject to the Arnold cat map for five iterations. Notice the unstable manifolds along which the pixels align, and how degeneration occurs with time. It is a peculiarity of the cat map though that there occurs a time when the initial image will exactly reappear, history will repeat endlessly. The first image appears smaller due to a white boundary, there is no loss of information in this process, the picture is merely scrambled. The original picture is taken without permission from <http://politicalhumor.about.com/>, where I highly recommend a visit to understand modern chaos in practice.

where $a_{k_1 k_2}(n) = a_{M^n k}(0)$. From the fact that M has real eigenvalues, one larger than 1, implies that $\|M^n k\|$ increases with time n for chaotic maps, for all k except $(0, 0)$. (We have assumed for simplicity that M is symmetric, this is not of course essential). That is $a_{00}(n) = a_{00}$ for all n .

What we have done is transfer the cat map dynamics to a map on the “dual” Fourier space wavenumber lattice, on which the dynamics is a simple linear hyperbolic map. Note in particular that there is no “modulo 1” in this map. Therefore the small wavenumber coefficients get rapidly destroyed, as some higher wavenumber ones get “excited”. In fact all this occurs exponentially rapidly. Thus the smooth density with predominantly small wavenumbers tends to be a highly oscillatory one, except for $a_{00} = 1$ for all time. Thus it is *not strictly true that the density will tend to the uniform density ($\rho = 1$)*, however, it does so in a *weak* sense. that is

$$\int_{\Omega} f(q, p) \rho(q, p; n) dq dp \longrightarrow \int_{\Omega} f(q, p) dq dp. \quad (1.55)$$

as $n \rightarrow \infty$, for sufficiently smooth functions of phase space $f(q, p)$.

Thus the approach to equilibrium in Hamiltonian systems proceed in somewhat subtle ways, the complex network that Poincaré talked about, the homoclinic tangle leaves its imprint on the evolving density by means of high wavenumber features that would get observationally blurred, leaving behind an appearance of a smooth uniform, “microcanonical” ensemble.

Chapter 2

Hamiltonian Chaos: Quantum Mechanics

2.1 Introduction

The founders of quantum mechanics were adepts at the classical. In many cases classical intuition guided them along, till they reluctantly were forced to give in to notions that were genuinely alien then. For instance Schrödinger was guided by the analogy between wave optics and geometric (ray) optics, and made use of the Hamilton Jacobi theory heavily. It was with great reluctance that he introduced the imaginary unit $\sqrt{-1} = i$ fundamentally into physics. When he first wrote the equation $H\psi = E\psi$ and passed this on to Lorentz, Lorentz said it couldn't be quite right as an equation with H , that is energy must have somewhere time in it. See our very first Hamiltonian equations of motion, the Hamiltonian was crucially involved in finding time derivatives. After Schrödinger went back to the drawing board, he apparently came up with $H\psi = i\hbar \partial\psi/\partial t$, and was very unhappy with it, as it involved i . After one year he resolved this by applying H twice to get the real equation $H^2\psi = -\hbar^2 \partial^2\psi/\partial t^2$. Only to realize that this cannot be right in general as the Hamiltonian can after all contain time explicitly, such as in the 1.5 DoF Hamiltonians we have been discussing. Thus it seemed that with reluctance he accepted the now famous Schrödinger equation which is our starting point.

The quantization of chaotic systems must need no motivation, considering the centrality of Hamiltonians in physics, considering the fundamental nature of quantum mechanics, and the alleged ubiquity of chaos, even in Hamiltonian systems. For instance going beyond the simplest atom, the hydrogen atom, to the Helium atom at once forces us to consider a problem in quantum chaos, as the two electrons in the field of the protons in the nucleus, is equivalent to a restricted three-body problem that is known to be chaotic. Even in the simplest of atoms, the H atom, if a sufficiently strong magnetic field was applied the electronic motion when treated classically is chaotic. If time dependent fields are applied almost anything (except the harmonic oscillator) is chaotic. All of these situations have also been realized experimentally.

The effects of quantum chaos on transport has been studied through measurements of magnetoresistance in quantum dots. These are simple generalizations of the 1D wells that we study in a first quantum mechanics course, only now they are 2D and can have different shapes. The motion of the electrons inside these is like the motion of a ball on billiard tables, and this class of billiard problems have been at the center of many classical as well as quantum studies. Experimental work on such systems has been on for more than two decades now. Recent explorations of the possibility of a quantum

computer, has also brought to the forefront issues of the effect of chaos on the functioning of many-body quantum computers. In particular the “entangling” power of quantum chaos is a current research topic. Entanglement which measure how nonseparable quantum systems are in a genuinely quantum way, is influenced by chaos in an apparently very nontrivial manner. Apart from all these “systems”, the fundamental nature of quantized chaotic systems could lie at the foundations of quantum statistical mechanics. There is also a suggestion that decoherence, which is the entanglement of a system with its environment, is strongly influenced by chaos in the system and/or environment.

More recently quantum chaos has seen a resurgence with applications in condensed matter systems and in many cold-atom experiments that probe few-body physics. There is unprecedented experimental control that keeps systems in a pure state over a long enough time in a non-stationary state, allowing probes of thermalization and chaos. So called “infinite-temperature” phase transitions, such as many-body-localization delve on a chaotic to localized transition. Furthermore there is interest from the high-energy-quantum gravity side with quantum chaos in black-holes. In fact an interesting subject of study is what has been come to be called “scrambling”, which tries to quantify how “information” gets redistributed in a many-body system, and black-holes are conjectured to be nature’s fastest scramblers. In general there is now a very active effort in understanding quantum many-body chaos, relating it to thermalization and so on. In this context, the so-called Eigenstate-Thermalization-Hypothesis (ETH) is an interesting attempt for arriving at statistical physics from deterministic dynamical systems.

The area of quantum chaos is roughly dominated by the following approaches:

1. **Phenomenology:** Numerical experiments abound and are central to our understanding, much like the classical case. This provides the basis of many theories and modelling efforts.
2. **Semiclassics:** The semiclassical theory of anything beyond 1D (no chaos!), involves nontrivial extensions of the WKB method. Gutzwiller’s **periodic orbit theory**, based on the path integral formalism and developed in the late 60’s, early 70’s and refined over the years forms an important tool in understanding quantum chaos. Another semiclassical tool that has found practical applications and helped intuitive understanding is the technique of semiclassical wavepacket propagation.
3. **Random matrix theory:** Chaos implies ergodicity, mixing, and an invariant measure classically. Thereby we can calculate averages knowing the invariant density. Quantum mechanically it has been found for about 34 years now that the methods originally devised for “complex” many body nuclei were applicable to low-dimensional chaotic systems. These methods fall under the class of problems which consider the Hamiltonian to be **random matrices** that obey the broad symmetries of the Hamiltonian of the system, such as parity, time-reversal symmetry etc.. Thus modelling using random matrix theory (RMT) has been found to be of great importance and use in quantum chaos. RMT was developed initially by Wigner, Dyson and Mehta. Today it is also a very active area of research in Mathematics and Mathematical physics, with a bewildering range of applications.
4. **Experiments:** Experiments from many fields (atomic, nuclear, mesoscopic, quantum optics, cold-atoms, Josephson-junction qubits, ...) deal with quantum chaos, due to the basic character of the investigations, after all we are only talking of the Schrödinger equation. While the earliest experiments involved multiphoton ionization of hydrogen atoms in Rydberg states subjected to microwave radiation, experiments later ranged from quantum dots to laser cooled sodium atoms in pulsed fields, and resonant tunneling across quantum wells in magnetic fields. Recent experiments using “transmon” qubits and optical lattices have dealt with chaos in few-body systems. There are

another class of experiments that are truly “electromagnetic” than quantum, in the sense that they simulate the Schrödinger equation with 2D microwave cavities (in which case the Helmholtz equation for the electric field becomes identical to the Schrödinger equation for the wavefunction of a particle freely moving inside a billiard whose shape is that of the 2D cavity.)

We may also classify the “objects” or “systems” of quantum chaos, that have been studied over the years, list is indicative and not exhaustive. The field of quantum chaos started with the independent and simultaneous publication of two papers, one on the quantized standard map by a combination of American (Joseph Ford), Italian (G. Casati) and Russian (B. Chirikov, F. M. Izrailev) efforts, while the other was on general planar 2D maps by a combination of American (N. L. Balazs), French (A. Voros) and British (M. V. Berry and M. Tabor) efforts, in 1979. Thus in fact the earliest quantized chaotic systems where quantizations of 1.5 DoF systems, and area preserving abstract maps that we have looked at classically in the previous chapter. Thus we begin the classification with these.

- 1. Quantum Maps:** These come in two flavours: (a) quantizations of 1.5 DoF systems, mostly of the “kicked” variety that we saw lead to explicit stroboscopic maps; (b) quantization of abstract dynamical systems, such as the baker map, and the cat map. Although in some cases (like the cat map) there have been mappings on to kicked systems. Almost all studies so far on this have been restricted to 2D area preserving mappings, although recent studies of 4D maps, and studies of entanglement using these exist.

Experimentally these have been studied using pulsed fields that provide a very good approximations to delta function impulses. One important phenomenon studied here is the dynamical localization of wavepackets. Experimental realizations of the baker map have been proposed and implemented using simple quantum gates. The kicked quantum top has been realized in both cold-atom and in transmon experiments.

- 2. Billiards:** Billiards are variously shaped cavities inside which particles travel freely and suffer specular reflections at the boundary. Mainly, 2D billiards have been studied. Apart from the circular, elliptical and rectangular 2D cavities, which are integrable, others studied are either chaotic or what is called “psuedo integrable”. This is an intriguing set of models with application to quantum dots, where experiments using various shaped billiards have revealed that the presence or absence of chaos has effects on conductance in ballistic dots.
- 3. Nonlinear Oscillators:** Nonlinear oscillators, again mostly two oscillators have been studied. The phenomena of localization has been found here as well. These are of great importance in the study of atoms in strong external fields. In suitable coordinates these problems can be reduced to chaotic nonlinear oscillators.
- 4. The Riemann Zeta function:** This rather odd addition to the “systems” is the tantalizing connections between number theory, analysis and chaos. The celebrated, largely unresolved, Riemann hypothesis conjectures that the (nontrivial) zeros of the zeta function lie on the $Re(z) = 1/2$ line. The zeta function obeys certain functional equations that look (almost) like the Gutzwiller semiclassical formulas, and the zeros, when treated as energy eigenvalues, are distributed according to a signature RMT distribution that is obeyed by time-reversal violating system. The millions of zeros of the zeta function have been used for statistical analysis, as if they are from a quantized chaotic system. Also the extensive theory of the zeta function has been used to gain insights into the semiclassics of quantum chaos.

A spirited hunt was on to find the Hamiltonian whose eigenvalues are the nontrivial (imaginary parts of) zeros of the zeta function, with the clues that its classical limit is chaotic and that it was not time reversal invariant, that its periodic orbits had periods that were the prime numbers and actions that were the log of the primes! The hunt is still on, although there are some developments on certain other parallel lines.

5. **Scattering systems:** We mention these separately, as we have not really talked about scattering, but chaotic scattering is quite common and has been studied mostly with the help of billiards. Experiments have been done using 2D microwave cavities.
6. **Spin Chains:** These are of rather recent origin: many body systems, such as spin chains studied in condensed matter physics. The Hubbard model, the Ising model in transverse and longitudinal fields, The Heisenberg Hamiltonian with a disordered field etc. are being explored these days. Although these systems have no classical limits, their quantum spectra resemble those whose classical limits are chaotic. For example RMT can be applied there in some ways. However the many-body nature of the systems give it an uniqueness that is not yet understood. They are now being used to study scrambling, OTOC, etc.. In fact there are some spin models (the main one being the SYK (Sachdev-Ye-Kitaev)) that are supposed to have similar (same?) physics as black-holes.
7. **Quantum Chromodynamics:** There has been some work that indicates that fundamental theories such as QCD would have connections to quantum chaos. As may be imagined, since we have not really gone much beyond 2DoF, a field theory is quite far. However again evidence from RMT statistics implies that chaos is present in QCD. This should not really come as a surprise, the very first application and motivation for RMT came from excited states of heavy nuclei.

2.1.1 But is there quantum chaos?

It is a question that is often asked, so we should address it first. Depends. If you go to a restroom having in mind a restaurant, you may not find what you looked for. Quantum and classical are separated by a singular limit and we cannot expect them to speak the same language, and they do not. Phase spaces give way to Hilbert spaces and trajectories to evolving states.

The usual objection raised is that there can be no “sensitive dependence on initial conditions”, as if we take two state $|\psi_A(0)\rangle$ and $|\psi_B(0)\rangle$, then their distance does not change with time as the evolution is unitary, that is $\langle\psi_B(t)|\psi_A(t)\rangle = \langle\psi_B(0)U^{-t}U^t|\psi_A(0)\rangle = \langle\psi_B(0)|\psi_A(0)\rangle$. Also it is pointed out that Schrödinger’s equation is linear whereas Hamiltonians is nonlinear and we know that linear-nonlinear is a “deal-breaker”. However this difference happens as we are comparing quantum states to points in phase space, whereas they are more correctly compared to distributions in phase space. In fact the phase space representation of a state, pure or mixed, is via its Wigner function which gives a distribution in phase space. The evolution of densities in phase space is via the *linear* Liouville equation. Recall that the classical densities also evolve via the *unitary* Perron-Frobenius operator, see Eq. (1.49).

2.1.2 Spectrum of Chaotic systems: Eigenfunctions

If H is a time-independent Hamiltonian, its eigenvalue equation

$$H|\psi_n\rangle = E_n|\psi_n\rangle \tag{2.1}$$

is a central one and $|\psi_n\rangle$ is the n^{th} eigenfunction and E_n the corresponding energy. Quantum eigenfunctions, being states that are time independent, are semiclassically associated with classical invariant sets. For classically chaotic systems, the only such set with full measure is the energy shell. There are smaller invariant sets, for instance there are an infinite number (dense, recall the baker map!) of periodic orbits whose measure is zero. It was not expected that these influence the eigenfunctions. This gave rise to the Berry-Voros hypothesis which said that the Wigner function, a phase space representation, of typical eigenstates will be uniformly spread on the energy shell (like the microcanonical ensemble of statistical physics). Given any state $|\psi\rangle$ its Wigner function is

$$W_\psi(\mathbf{q}, \mathbf{p}) = \frac{1}{(2\pi\hbar)^d} \int_{-\infty}^{\infty} \langle \mathbf{q} + \mathbf{X}/2 | \psi \rangle \langle \psi | \mathbf{q} - \mathbf{X}/2 \rangle \exp(i\mathbf{X} \cdot \mathbf{p}/\hbar) d\mathbf{X} \quad (2.2)$$

Berry-Voros hypothesis relates the Wigner function of an energy eigenstate (of a chaotic system) $|\psi_{E_n}\rangle$ of energy E with

$$W_E(\mathbf{q}, \mathbf{p}) = \frac{\delta(E - H(\mathbf{q}, \mathbf{p}))}{\int d\mathbf{q} d\mathbf{p} \delta(E - H(\mathbf{q}, \mathbf{p}))}. \quad (2.3)$$

The marginals of the Wigner function, obtained by integrating out either \mathbf{q} or \mathbf{p} gives the state intensity in \mathbf{p} and \mathbf{q} representations respectively. If we integrate the momentum out assuming a Hamiltonian of the standard form, this then gives the first, perhaps very grainy, picture of an chaotic eigenstate's intensity distribution in space:

$$|\psi_E(\mathbf{q})|^2 = \frac{(E - V(\mathbf{q}))^{d/2-1} \Theta(E - V(\mathbf{q}))}{\int dq (E - V(\mathbf{q}))^{d/2-1} \Theta(E - V(\mathbf{q}))} \quad (2.4)$$

This implies that on classical boundaries when $E = V(q)$, generalizations of the 1-D turning points, chaotic states tend to **vanish**. Notice how different this is from 1-DoF systems such as the Harmonic oscillator whose eigenfunction intensities are maximum at the turning points. It is also very different from eigenfunctions of higher dimensional integrable systems that tends to have caustics at the boundaries and have large eigenfunction components there. Note that for $d = 2$ -DoF, the smallest when we can have chaos, this predicts a **uniform distribution** over the available coordinate space. There is an assumption underlying these that the intensities are smoothed over with a local averaging, averaging over many oscillations or the smallest wavelengths that are locally present. Once this averaging is done, this predicts a distribution that is constant and $1/A$, where A is available area in the coordinate space for that energy.

Further implications of this model concerns the correlation function

$$C(\mathbf{X}, \mathbf{q}) = \langle \psi(\mathbf{q} + \mathbf{X}/2) \psi^*(\mathbf{q} - \mathbf{X}/2) \rangle / \langle |\psi(\mathbf{q})|^2 \rangle \quad (2.5)$$

where the average indicates a certain small averaging over space to coarse grain the state. This measure the correlations between amplitudes at \mathbf{q} and \mathbf{X} . As above, the denominator is the marginal of the Wigner function, obtained by integrating over \mathbf{p} , and the numerator is actually just the Fourier transform of the Wigner function. Thus if we assume a microcanonical Wigner function this should give us $C(\mathbf{X}, \mathbf{q})$. Thus using the result for the intensity above (upto constants?),

$$C(\mathbf{x}, \mathbf{q}) = \frac{1}{(E - V(\mathbf{q}))^{d/2-1}} \int_{-\infty}^{\infty} e^{-i\mathbf{x} \cdot \mathbf{p}} \delta \left(E - V(\mathbf{q}) - \frac{1}{2} \mathbf{p}^2 \right) d\mathbf{p} \quad (2.6)$$

Now let the angle between \mathbf{x} and \mathbf{p} be θ , then the volume element is proportional to $p^{d-1} \sin^{d-2} \theta dp d\theta$, and we get

$$C(\mathbf{x}, \mathbf{q}) = \frac{1}{(E - V(\mathbf{q}))^{d/2-1}} \int_0^\infty dp \int_0^\pi d\theta e^{-ixp \cos \theta} \delta \left(E - V(\mathbf{q}) - \frac{1}{2m} p^2 \right) p^{d-1} \sin^{d-2} \theta. \quad (2.7)$$

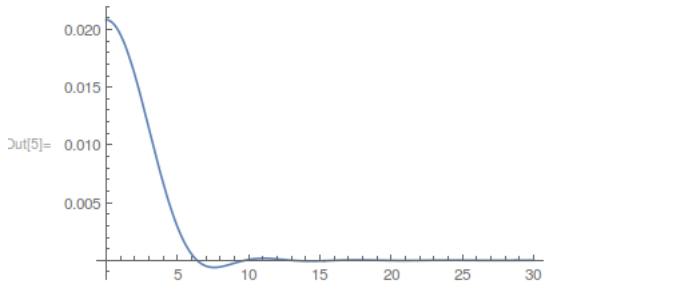
The integral over p can be done easily enough (perhaps again up to constant factors), and we get

$$C(\mathbf{x}, \mathbf{q}) = \int_0^\pi e^{-ix\sqrt{2m(E-V(\mathbf{q}))} \cos \theta} \sin^{d-2} \theta d\theta. \quad (2.8)$$

Finally this is evaluated in terms of Bessel J functions:

$$C(\mathbf{x}, \mathbf{q}) = \Gamma(d/2) \frac{J_{d/2-1}(xp/\hbar)}{(xp/\hbar)^{d/2-1}}, \quad p = \sqrt{2m(E - V(\mathbf{q}))}. \quad (2.9)$$

```
In[5]:= Plot[BesselJ[3, x] / x^3, {x, 0, 30}, PlotRange -> All]
```



Properties of the Bessel function ensure that this is small if $x \gg \hbar/p$ (see figure), thus for separations larger than about a “de Broglie” wavelength the chaotic wavefunctions have practically no correlations. Also the correlations are isotropic, both of these are not the case for regular wavefunctions. This argument based on the Berry-Voros hypothesis indicates that eigenfunctions of chaos are like **random functions** and was the first prelude to the applications of random matrix theory to these systems. Thus the eigenfunctions were thought of as “random waves”, and then many numerical computations were done in the 80’s, which supported to some extent this picture but also threw up very significant surprises.

2.1.3 Billiards

Historically, 2D billiard eigenfunctions were computed first. Originally by McDonald and Kaufman in 1979 and later by Heller in 1984. The first study pointed out the complex nodal patterns—where the wavefunction vanishes on curves, while the second pointed out that while many eigenfunctions appeared ergodic in the sense of being spread out, there was also plenty of prominent structures.

We now reproduce some of the results of McDonald and Kaufman from a later work in 1988 (Phys. Rev. A, Vol. 37, pg 3067), which deals with testing some of the conclusions from above.

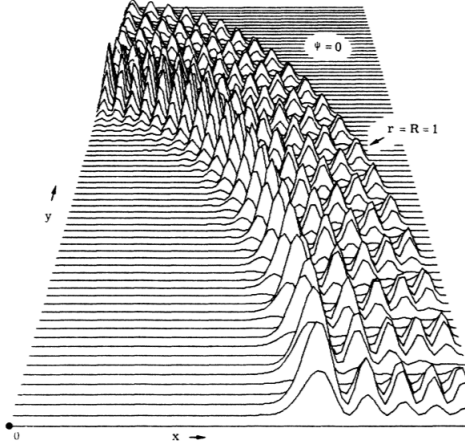


FIG. 4. Intensity distribution $|\psi_{m,n}|^2(x,y)$ in positive quadrant ($x,y > 0$) of the ($\gamma=0$) circle. This mode is $\psi_{m,n} = \psi_{40,5} = J_{40}(k_{40,5}r)\sin 40\theta$ with eigenvalue $l_{40,5} = 65.012$.

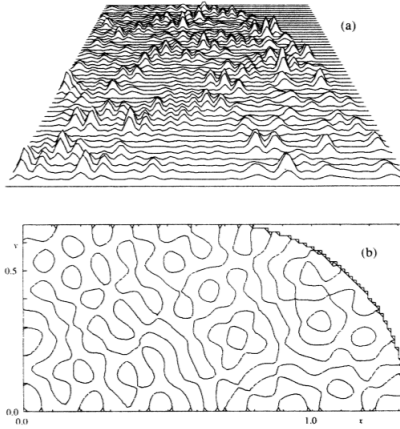


FIG. 6. Typical eigenfunction structure for $\gamma=1$ stadium, again plotted in the positive quadrant (this eigenvalue is $k = 65.326$). (a) Perspective of intensity distribution. (b) Nodal curves.

Shown are the cases of the integrable billiard and the chaotic stadium billiard. The structure of the eigenfunctions are indeed very different, although it is not clear that it is “uniformly distributed” in the stadium case. However the nodal patterns look “complicated” and have since been related to percolation problem. It maybe said that nodal patterns are ill-understood even for integrable systems (compared with the well known zeros of 1-D wavefunctions). For an absorbing recent review see “Nodal portraits of quantum billiards: Domains, lines, and statistics” Sudhir Ranjan Jain and Rhine Samajdar

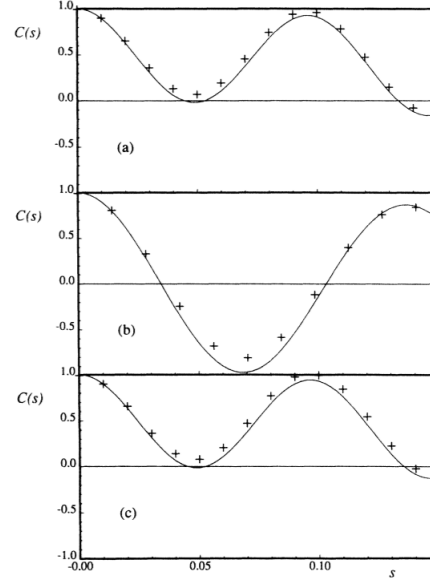


FIG. 5. Locally averaged spatial correlation function $C(x,s)$ for the circular ($\gamma=0$) mode of Fig. 4. The point x is fixed at $(r,\theta)=(0.866, 0.867)$ and the correlation is plotted as a function of $|s|$ for three angles ϕ of s relative to the x axis. Crosses denote numerical measurements, solid line is theory based on the real part of Eq. (19). (a) $\phi=0$. (b) $\phi=\pi/4$. (c) $\phi=\pi/2$.

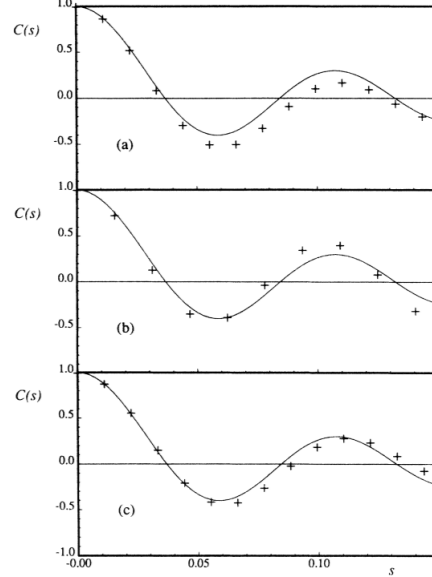


FIG. 7. Locally averaged spatial correlation function for $\gamma=1$ stadium mode of Fig. 6. The reference point x is fixed at $(x,y)=(0.76, 0.46)$ and $C(x,s)$ is plotted against $|s|$ for three angles ϕ of s relative to the x axis. Crosses denote numerical measurements, solid curve is theory based on Eq. (21). (a) $\phi=0$. (b) $\phi=\pi/4$. (c) $\phi=\pi/2$.

Rev. Mod. Phys. 89, 045005 (2017). The spatial correlation functions bear out the analysis pretty well. In the integrable case they are large and anisotropic, while in the chaotic stadium case, they follow the $J_0(kx)$ function oscillation as predicted by Eq. (2.9), where k is the wavenumber that is determined by the energy eigenvalue only in the case of billiards.

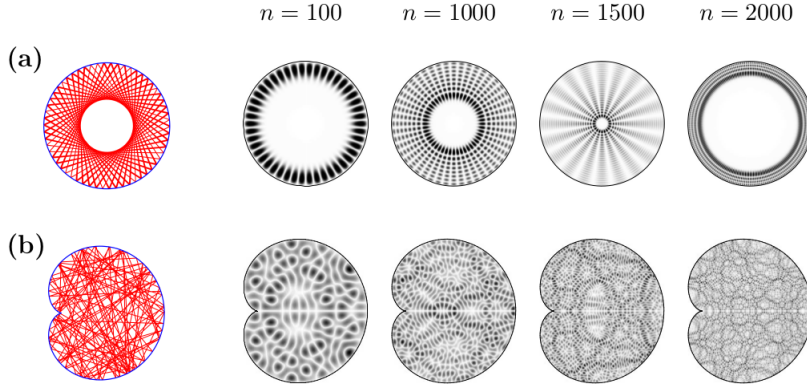


Figure 2: The eigenstates of (a) the integrable circular billiard and (b) the chaotic cardioid billiard reflect the structure of the corresponding classical dynamics. Shown is a density plot of $|\psi_n(\mathbf{q})|^2$ where black corresponds to high probability.

Further numerical results for billiards were obtained and see above for a few more characters now for the chaotic billiard (from Arnd Backer, Habilitation thesis 2007). These do seem to indicate that highly excited states may equidistribute after suitable averaging. Berry also introduced a “random wave model” to better understand these states and maybe considered a precursor to applications of random matrix theory. The idea is that in a chaotic billiard at any given point there are trajectories with all possible directions (as opposed to say the integrable central force problem, wherein they can have only 2). If we associate a wave with the trajectory, then the wavefunction in a billiard is a superposition of many plane waves. Thus consider the Random wave model wavefunction to be,

$$\psi_{RW}(x, y) = \sqrt{\frac{2}{AN}} \sum_{n=1}^N a_n \cos(k_x x + k_y y + \phi_n) \quad (2.10)$$

where a_n are randomly drawn amplitudes from a normal distribution $\mathcal{N}(0, 1)$ of 0 mean and unit variance, and $k_{x,y}$ are the wavenumbers such that their direction is uniformly random while their magnitude is fixed as $k_x^2 + k_y^2 = E$. The phases ϕ_n are uniform in $[0, 2\pi]$. The normalization constant is determined from large N limit and A is the area (or volume) of the allowed region, say the area of the billiard.

2.1.4 Scars of the classical

However numerical investigation of the eigenfunctions of the chaotic stadium billiard by Eric Heller in 1984 showed that many of the eigenfunctions were “decorated” with strong enhancements in intensity that could be unambiguously identified with classical periodic orbits. Since this is a chaotic system, these **orbits are isolated and unstable**. Heller called these “scars” of periodic orbits in quantum wavefunctions.

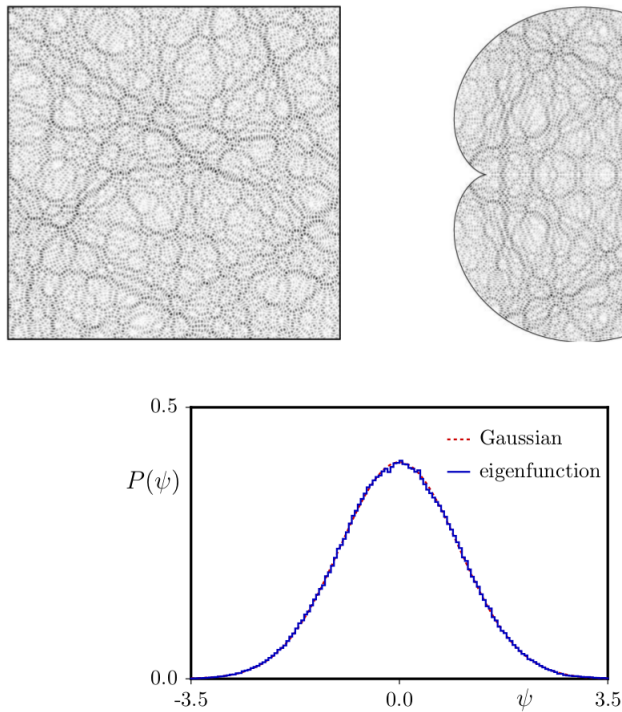


Figure 2.1: Top: left: from the random wave model, right: an excited state of the cardioid with the same energy. Below is the amplitude distribution that fits well with a zero centered normal distribution whose variance is $1/A$, where A is the billiard area (figure from AB habilitation).

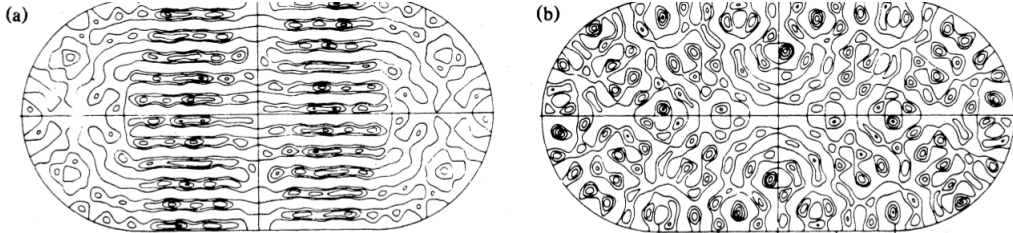


FIG. 1. (a) Localized and (b) chaotic states of the stadium potential; only the negative contours are shown. From Ref. 15, with permission.

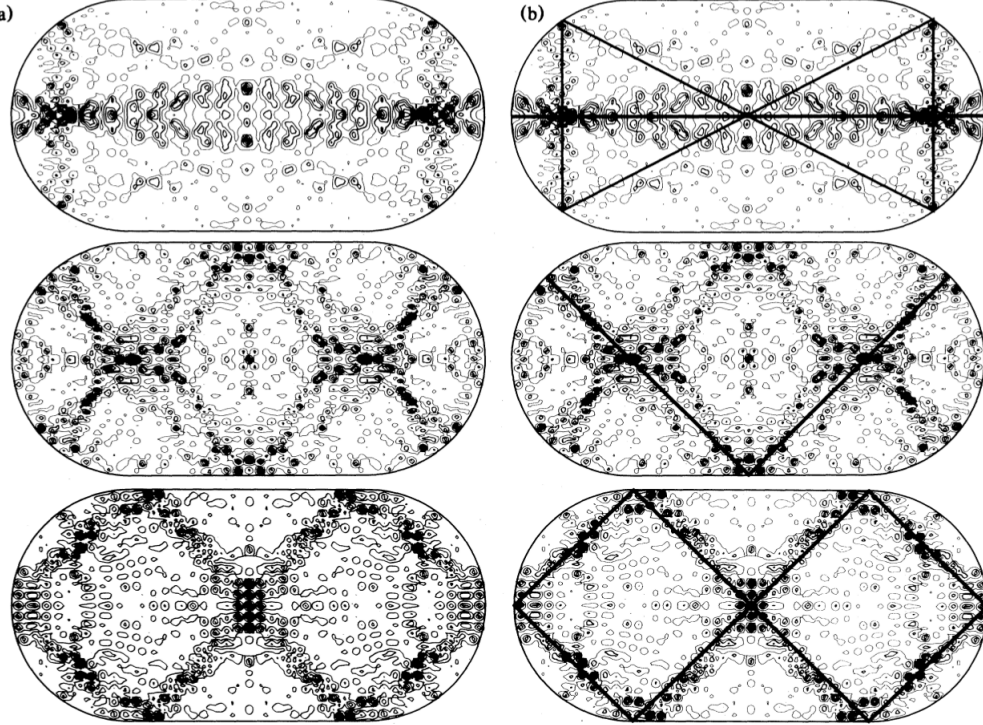


FIG. 2. Left column, three scarred states of the stadium; right column, the isolated, unstable periodic orbits corresponding to the scars.

Since these investigations many many examples have been found. Heller has put forward certain explanations for this phenomena based on wavepacket dynamics, while Bogomolny and Berry have advanced semiclassical theories based on Gutzwiller's periodic orbit theory. Today we know that apart from periodic orbits there are also scars of homoclinic and heteroclinic orbits. However our understanding is far from complete, in the sense that we cannot say which eigenfunction will be influenced by which classical orbits. Heller gave a criteria that restricts those periodic orbits that could scar the wavefunctions, which effectively cuts off long periodic orbits. Almost all scarring studies have been done with 2DoF systems or quantum maps. Experimental evidence exists from resonant tunneling experiments and microwave cavity billiards. Recent studies have started exploring scars and weak ergodicity breaking in many-body systems ("Weak ergodicity breaking from quantum many-body scars" C. J. Turner et. al., Nature Physics (2018))

2.1.5 Nonlinear oscillators

For the coupled quartic oscillator Hamiltonian (see Fig. (1.3.2) and Eq. (1.36))

$$H = p_x^2 + p_y^2 + x^4 + y^4 + \alpha x^2 y^2$$

similar studies with spectra have long been done, there are important differences between these and billiards, however all the phenomena, including scarring have been observed.

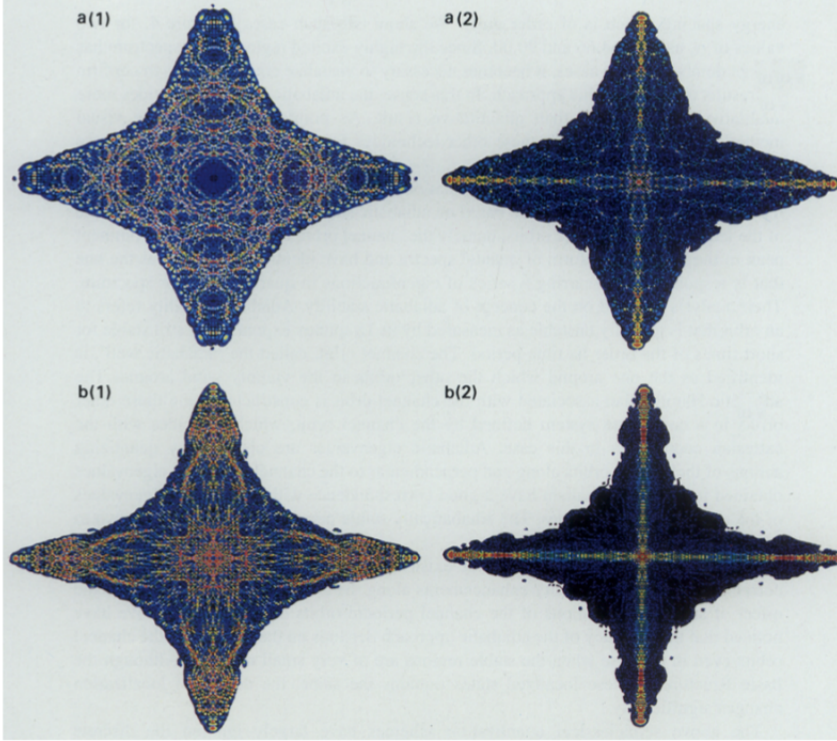


Figure 4. The configuration space intensities for two consecutive states for (a) $\alpha = 64.66$, states 1376 and 1377 with energies 2770.2953 and 2770.5087 respectively. (b) $\alpha = 90.00$, states 1857 and 1858 with energies 3642.9626 and 3643.0294 respectively. The colour code for all images is such that red is the maximum, blue is low and black is zero.

Shown are two consecutive quantum states for two different values of α (source: "Chaos and localization in coupled quartic oscillators" M S Santhanam et. al., Pramana 1997 special issue on nonlinearity and chaos). While one of them resembles the chaotic billiard states, the other is strongly localized by an orbit that could be unstable (top right) or stable (bottom right), which affects the extent of localization. Shown in Fig. (2.1.5) is the **entanglement entropy** for the first 1000 states and we see that there is large entanglement for chaotic states and much smaller for the localized or regular ones. It is well-appreciated now that although quantum entanglement is uniquely quantum it is very much affected by the classical stability and the presence of chaos. For pure two-party states it is quite clear why chaos enhances the entanglement. Experiments, again with cold atoms have demonstrated this as well.

2.2 Quantum Maps: Generalities

Historically, quantum maps were studied even earlier (in 1978/79) than billiards or anharmonic oscillators. The reason is the same as classical maps were useful it is/was expected that quantum ones will be very simple and perhaps even soluble. They certainly do provide a more easier numerical approach and are often just in a finite dimensional Hilbert space. As Floquet systems, they have also been experimentally realized for a while now.

Quantum maps are quantizations of classical maps. Classical 2D area preserving maps are *symplectic*

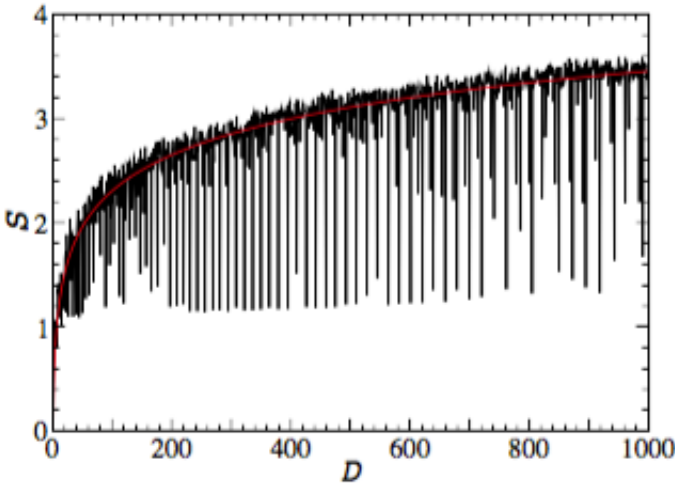


Figure 2.2: Quantum entanglement (von Neumann entropy of the reduced states of 1 oscillator) for the first 1000 states of the two coupled quartic oscillator system. The highly localized states that appear systematically across the spectrum have much smaller entanglement than the typical chaotic states that have a logarithmic growth. (From Santhanam, Sheorey, AL, Phys. Rev. E., 2008).

or what is more commonly called *canonical* transformations. Thus quantum maps may be thought of as the quantum equivalents of canonical transformations. The task is, given a canonical quantization, to find its quantum equivalent. The quantum equivalent is an unitary operator, and it is not immediately clear whether this is possible. For the class of maps derived from kicked Hamiltonians we can derive the quantum map quite easily as will be shown below.

We will first deal with the broad class of canonical transformations (maps) that comes from kicked systems. Consider the Hamiltonian:

$$H = H_0 + V \sum_{n=-\infty}^{\infty} \delta(t/T - n). \quad (2.11)$$

H_0 and V are time independent operators. There is no need to assume anything about the number of DoF. The Schrödinger equation we want to solve is

$$i\hbar \frac{\partial}{\partial t} |\psi\rangle = H_0 |\psi\rangle + V \delta_T(t) |\psi\rangle; \quad (2.12)$$

given an initial state $|\psi(0)\rangle$, we wish to solve for $|\psi(t)\rangle$. Recall that $\delta_T(t)$ is an abbreviation for the train of delta impulses. Recall that the classical map related phase space variables just after consecutive kicks, see Eq. (1.27). Therefore we may consider the quantum map to be that operator, say U , that connects states just after consecutive kicks. Due to the periodicity of the perturbation, this is independent of the kick number itself, and from elementary quantum mechanics this is an unitary operator. Thus if we write the state just after kick n as $|\psi(n^+)\rangle$ we are seeking that U such that

$$U |\psi(n^+)\rangle = |\psi(n+1^+)\rangle. \quad (2.13)$$

From just after kick n to just before kick $n+1$, the delta function term is effectively absent in Eq. (2.12). Thus we have:

$$|\psi(n+1^-)\rangle = \exp(-iH_0T/\hbar) |\psi(n^+)\rangle. \quad (2.14)$$

Now we have to deal with integration over a kick, during which time the wavefunction changes abruptly. Integrating the Schrödinger equation over the infinitesimal time about the kick, eliminates the H_0 part of the Hamiltonian, or alternatively we could say that the kick dominates the Hamiltonian during this time. Therefore consider the general equation:

$$i\hbar \frac{\partial}{\partial t} |\psi\rangle = V g(t) |\psi\rangle, \quad (2.15)$$

where $g(t)$ is any function of time t . It is easy to verify that it is solved by

$$|\psi(t')\rangle = \exp\left(-\frac{iV}{\hbar} \int_t^{t'} g(t) dt\right) |\psi(t)\rangle, \quad (2.16)$$

this effectively being a (dynamic) rescaling of time. In our case $g(t) = \delta_T(t)$ and we get using $t' = n + 1^+$, $t = n + 1^-$,

$$|\psi(n+1^+)\rangle = \exp(-iVT/\hbar) |\psi(n+1^-)\rangle. \quad (2.17)$$

Combining this with Eq. (2.14) we get:

$$|\psi(n+1)\rangle = \exp(-iVT/\hbar) \exp(-iH_0T/\hbar) |\psi(n)\rangle, \quad (2.18)$$

where we have dropped all the + superscripts, all the states are now understood to be immediately after the stated times. Thus we have the quantum map to be the unitary operator:

$$U = \exp(-iVT/\hbar) \exp(-iH_0T/\hbar) \quad (2.19)$$

This is the quantization of the classical map in Eq. (1.27).

2.2.1 Comments

The form of the unitary operator, or quantum map, is as a product of two unitary operators, the first one is the “free” evolution corresponding to the Hamiltonian H_0 , while the other is the kick. If $[H_0, V] = 0$, that is these two operators commute then the evolution operator is simply $\exp(-i(H_0 + V)T/\hbar)$, equivalent to a continuous flow. The most interesting, and general case is when this does not happen. If the system has 1DoF (so that the whole Hamiltonian has 1.5 DoF), then this can mean the difference between order and chaos. Without the kicks the 1D Hamiltonian is simply $H_0 + V$, there is no classical chaos, the unitary operator over a time T is also $\exp(-i(H_0 + V)T/\hbar)$. Thus for 1D quantum systems the difference between e^{A+B} and $e^A e^B$ could spell the difference between order and chaos.

It must be noted that but for the impulsive time dependence we would be hard put to write explicitly the quantum map. For general time dependences, fully numerical integration has to be resorted to to write the corresponding quantum map or the Floquet operator. Since the Hamiltonian is time dependent the usual description of stationary states and energy eigenvalues does not exist. However the quantum map, is stationary in the sense that it does not depend on the kick number, and is a special case of the Floquet operator for general time dependence.

Iterating the classical map is equivalently done in quantum maps as repeated multiplication by the operator U , thus:

$$|\psi(n)\rangle = U^n |\psi(0)\rangle. \quad (2.20)$$

The powers of an operator is essentially determined by its eigenvalues and vectors and hence the problem of time evolution is an eigenvalue problem. The eigenangles of U take the role of the energies and the

eigenvectors of U are the “stationary” states. Since U is an unitary operator its eigenvalues lie on the unit circle, the eigenvalue equation may be written as:

$$U|\phi_k\rangle = \exp(i\phi_k)|\phi_k\rangle. \quad (2.21)$$

where $0 \leq \phi_k < 2\pi$ are real numbers, the eigenangles, and also referred to as the “quasi-energies”. The index k may be discrete, or continuous, as the eigenangles are discrete or continuous. In fact the nature of the spectrum of operators such as U even for 1D systems is notoriously difficult to predict, it may also be of a singular continuous kind, where the spectrum is a Cantor set, a fractal. These different kinds of spectra impact crucially properties of quantum transport. Note that

$$|\psi(n)\rangle = U^n |\psi(0)\rangle = \sum_k \exp(i\phi_k n) |\phi_k\rangle \langle \phi_k| \psi(0)\rangle. \quad (2.22)$$

From the reality of the eigenangles it follows that quantum evolution is quasi-periodic, especially if the spectrum is discrete. If the spectrum is continuous this need not be the case.

We now quantize the maps that were displayed in the classical section 1.3.1.

2.2.2 Quantum maps on the plane and cylinder

Quantum Linear Map

The quantum map corresponding to the classical map in Eq. (1.29) is

$$U = \exp\left(-\frac{iT}{\hbar}\omega^2 q^2\right) \exp\left(-\frac{iT}{2\hbar} p^2\right), \quad (2.23)$$

where of course p and q are operators satisfying the Heisenberg commutation relation: $[q, p] = i\hbar$. The quantum linear map is completely solvable, just like the classical linear map. This can be seen from the fact that an application of the Campbell-Baker-Hausdorff (CBH) theorem will reduce the product of the two exponentials to a single exponential with an effective quadratic Hamiltonian. Therefore for cases where the classical map is filled with elliptic orbits, the quantum spectrum is identical to the Harmonic oscillators, the eigenangles are equispaced in the case the corresponding classical map is stable. If the classical map is unstable, there is a continuous spectrum in the quantum case and the eigenfunctions are parabolic-cylinder functions.

Quantum Standard Map

The quantum map corresponding to the classical map in Eq. (1.30) is

$$U = \exp\left(\frac{igT}{(2\pi)^2 \hbar} \cos(2\pi q)\right) \exp\left(-\frac{iT}{2\hbar} p^2\right). \quad (2.24)$$

While the classical map was shown to depend on only one (scaled) parameter, $K = T g$, in the case of the quantum map we see that there are *two* effective parameters: gT/\hbar and T/\hbar . Thus \hbar enters in a crucial manner, and a scaled Planck constant determines many behaviours of the standard map. We will return to the standard map shortly, but note that we have not taken into account any modulo operation so far. As it exists the above would be the quantization of the standard map on the entire plane. The nature of the spectrum of the above operator (whether discrete, continuous, singular) has been the topic of much

research and there has been a mapping of this map to an tight-binding model of condensed matter physics. It has been at the center of many quantum chaos studies including atom-optics experiments.

Quantum Harper Map

It immediately follows from the above that a quantization of the Harper map without the modulo conditions is

$$U = \exp\left(-\frac{igT}{(2\pi\hbar)} \cos(2\pi q)\right) \exp\left(-\frac{iT}{2\pi\hbar} \cos(2\pi p)\right). \quad (2.25)$$

2.2.3 Standard map on the cylinder

While both the standard and Harper maps were easy to study classically, at least in terms of their phase space trajectories, the quantum maps pose severe problems, they are infinite dimensional and there is no guarantee that the spectrum is discrete. The classical maps lived on cylinders and tori and thereby simplified matters considerably. For instance the kicked pendulum configuration space is the circle S^1 and not the line. Therefore we could quantize these maps on cylinders and tori. Cylindrical phase spaces we are more familiar with. There is an angle $0 \leq q < 1$, and an angular momentum $-\infty < p < \infty$ pair, If $|q\rangle$ are angle kets, the angular momentum kets are $|m\rangle$ such that $p|m\rangle = mh$

$$|m\rangle = \int_0^{2\pi} e^{2\pi imq} |q\rangle dq; m = 0, \pm 1, \pm 2 \dots, \quad (2.26)$$

the transformation function between momentum and angle is:

$$\langle q|m\rangle = e^{2\pi imq}. \quad (2.27)$$

Thus the standard map on the cylinder in the momentum (the word angular is dropped) is given by the **infinite dimensional matrix**

$$U_{mm'} = \langle m | \exp\left(\frac{igT}{(2\pi)^2\hbar} \cos(2\pi q)\right) \exp\left(-\frac{iT}{2\hbar} p^2\right) | m' \rangle. \quad (2.28)$$

Inserting complete $|q\rangle$ states, we get

$$e^{-i4\pi^2 T m'^2 \hbar^2 / (2\hbar)} \frac{1}{2\pi} \int_0^{2\pi} e^{igT \cos(\theta) / (4\pi^2)} e^{2\pi i \theta (m' - m)} d\theta. \quad (2.29)$$

We have made the substitution $2\pi q = \theta$ and used the eigenvalues of the momentum operator $(2\pi m\hbar)$. Using the standard definition of the Bessel (J) function:

$$J_n(z) = \frac{1}{2\pi} \int_0^{2\pi} \exp(-i(n\theta - z \sin(\theta))) d\theta,$$

and the standard property of integer order Bessel functions: $J_{-n}(z) = (-1)^n J_n(z)$ we get:

$$U_{mm'} = (-i)^{m'-m} J_{m'-m}(gT/4\pi^2\hbar) \exp(-i2\pi^2 T m'^2 \hbar), \quad (2.30)$$

$$= (-i)^{m'-m} J_{m'-m}(K/\tau\hbar) \exp(-i\tau m'^2 \hbar/2). \quad (2.31)$$

Here we have reintroduced the *classical* effective parameter $K = gT^2$ (see the classical map), and introduced $\tau = 4\pi^2 T$ to show that there is effectively one more parameter.

Note that we have already chosen our units so that the moment of inertia, I , of the rotator is unity, and the units of \hbar are of I/τ , which may be considered a characteristic action in the system. Therefore one may define an effective scaled dimensionless Planck constant as $\hbar\tau/I = \hbar\tau$, as $I = 1$, which measures roughly “how many classical actions are there in an \hbar ”. Thus the classical limit is the limit $\hbar\tau \rightarrow 0$. Since always the scaled Planck constant appears in the combination $\hbar\tau$, we may set $\tau = 1$ and loosely talk of $\hbar \rightarrow 0$. Often one is bewildered how fundamental constants are blithely treated as variables and limits are taken, it is always implied in these cases that some scaled constant is involved. This can always be done as long as the fundamental constant is *not dimensionless*.

This matrix U is the quantum standard map on the cylinder. All the complications of the classical standard map, from the KAM theorem, the Poincaré Birkhoff theorem, to the homoclinic tangle and hard chaos, all illustrated in Fig. (1.5), must appear as $\hbar \rightarrow 0$ from this matrix, and must be in some quantized avatar otherwise. One of the first, and enduring, questions, of quantum chaos, was exactly how this happens. As M. V. Berry points out, there are two questions that are often conflated here: (a) How does the classical limit emerge from the quantum. The answer, if complicated, is already known in the sense that the classical limit is known. (b) Do any new phenomena occur in the semiclassical regime, something that is not classical, that perhaps survives from the quantum regime? Can this even survive the classical limit? As Berry again points out, this question would be nonsensical as long as the limit were not *singular*. The classical-quantum limit is completely different from say the relativistic-nonrelativistic limit in the sense that we cannot set $\hbar = 0$ and get the classical limit (as we may set $c = \infty$ and get the nonrelativistic limit).

The structure of the unitary operator U is that of a *banded matrix*. This follows from $|U_{mm'}| = |J_{m-m'}(K/\tau\hbar)|$. From properties of the Bessel function we know that $J_n(z)$ decays exponentially for $n > z$, thus the effective (half) band width of U is $K/\tau\hbar$. We see from this that in the classical limit the matrix tends to become full, so also in the large classical chaos limit when K is large. A full matrix has much more complicated spectra, at least potentially, than a banded one.

One of the first questions asked of the quantum standard map, is whether it allows unlimited diffusion of the momentum of the pendulum. We know (see also “problem” in classical standard map section) that classically $\langle p^2(t) \rangle = D t$, the kinetic energy, ensemble averaged over an initial conditions ensemble, increases linearly. Quantum mechanically an initial ensemble is already provided by a state, say take $|m = 0\rangle$ state, which is one of angular momentum zero. It is uniformly spread in the q space, and therefore we can think of this as the quantum equivalent of an ensemble of initial conditions with $p = 0$ and uniform spread in angle. Therefore we evaluate:

$$|\psi(t)\rangle = U^t |0\rangle; \langle p^2(t) \rangle = \langle 0 | U^{-t} p^2 U^t | 0 \rangle = 4\pi^2 \hbar^2 \sum_m m^2 |\langle 0 | U^t | m \rangle|^2, \quad (2.32)$$

where in the last equality we have inserted momentum states. Shown in Fig. (2.3) is a doodle of the quantum-classical cases. Note that this is an “easy” computation these days with powerful computers, however we have to truncate the infinite dimensional matrix somewhere, and this determines the time t till which our numerical calculation can be done. This is checked by ensuring that the norm of the vector $|\psi(t)\rangle$ is reasonably close to 1. A truncation leads to nonunitary matrices. The truncation becomes effective only if the matrix is banded and therefore from the above we see the difficulty posed by both the large chaos, and the semiclassical regimes.

The kinetic energy (actually twice the kinetic energy is shown in figure) of the quantum pendulum (or rotator) increases nearly linearly along with the classical till a time t^* , after which it deviates, falls short and starts to oscillate. Whether this will continue to be bounded or will increase depends on the nature of the quantum spectrum and there are very few rigorous results on this. It is believed from

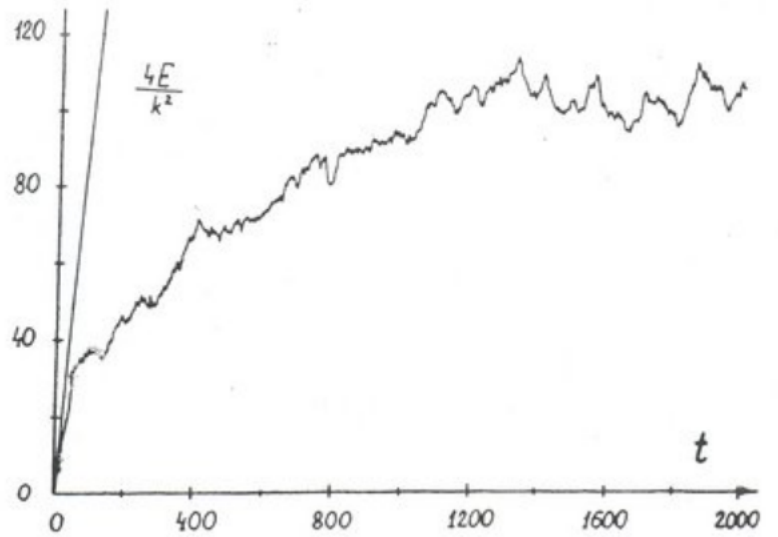


Figure 4: Dependence of rescaled rotator energy $E/(k^2/4)$ on time t for $K = kT = 5, \hbar = 0.25 (k = 20, T = 0.25)$; the full curve shows numerical data and the straight line gives the diffusive energy growth in the classical case (from [23]).

Figure 2.3: Classical vs Quantum diffusion, borrowed from Scholarpedia which borrows from original article in 1979, by Casati, Ford, Izrailev and Chirikov.

many numerical investigations that the energy does not indefinitely increase. The fact that the energy of the rotator is bounded implies that all the eigenstates of the quantum map are *localized* in momentum space. This among things gave rise to the understanding that quantum mechanics somehow smoothens classical chaos, and makes it less random.

While dynamical localization is a quantum effect there is another peculiar feature known as **quantum resonances**. From the operator in Eq. (2.30), we notice that if the scaled Planck constant $\tau\hbar = 4\pi$ the kinetic energy term goes to an identity and this implies that $\langle p^2(t) \rangle \sim t^2$, the energy grows **ballistically**, much faster than the classical. It has been shown that this is true for $\tau\hbar$ being any rational multiple of 4π and has also been seen in cold-atom experiments. To show that it grows ballistically, note that only the potential term is effective and therefore it is straightforward to solve in the position basis:

$$\psi(q, t) = \psi(q, 0) \exp\left(-i\frac{Kt}{\tau} \cos(2\pi q)\right). \quad (2.33)$$

If we start from the $m = 0$ eigenstate, $\psi(q, 0) = 1$, a constant and it is easy to see that

$$\langle p^2(t) \rangle = - \int_0^1 \psi^*(q, t) \frac{\partial^2}{\partial q^2} \psi(q, t) \sim t^2. \quad (2.34)$$

Thus quantum localization is observed when $\tau\hbar$ is irrational, the typical case.

Exercises

1. Establish that U is indeed an unitary matrix.

2. Write a program in your favourite language to calculate the matrix elements of U .
3. Find the powers of U by repeated multiplication and for the initial state $|m = 0\rangle$ find how the expectation value of the kinetic energy behaves in time. Note that one does not have to store the matrix elements if the elements are easy to find each time. Keep track of the normalization to see that it is not tending to 0. Suggested parameters are $\hbar\tau = 1$, $K = 5$, $N = 1000$, where N is the matrix dimension to which U is truncated. Note that for these parameters the band width is 5. if we go to a smaller $\hbar\tau$ like 0.01, the half width will be 500 and $N = 1000$ would be too small. Try it!

The time t^* at which quantum-classical correspondence breaks down is an important time scale in much of quantum chaos. The general understanding is that it is at this time that the discreteness of the quantum spectrum is starting to be felt. However in the quantum standard map (also called kicked rotor etc.) the time is a “diffusive time scale” and longer than the corresponding Ehrenfest time. There are more time scales in quantum chaos and a detailed study of these is quite involved and even incomplete. We do not attempt that here. It may be mentioned finally that such quantum localization of classical chaos was found experimentally by pulsing cold sodium atoms and the break time agreed well with theoretical predictions. Localization and delocalization remains a topic of research. One way the localization can be understood is by mapping the eigenvalue problem to a tight-binding model and show that the onsite potential is psuedo-random and invoke Anderson localization. The connections between transport properties in such disordered systems, and “simple” chaotic systems is intriguing and has been studied to some extent.

2.2.4 Quantum maps on the torus

The quantum standard map on the cylinder is a scattering system, in the sense that unlimited diffusion in momentum can take place. If we want to study 2D Hamiltonian systems, the PSOS at any given energy in bound systems is finite, such as that shown in Fig. (1.3.2), and therefore if we wish to study the effects of chaos, without the complication of scattering we have to study area preserving maps on compact phase spaces, such as tori. Indeed the two modulo conditions, on both q and p are possible for the standard map, the Harper map and is the natural phase space of the the baker and cat maps. Thus quantum maps on tori have been studied fruitfully as models of quantum 2 DoF nonintegrable Hamiltonian systems. However as the kinematics (states) on the torus may not be well-known we first discuss this.

Quantum kinematics on the torus

Consider the unit $q-p$ torus $[0, 1] \times [0, 1]$ as the classical phase space. Since the restriction of both q and p to be angle like variables leads to finite quantum mechanics that is not often treated in standard books, we will develop this to the extent possible here. Imposing periodic boundary conditions on both position and momentum, results in a state space of finite dimensions. Let the position and momentum eigenstates be $|q_n\rangle$, and $|p_n\rangle$, $n = 0, 1, \dots, N - 1$, where N is the dimensionality of the Hilbert space. Assume that these form orthonormal basis sets. Recall from continuum quantum mechanics that $\exp(-i\hat{p}a/\hbar)$ is the position translation operator in the sense that $\exp(-i\hat{p}a/\hbar)|q\rangle = |q + a\rangle$, while $\exp(i\hat{q}b/\hbar)$ is the momentum translation (or boost) operator. Here a and b are arbitrary real numbers. Since there are only N discrete states, it is finite translation operators that take on special significance for finite quantum mechanics. Strictly speaking we should deal with unitary operators rather than the generating

Hermitian ones, as there are no infinitesimal translations of a finite number of states. Therefore rather than deal with position and momentum operators we deal with position and momentum *translation* operators.

The position translation operator, denoted by T_q , is such that

$$\langle q_n | T_q = \langle q_{n+1}|, \text{ and } \langle q_n | T_q^N = \langle q_{n+N} | = \exp(2\pi i \beta) \langle q_n |. \quad (2.35)$$

Here $0 \leq \beta < 1$, is the phase accumulated as one goes along the q direction. For periodic boundary conditions $\beta = 0$, for anti-periodic, it is $\beta = 1/2$. Phases such as these are very useful in controlling quantum symmetries. The physical interpretation of this phase is possible as a magnetic flux line threading the particles circular configuration space. The phase then appears as the Aharonov-Bohm phase and is useful in controlling time-reversal symmetry. The translation operator in momentum, T_p , is similarly defined.

$$T_p |p_n\rangle = |p_{n+1}\rangle, \text{ and } T_p^N |p_n\rangle = |p_{n+N}\rangle = \exp(2\pi i \alpha) |p_n\rangle. \quad (2.36)$$

Here $0 \leq \alpha < 1$, similarly controls parity symmetry. We find the relationship between the two basis, the position and momentum, by requiring that the momentum states be eigenstates of the position translation operator and vice-versa; just as in usual quantum mechanics.

Exercises.

4. Using the above definitions, prove that the translation operators T_p and T_q are indeed unitary. Write down the T_p operator in momentum basis and the T_q operator in position basis for $N = 4$.
5. Show by direct verification that

$$|p_m\rangle \equiv \frac{1}{\sqrt{N}} \sum_{n=0}^{N-1} \exp\left(\frac{2\pi i}{N}(n+\alpha)(m+\beta)\right) |q_n\rangle \quad (2.37)$$

is an eigenvector of T_q , that is

$$T_q |p_m\rangle = \exp\left(\frac{2\pi i}{N}(m+\beta)\right) |p_m\rangle. \quad (2.38)$$

Similarly

$$T_p |q_n\rangle = \exp\left(\frac{2\pi i}{N}(n+\alpha)\right) |q_n\rangle. \quad (2.39)$$

From this exercise we get the important transformation function which is nothing but a discretized and generalized version of the Fourier transform of usual quantum mechanics, that transforms position states to momentum eigenstates.

$$\langle q_n | p_m \rangle = \frac{1}{\sqrt{N}} \exp\left(\frac{2\pi i}{N}(n+\alpha)(m+\beta)\right) \equiv G_{nm} \quad (2.40)$$

Thus although we avoid writing down position and momentum operators, the rest of the machinery is very much there on the torus, and appropriate discretization is involved. We may also identify “position” and “momentum” eigenvalues from the eigenvalues of the translation operators as $q_n = (n+\alpha)/N$

and $p_m = (m + \beta)/N$. Notice that we have now a 2 parameter family of quantizations and this freedom with boundary conditions is absent in ordinary quantum mechanics. It is interesting that the Aharonov-Bohm phase appears in finite quantum mechanics unobtrusively and in fact there is one more phase which comes from momentum periodicity.

Exercise.

6. One may ask what about the uncertainty relation $[q, p] = i\hbar$? As is well known this translates into the fact that unitary translation operators along q and p , do not commute, which is a reflection that there is no sensible phase space in quantum mechanics. Show that the analogue of the uncertainty relation is the non-commutativity of T_q and T_p described by

$$T_p T_q = e^{-2\pi i/N} T_q T_p. \quad (2.41)$$

For simplicity put $\alpha = \beta = 0$. Hence find λ_{rs} where $T_p^r T_q^s = \lambda_{rs} T_q^s T_p^r$ for some integers r and s . Also investigate the role of the phases.

Where is \hbar ? From comparing the transformation function with the continuum formula for $\langle q|p\rangle$ we may infer that $N = 1/\hbar$. This also follows from semiclassical arguments of state counting: as there are N states on the unit phase space, and there is one state per \hbar , it follows that

$$\hbar = \text{Total area of phase space}/\text{Total number of states} = 1/N. \quad (2.42)$$

This is of course the effective scaled Planck constant. The classical limit is then the large N limit, $N \rightarrow \infty$.

Problem.

7. Show that G_N , the finite Fourier transform matrix is an unitary matrix.
8. We discussed that quantum maps of area preserving transformations were unitary operators. May G_N be the quantum map corresponding to some classical map? For simplicity taking the phases α, β to be 0, show that G_N corresponds to the simple classical transformation of a 90 degree rotation of the unit square about its center. Note how this dovetails with the fact that $G^4 = 1_N$, where 1_N is the N dimensional identity. Hence show that the eigenvalues of G_N are only ± 1 and $\pm i$. Thus G_N , the finite Fourier transform has an interesting and intuitive interpretation of a rotation, a simple operation that is at the bottom of integrable systems.

Quantum phase-space representations: Coherent States on the Torus

Coherent states on the torus are the equivalent of the coherent states that one studies in quantum mechanics as eigenstates of the harmonic oscillator annihilation operator. We use them essentially to visualize quantum states in a “phase space”, as coherent states are of minimal $q - p$ uncertainty and therefore come closest to being phase space points. They are the quantum microscope through which we hope to see the quantum-classical border with more precision.

First we need a “fiducial” state which is the analogue of the harmonic oscillator ground state, the first coherent state (recall $\hat{a}|0\rangle = 0$, so that $|0\rangle$ is a coherent state). Saraceno proposed using the ground state of the Hamiltonian

$$H_h = 2 - \frac{1}{2} \left(T_q + T_q^\dagger + T_p + T_p^\dagger \right), \quad (2.43)$$

which is the quantization of $2 - \cos(2\pi\hat{q}) - \cos(2\pi\hat{p})$ on the torus (see this from the analogy of the translation operators on the torus to the usual translation operators). Examine the classical Hamiltonian to see that the energy is bounded between 0 and 4, which is also the bound for the eigenvalues of H_h . Expanding about $q = p = 0$ we see that it is a Harmonic oscillator in the linear approximation. Thus we can expect this state to be localized at the $q = p = 0$ and be one of minimal uncertainty. Calling this state $|00\rangle$ (not to be confused with a tensor product state) we may then define:

$$|pq\rangle = T_p^p T_q^{-q} |00\rangle, \quad 0 \leq p, q \leq N-1, \quad (2.44)$$

so that $|pq\rangle$ is the coherent state that we seek, as it translates in position by q and momentum by p . In particular if ψ is any state $|\langle pq|\psi\rangle|^2$ tells us how this state is spread in momentum and position simultaneously. It is known as the **Husimi or coherent state representation**.

It is a simultaneous view of two incompatible quantities: the Electrical engineers use a very closely related Gabor transform, which is a windowed Fourier transform, to see signals simultaneously in frequency and time space.

Exercise

9. Analyse more carefully the fiducial state $|00\rangle$ as defined above. Derive an approximate expression for this from the harmonic oscillator approximation of the Harper Hamiltonian. Diagonalize H_h numerically for some large N , such as $n = 50$, and compare this ground state with that found approximately. What about the excited states? For how long do we expect the harmonic oscillator approximation to be valid?

This ends our discussion of the kinematics on the toral phase space.

2.2.5 General toral quantum maps

Consider the quantization of the kicked Hamiltonian in Eq. (1.22) and the resultant classical map of Eq. (1.27). Recall that the map is from just after a kick to just after the next kick. Therefore first there is the “free motion”, and then the kick. This results, as discussed earlier, in the quantum map:

$$U = \exp(-iV(\hat{q})/\hbar) \exp(-if(\hat{p})/\hbar). \quad (2.45)$$

We now wish to treat the map restricted to a unit torus, which requires that f and V be periodic functions of unit period. Thus we write the quantum map in the position basis as:

$$U_{nn'} = \langle q_n | U | q_{n'} \rangle = \langle q_n | \exp(-if(\hat{p})/\hbar) | q'_{n'} \rangle e^{-2\pi i NV \left(\frac{n'+\alpha}{N} \right)}, \quad (2.46)$$

where we have used $\hbar = 1/N$ and inserting complete momentum states we get

$$\langle q_n | \exp(-if(\hat{p})/\hbar) | q'_{n'} \rangle = \frac{1}{N} \sum_{m=0}^{N-1} e^{-2\pi i N f \left(\frac{m+\beta}{N} \right)} e^{\frac{2\pi i}{N} (m+\beta)(n-n')}. \quad (2.47)$$

Piecing them together

$$U_{n'n} = \frac{1}{N} e^{-2\pi i NV \left(\frac{n'+\alpha}{N} \right)} \sum_{m=0}^{N-1} e^{-2\pi i N f \left(\frac{m+\beta}{N} \right)} e^{\frac{2\pi i}{N} (m+\beta)(n-n')}. \quad (2.48)$$

While this may appear somewhat messy, its essential underlying simplicity must be appreciated. Nothing much further can be done with this form in this generality. The finite unitary U is the quantum map corresponding to the general family of maps in Eq. (1.27), with modulo 1 conditions in both q and p . An example is the Harper map for which both f and V are simply cosines.

Exercise.

10. Write a code for the quantum Harper map. Evaluate numerically the matrix elements and explicitly verify that it is unitary, that is $U^\dagger U = I_N$.

2.2.6 Quantum standard map on the torus

In this case $f(p) = p^2/2$ does not appear naturally as a periodic function. However we define the action of the free motion on an momentum eigenstate in the obvious manner:

$$\exp \left(-i \frac{\hat{p}^2}{2\hbar} \right) |p_m\rangle = \exp \left(-\frac{i\pi}{N} (m+\beta)^2 \right) |p_m\rangle. \quad (2.49)$$

and therefore we quantize the standard map on the torus in the position basis as ($V = -K \cos(2\pi q)/(2\pi)^2$):

$$U_{n'n} = \frac{1}{N} e^{\frac{iNK}{2\pi} \cos(2\pi \frac{n'+\alpha}{N})} \sum_{m=0}^{N-1} e^{-\pi i \frac{(m+\beta)^2}{N}} e^{\frac{2\pi i}{N} (m+\beta)(n-n')}. \quad (2.50)$$

In the case that $\beta = 0$, we can do the sum exactly, as this was done by Gauss quite some time back and constitutes an example of an exact *Gaussian sum*. The objection that p^2 is not periodic is addressed in this case by restricted the value of N to even integers. This ensures that $e^{-i\pi m^2/N}$ has the periodicity of N . We get after the summation a simple formula for the quantum standard map on the torus:

$$U_{nn'} = \frac{e^{i\pi/4}}{\sqrt{N}} e^{\frac{iNK}{2\pi} \cos(2\pi \frac{n'+\alpha}{N})} e^{\frac{i\pi}{N} (n'-n)^2}. \quad (2.51)$$

If the other phase $\alpha = 0$ as well (parity remaining a good quantum number), then the quantum map is even simpler looking,

$$U_{nn'} = \frac{e^{i\pi/4}}{\sqrt{N}} e^{\frac{iNK}{2\pi} \cos(\frac{2\pi n'}{N})} e^{\frac{i\pi}{N} (n'-n)^2}. \quad (2.52)$$

2.2.7 Quantum bakers map

The bakers map was the simplest classical 2D area preserving transformation that we studied, in the sense that it was exactly solvable for all orbit types, periodic or otherwise, its Lyapunov exponent, topological entropy etc. are easy to find, it is in short an exactly solvable model of chaos. Therefore it is natural for us to seek a quantum version of the map. Perhaps it will also be exactly solvable? It was with this motivation that the bakers map was first quantized in 1988-89, however, despite its structural

simplicity it is not exactly solvable in the sense that we do not yet know how to solve for the spectrum of the quantum problem.

One reason why the baker was quantized fairly late was that it does not have a kicked Hamiltonian generating it. However there is a generating function generating it. Here we will merely state the quantum baker map and restrict ourselves to some motivating comments. Given a particular choice of toral boundary conditions (α, β) , recall that we have the finite Fourier transform which we denoted by G_N as the transformation function between position and momentum in Eq. (2.40). This will form the central quantity in the quantum baker map which in the position representation is:

$$B = G_N^{-1} \begin{pmatrix} G_{N/2} & 0 \\ 0 & G_{N/2} \end{pmatrix}. \quad (2.53)$$

Here $G_{N/2}$ is the $N/2$ dimensional Fourier transform (FT), and we require that N be an even integer. Thus we see that the quantum baker map is a simple combination of finite Fourier transforms. In terms of signals, it instructs us to split the signal into two halves and do a FT in each part individually, then combine the two outputs and do an inverse FT on the whole lot. Indeed it seems a very simple transformation, but this is the quantized version of the paradigm chaotic system: the left shift dynamics.

The bakers map first quantized by Balazs and Voros has since undergone several versions of justifications and other operators have also been proposed. We will take a route to it through generating functions that also throw interesting light on quantum-classical correspondences. As we had noted earlier, quantum maps are quantizations of classical canonical transformations.

Canonical Transformations and Propagators: A digression

Recall that a canonical transformation is specified by a generating function and this comes in 4 flavors (Goldstein!), F_1 , F_2 , F_3 and F_4 , such that

$$F_1(q, Q) : p = \partial_q F_1, P = -\partial_Q F_1; \quad (2.54)$$

$$F_3(p, Q) : q = -\partial_p F_3, P = -\partial_Q F_3; \quad (2.55)$$

The generating functions F_2 and F_3 are said to be of a “mixed” kind, referring to their dependencies on the position and momentum. For the sake of simplicity we treat 1DoF and time independent transformations, the extensions do not add any essential complication.

Now we write the corresponding quantum propagators:

$$\langle Q|K|q\rangle \sim \exp(-iF_1(q, Q)/\hbar); \quad \langle P|K|q\rangle \sim \exp(-iF_2(q, P)/\hbar); \quad (2.56)$$

$$\langle Q|K|p\rangle \sim \exp(-iF_3(p, Q)/\hbar); \quad \langle P|K|p\rangle \sim \exp(-iF_4(p, P)/\hbar). \quad (2.57)$$

The propagators have 4 possible representations, two of which are mixed, and correspond exactly to the 4 classical generating function types. Notice that this has the intuitive structure of the propagator “taking the old variables to the new”. The classical relation between the generating functions is via Legendre transformations (for instance $F_2 = F_1 + PQ$, F_1 is Legendre transformed wrt Q), while the quantum propagators are related to each other via the Fourier transform. The “~” symbol is to indicate that the relationship is semiclassical. However *if the transformation is linear the relationship is exact* Upton normalizations.

For instance take the identity transformation ($Q = q$, $P = p$), which is generated by $F_2 = qp$ (verify it), then since a classical identity transformation can be expected to be a quantum identity

transformation we get $\langle P|Id|q\rangle = \langle P|q\rangle \sim \exp(-iPq/\hbar)$, a result we know is an equality if we put in the factor $1/\sqrt{2\pi\hbar}$. Thus the FT is the identity in the mixed representation. Consider the exchange of q and P , ($Q = p$, $P = -q$), which is actually a 90 degree anticlockwise rotation in phase space generated by $F_1 = qQ$. The corresponding quantum map is $\langle Q|K|q\rangle \sim \exp(-iqQ/\hbar)$, which is again the FT. Thus the FT is a 90 degree rotation in the pure position representation. This is also the solution to a problem posed earlier in the context of quantum maps. As another example, we know that Hamiltonians generate infinitesimal time translations, which leads us to $\langle P|K(dt)|q\rangle \sim \exp(-iH(q, P)dt/\hbar)$, while its Fourier transform would give us the propagator in position representation; but as mentioned earlier the FT is classically (and semiclassically) a Legendre transform. The Legendre transform of the Hamiltonian is of course the Lagrangian and we can write $\langle Q|K(dt)|q\rangle \sim \exp(-iL(q, Q)dt/\hbar)$, which is the mysterious formula in Dirac's book that spurred Feynman to develop the path-integral formalism of quantum mechanics. It also explains the confusion we often fall into while asking why the Lagrangian should appear in the propagator rather than the Hamiltonian, the answer is that the Hamiltonian would appear in a mixed representation of the propagator. That should be expected as indeed Hamiltonians generate translations in the "mixed space" of phase space.

We return to the baker map. Recall that the $L \rightarrow B$ part of the baker map is $(q' = 2q, p' = p/2)$, which is generated by the canonical transform $F_2(q, P) = 2qP$, where we identify $(q' \equiv Q, p' \equiv P)$. Therefore this half is given by the operator B whose mixed representation is $\langle P|B|q\rangle \sim \exp(-i2qP/\hbar)$, which is almost the FT but for the factor 2 in the exponent. On the torus, this becomes $G_{N/2}$, see that this indeed has the right structure. However this is only for those $(q < 1/2, P < 1/2)$, in the phase space. In the Hilbert space this translates to those $(q_n < 1/2, P_m < 1/2)$ or $(n < N/2, m < N/2)$. Similar arguments hold for the other half of the baker map and we get the quantum baker in the *mixed* representation by the matrix:

$$B_{\text{mixed (P-q) representation}} = \begin{pmatrix} G_{N/2} & 0 \\ 0 & G_{N/2} \end{pmatrix}, \quad (2.58)$$

from which we multiply by G_N^{-1} to take the baker to the pure position representation. This completes our motivation of why Eq. (2.53) should qualify as a quantum baker. Other arguments also favour this simple matrix. It is well known that quantization is not an unique process, and while there exist a few other quantizations, they are all equivalent (or believed to be) in the semiclassical regime. The simplicity of the Balazs-Voros baker makes it still the simplest model of quantum chaos. Saraceno found that antiperiodic boundary conditions ($\alpha = 1/2, \beta = 1/2$) maximally preserves the classical symmetry of reflection about the center of the square.

Exercise.

11. Find explicitly the matrix elements of the quantum baker map in the position representation.
12. What is the quantum baker map in the momentum representation?
13. Define the operator R such that $R|q_n\rangle = |q_{N-n-1}\rangle$. Find the action of R on the momentum states. Hence prove that R corresponds classically to the act of reflection about the center of the square of the square: $(q \rightarrow 1 - q, p \rightarrow 1 - p)$. Show that the classical map commutes with this reflection.
14. Prove that $[R, B] = 0$ if $\alpha = 1/2, \beta = 1/2$.
15. Write a program to calculate the matrix elements of B and verify that indeed B is unitary and that it commutes with R .

2.3 Eigenfunction of quantum maps

We have taken a long time to set up unitary operators for quantum maps. Hamiltonian, time independent systems, such as the nonlinear oscillators or billiards have also been studied and their quantization is straightforward. The advantage of the quantum maps, is that if they are on the torus, they are finite dimensional and face no truncation issue. In all these case we can usefully ask how the spectra, that is eigenvalues and eigenfunctions behave. In the case of unitary Floquet operators, such as the standard of bakers map, we have

$$U|\phi_j\rangle = \exp(i\phi_j)|\phi_j\rangle, \quad 0 \leq j \leq N-1, \quad (2.59)$$

and in the case of Hamiltonian H as always:

$$H|\psi_n\rangle = E_n|\psi_n\rangle, \quad n = 1, 2, \dots \quad (2.60)$$

We emphasize that none of the operators discussed thus far have been analytically diagonalized. Use any of the standard matrix diagonalization routines to diagonalize the matrices for some fixed N (effective inverse Planck constant) and parameter values when studying the stationary states. When N is a power of 2 many eigenstates of the quantum baker map can be found to an excellent approximation via an ansatz that involves a beautiful and simple sequence called the Thue-Morse.

It is accurate to say that eigenfunctions remain poorly understood even for 2DoF systems. When the baker map was first quantized, the bakers looked at the eigenfunctions in the position representation and concluded that they were mostly erratic, or random looking. However when subsequently coherent states were used to look at the functions a bewildering variety of patterns became visible, most of which could be identified with some classical feature, such as **periodic orbits, or homoclinic orbits, or stable and unstable manifolds**, but the way they were appearing held no particular rule. With the techniques developed by us so far, this is quite easy to do, we diagonalize the quantum baker map, we have used $N = 50$ in the figure below, find all the N eigenfunctions $|\psi_i\rangle$, which would be in the position basis and then calculate the overlap:

$$|\langle pq|\psi_i\rangle|^2, \quad (2.61)$$

for each i , where $|pq\rangle$ is the coherent state discussed earlier and must simply be thought of as a minimum uncertainty wavepacket at (q, p) . The overlap is sometimes called the *Husimi representation*. This will tell us how the eigenfunction is spread in “phase-space.”

Figs (2.4) are 30 of the 50 eigenfunctions and will give some idea of what we are up against. Firstly notice that the wavefunctions are not really spread all over, there is prominent clumping to be seen, and that this is indeed associated with classical orbits is quite easily seen in the case of the bakers map, as the classical orbits are exactly known. For instance we can see the period 2 orbit $(2/3, 1/3), (1/3, 2/3)$ prominently in some eigenfunctions, we can also see period 3 and 4. To really convince oneselves, we need to superimpose the orbits with the eigenfunctions, and they would fall on each other. However in this “eigenfunction zoo” we only know *a posteriori* what orbits are scarring what functions. Besides it must be said that there is a lot of “grass” or small structure that is not immediately visible but which is nevertheless important.

After the example of a “hard chaos” system, the baker map, lets look at the quantum standard map which could have a mixed phase space depending on the parameter K . Say we take $K = 2$, in which case we have a prominent elliptic island around the fixed point at the origin and a large chaotic sea. In Fig. (2.5) we again show 30 of the 50 eigenfunctions for $N = 50$ case. Firstly it appears overall “cleaner”. It is useful now to go back to the classical standard map and look at the phase space for $K = 2$ in Fig. (1.5). See the remarkable classical-quantum correspondence that is there. Notice how

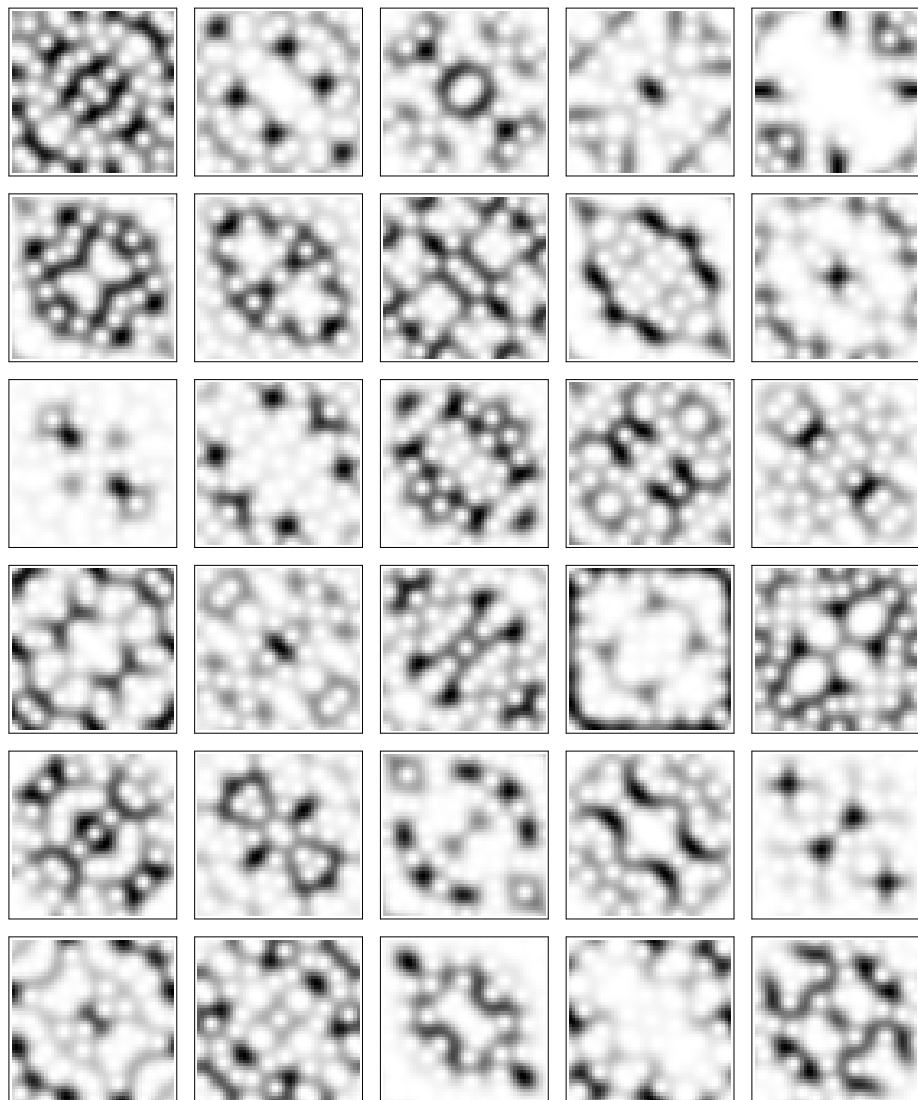


Figure 2.4: Quantum baker eigenfunctions for $N = 50$. The squares are the unit torus, notice intense scarring in some “clean” states by low period periodic orbits, 2, 3 and 4 orbit.

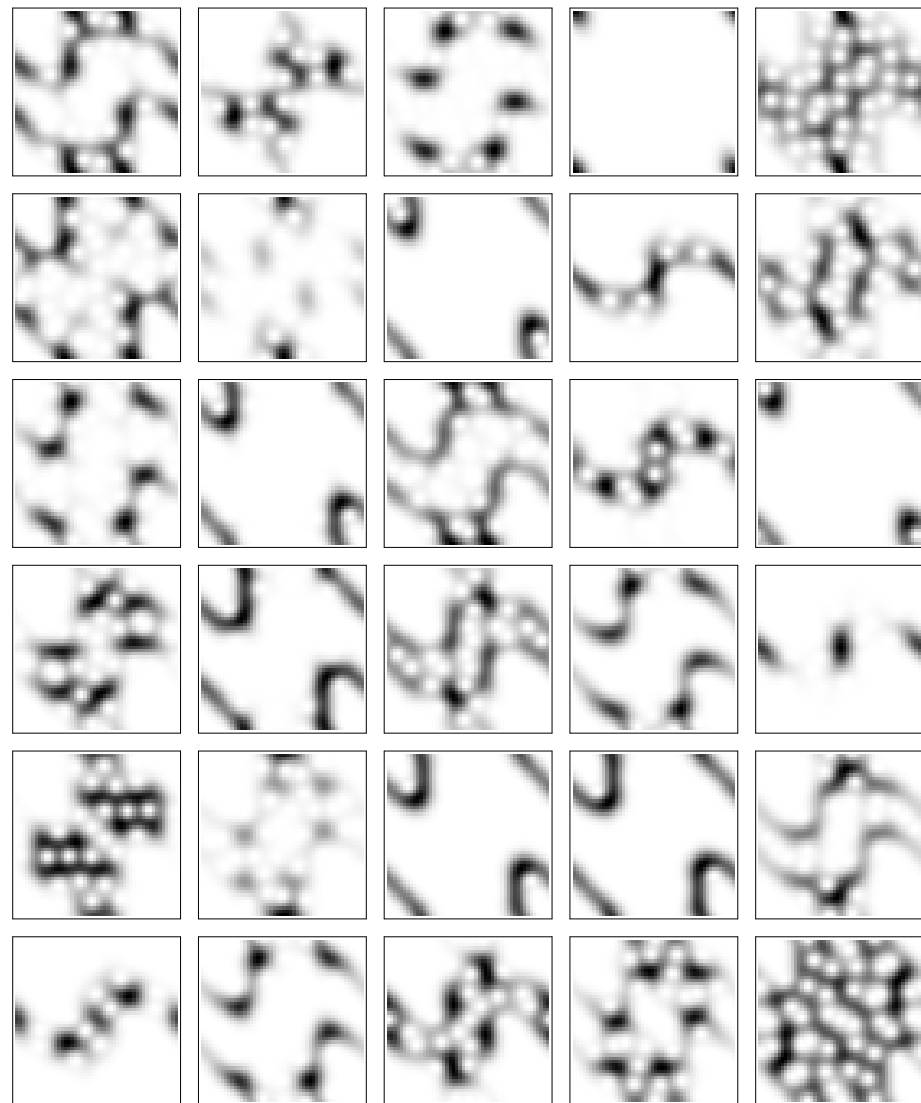


Figure 2.5: Quantum standard map eigenfunctions for $N = 50$. The squares are the unit torus, compare with the classical phase space in Fig. (1.5), and notice how all the eigenfunctions are either in the regular or in the chaotic regions.

there is a state that is only affected by the fixed point at the origin and how remarkably there is a state that is localized around the stable period 2 orbit $(0, 1/2), (1/2, 1/2)$. There are many that are affected by the elliptic orbits around the fixed point at the origin, and the rest are prominently located in the chaotic “sea” and look somewhat like the baker eigenfunctions. The other observation is that all the states seem to be either “scarred” by the regular orbits, or by the chaotic ones, not by both simultaneously. This was conjectured to be the case by Ian Percival in the early 1970’s, and while it is seen to hold for many 2DoF systems, it is not clear if this is valid in higher dimensions. Violations of these have come to light in certain periodic systems, and states that are localized in both chaotic and regular regions have been called “amphibious”.

A lot of work has gone into understanding functions, but there are many fundamental open questions concerning them. There is also a viewpoint that individual states may not be important, as there are too many and often they are too close in energy. Thus statistical and average properties may be of more experimental interest and indeed some finer semiclassical theories are possible if such averaging is done. We move on now to the eigenvalues.

2.4 Eigenvalues and quantum chaos

Eigenvalues of the Hamiltonian are the energies that are allowed and the information about whether we have quantized a chaotic system or not is left buried in this set of numbers. Unlike the eigenfunctions, these are just a series of numbers and hence amenable to a variety of analysis, and unlike eigenvectors, which have always to be studied in a particular basis, the eigenvalues are independent of this. Let $\{E_j\}$ series of energy eigenvalues. In the case of quantum maps or Floquet systems, we have the so-called quasi-energies, the eigenphases $\{\phi_j\}$. We will continue with the “ E ” terminology and notation but everything goes through for this as well.

First let us see how they “look” and just as with eigenfunctions, this may already give away something. Rather than looking at the eigenvalues at a particular parameter, it is immensely useful to follow them as a function of a parameter. For example consider again the Hamiltonian reproduced for convenience.

$$H = \frac{1}{2}(p_1^2 + p_1^2) + \frac{1}{4}\alpha(q_1^4 + q_2^4) + \frac{1}{2}\gamma q_1^2 q_2^2,$$

As α is decreased the oscillators become more classically chaotic. This is reflected in the flow of the spectrum shown in Fig. (2.6) as the eigenvalues become more reserved, they keep a distance and essentially repel each other at **avoided crossing**; this is clearer in the magnification. Such “spaghetti” plots give away the complexity of the system. We saw that both the circle and elliptic billiard are both integrable, but for a charged particle trapped in it the presence of a magnetic field can change the dynamics, it keeps the circle still integrable and renders the ellipse non-integrable due to a collision of the symmetry between the billiard and the cyclotron motion. As a function of the magnetic field then the energy levels behave completely differently as shown in Fig. (2.7). (from Nakamura, Thomas, Phys. Rev. Lett., 1988). A consequence of the differences is supposed to manifest in the zero-temperature diamagnetic susceptibility

$$\chi = \sum_{i=1}^n \frac{d^2 E_i}{dB^2}$$

where n is the number of (free) electrons in the billiard (quantum dot). The differences are marked as shown in Fig. (2.8); the integrable system showing usual Landau diamagnetic behaviour with the

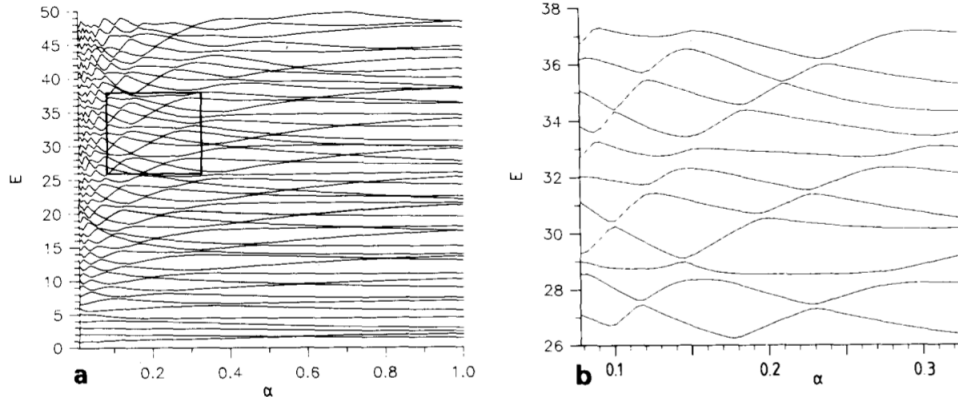


Fig. 4. (a) The lowest 48 eigenvalues for the quantized Hamiltonian (2.1.41) with $\gamma = 3$. For every value of α , the spectrum has been unfolded to one of mean spacing 1. As shown in the magnification (b), almost all crossings or close encounters between eigenvalues are avoided.

Figure 2.6: Energy vs parameter α for the coupled quartic oscillator

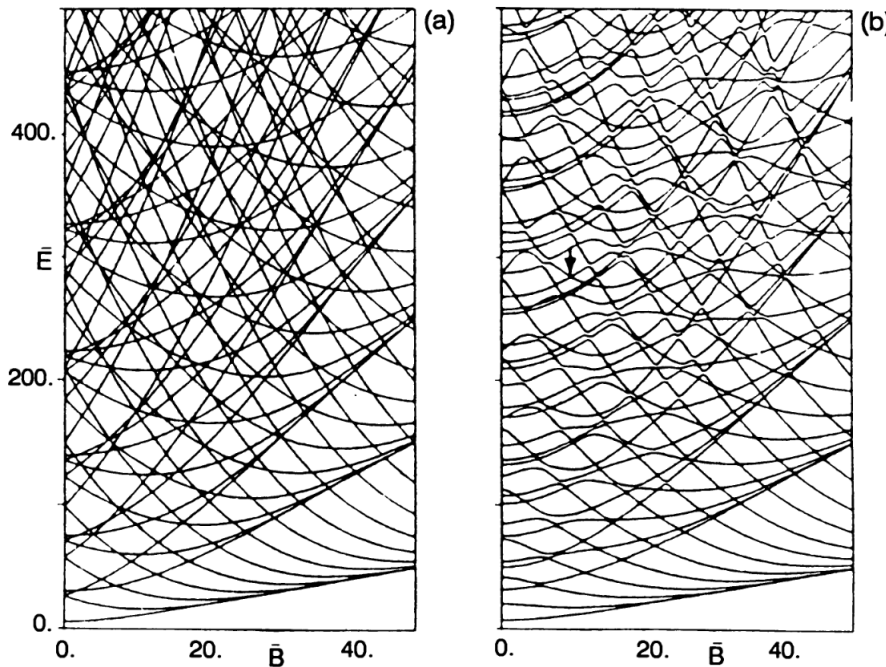


Figure 2.7: Energy vs magnetic field for a particle in a circle (integrable, left), ellipse (nonintegrable, right).

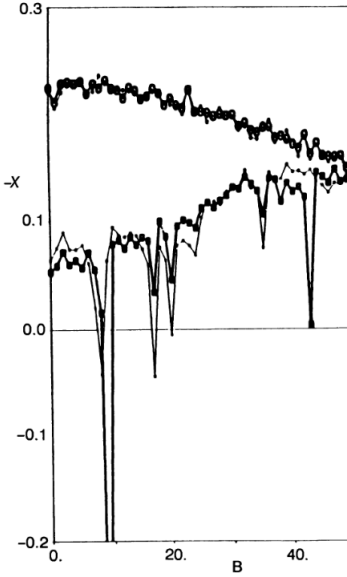


Fig. 29. Negative of diamagnetic susceptibility χ as a function of the magnetic field strength B for $n = 100$ occupied levels. The upper part corresponds to a circular billiard and the lower part to an elliptic billiard (taken from [99]).

Figure 2.8:

susceptibility decreasing from $B = 0$, whereas for the nonintegrable case it increases and shows sharp fluctuations whenever the level at the Fermi energy E_F undergoes an avoided crossing.

For yet another example, we reproduce from D. Delande's article in the Les Houches school on chaos and the quantum the Fig. (2.9). This concerns the Hydrogen atom spectrum as a function of an external magnetic field. Again due to clash of symmetries nonintegrability and chaos sets in for large (but no too large) fields (~ 5 Tesla).

2.4.1 The staircase function, density of states, and spectral fluctuations

So where does the chaos lurk in the numbers? First off the energies increase from the ground state up in essentially a smooth looking manner. Define the function $N(E) = \#$ of levels less than E , that is

$$N(E) = \sum_j \Theta(E - E_j), \quad (2.62)$$

this is the “staircase function” and the density of states is

$$\rho(E) = \frac{dN(E)}{dE} = \sum_j \delta(E - E_j). \quad (2.63)$$

The spectral staircase has a secular growth that can be approximated by a smooth function $\overline{N(E)}$ and its derivative is the smooth part of the density of states:

$$N(E) = \overline{N(E)} + N_{osc}(E), \quad \rho(E) = \overline{\rho(E)} + \rho_{osc}(E). \quad (2.64)$$

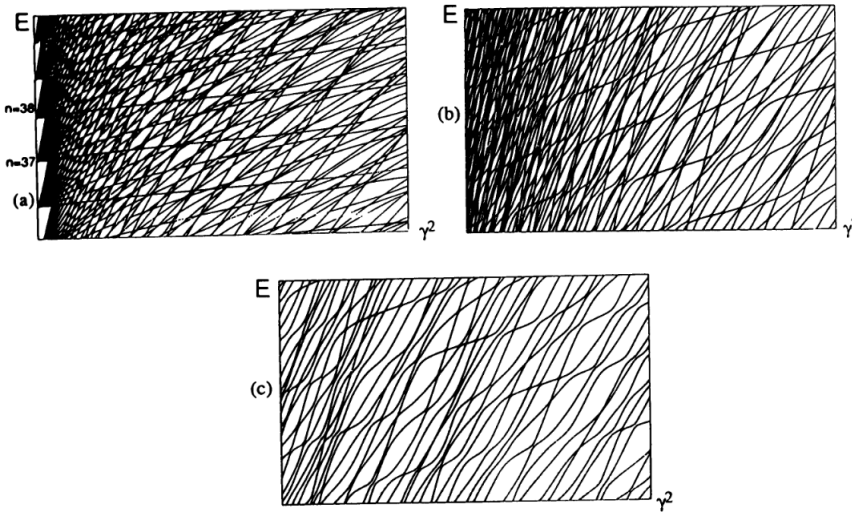


Fig. 18. Energy levels of the hydrogen atom versus the square of the magnetic field, at increasing scaled energy. (a) $0 \leq \gamma^2 \leq 1.4 \times 10^{-9}$; $-4 \times 10^{-4} \leq E \leq -3 \times 10^{-4}$; the classical motion is partly chaotic in the right part. Some large avoided crossings (resonances) are visible. (b) $10^{-9} \leq \gamma^2 \leq 1.4 \times 10^{-8}$; $-4 \times 10^{-4} \leq E \leq -3 \times 10^{-4}$; more and more avoided crossings appear as the chaotic part of the phase space increases. (c) $6 \times 10^{-9} \leq \gamma^2 \leq 1.3 \times 10^{-8}$; $-2.5 \times 10^{-4} \leq E \leq -2 \times 10^{-4}$; completely chaotic regime. There are only large avoided crossings.

Figure 2.9: Energy vs magnetic field for the H atom.

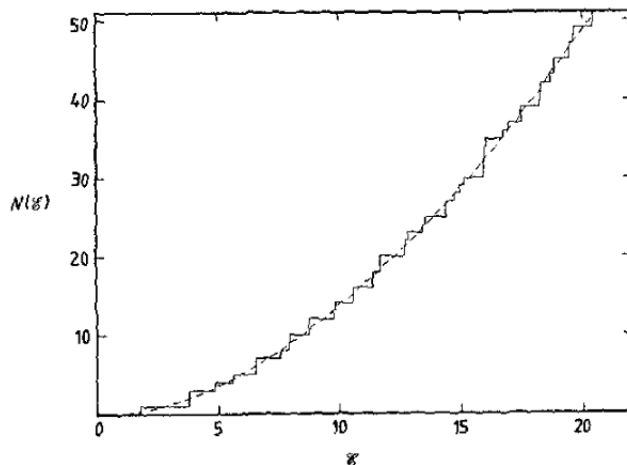


Figure 1. The comparison of the exact quantum integrated density of states (the 'staircase' function, $N(\epsilon)$) to the asymptotic mean number expected for the lowest 50 eigenvalues.

Figure 2.10: The spectral staircase function when the potential is simply x^2y^2 . From Tomsovic, J. Phys. A, 1991.

The density of states may be derived from the Heat kernel or partition function, as its inverse Laplace transform:

$$Z(t) = \text{tr}(e^{-t\hat{H}}) = \sum_j e^{-tE_j} = \int_0^\infty \rho(E)e^{-tE} dE. \quad (2.65)$$

The smooth part of the density states is approximated by approximating the partition function. The leading order term comes from simply treating H as the classical Hamiltonian and the trace is replaced by a phase space integral.

$$\int_0^\infty \overline{\rho(E)} e^{-tE} dE \approx \frac{1}{(2\pi\hbar)^d} \int e^{-tH(q,p)} d^d q d^d p. \quad (2.66)$$

The $1/h^d$ factor comes as semiclassically the number of quantum states in a phase space volume dV is dV/h^d . Alternatively this is a consequence of the “Thomas-Fermi” approximation that is evidently semiclassical:

$$\overline{N(E)} = \frac{1}{(2\pi\hbar)^d} \int \Theta(E - H(q, p)) d^d q d^d p. \quad (2.67)$$

For example for the quartic oscillators in Eq. (1.36)

$$\int_0^\infty \overline{\rho(E)} e^{-tE} dE \approx \frac{1}{(2\pi\hbar)^2} \int_{-\infty}^\infty \exp[-t(\mathbf{p}^2/2 + \alpha(q_1^4 + q_2^4)/4 + \gamma q_1^2 q_2^2/2)] dq_1 dq_2 d\mathbf{p}. \quad (2.68)$$

The kinetic energy term can be exactly integrated as they are gaussians and contribute a factor of $1/t$, the potential being homogeneous is now crucial, as substituting $q_1^4 t = u_1^4$ and $q_2^4 t = u_2^4$, removes all the t dependence and we get

$$\int_0^\infty \overline{\rho(E)} e^{-tE} dE \approx \frac{C}{(2\pi\hbar)^2} \frac{1}{t^{3/2}}, \quad (2.69)$$

where C is a constant, and gives on Laplace inversion

$$\overline{\rho(E)} \approx \frac{CE^{1/2}}{(2\pi\hbar)^2}, \text{ and hence, } \overline{N(E)} \approx \frac{CE^{3/2}}{(2\pi\hbar)^2}. \quad (2.70)$$

These quantities have an expansion in the energy with lower order terms, the Weyl expansion. For example the quartic oscillator has subleading corrections to the counting function going as $E^{3/4}$, the remaining being a constant and $\mathcal{O}(E^{-3/4})$. For 2D billiards there is a celebrated Weyl series:

$$\overline{N(E)} = \frac{\mathcal{A}}{4\pi} E - \frac{\mathcal{L}}{4\pi} \sqrt{E} + C + \dots, \quad (2.71)$$

where \mathcal{A} is the area of the billiard, \mathcal{L} its perimeter and C includes curvature terms.

Now the chaos is hidden in the **spectral fluctuations**, or the oscillating part:

$$N_{osc}(E) = N(E) - \overline{N(E)} \quad (2.72)$$

In general the **fluctuations in an integrable systems are more than in the chaotic**, see Fig. (2.11). For the integrable case the fluctuations grow with energy and for the chaotic case they are essentially bounded. The chaotic spectrum is said to be **rigid**. A quantitative characterization of the statistics of the fluctuations will be done in the next chapter when we consider random matrix theory. But we are now ready to do an important preparatory step.

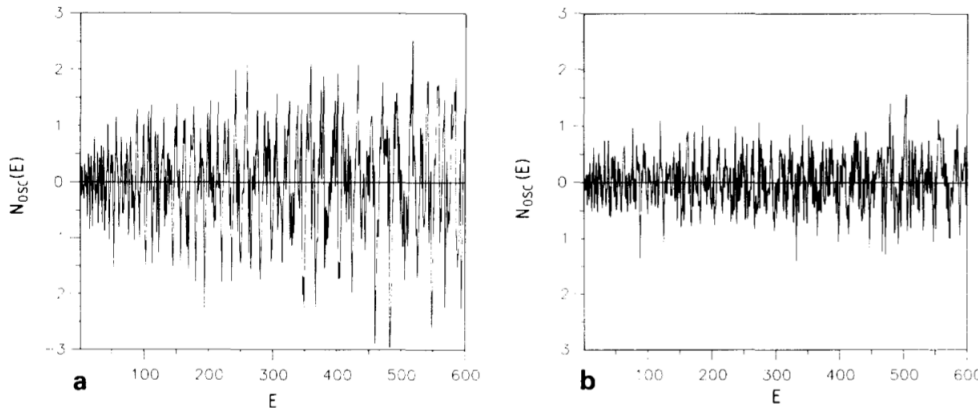


Fig. 3. Fluctuations of spectra around the mean integrated density of states. (a) Low-lying eigenvalues of an integrable system and (b) eigenvalues of a chaotic system. The Hamiltonian is that of eq. (2.1.41) quantized. The parameters are that of figs. 1a and 1d.

Figure 2.11: Refers to the Hamiltonian in Eq. (1.36) and to Fig. (1.3.2)

Unfolding energy levels

To compare fluctuations of the spectra of disparate Hamiltonians, they are all brought to one common denominator, one with unit level spacing on the average, so that the spectral staircase is fluctuating about the straight line E . Unfolding a spectrum is the mapping to

$$x_n = \overline{N(E_n)}. \quad (2.73)$$

The unfolded spectrum x_n will now have the desired properties and the fluctuations in these about the 45° line is studied.

2.4.2 Semiclassics of Eigenvalues

The story of eigenvalues is somewhat more happier if not entirely so. The general aim of semiclassics is to provide quantum information from purely classical one. For instance everything about the quantum harmonic oscillator can be found from classical properties. It is not at all clear whether this is possible in general. It must be emphasized that calculating quantum quantities using classical ones, does not mean that the phenomena are classical, of course not. It also does not mean that when quantum-classical correspondence there is an end to the use of semiclassics.

The Gutzwiller trace formula which connects the trace of the energy Green's function to a weighted sum over the periodic orbits on energy shells is the central object. This however requires quite an extensive treatment, we will here restrict ourselves to a part of it and give a flavor of the issues involved. Using quantum maps, the trace formula is also usefully studied. As one central object we will deal with the trace of the propagator in time:

$$\text{Tr}(U^T) = \sum_{i=0}^{N-1} \exp(iT\phi_i) \quad (2.74)$$

where U is some unitary map, the ϕ_i are the eigenangles. This implies that if we know the traces of the

powers of U we can know the eigenangles. This is seen by Fourier transforming both sides:

$$\sum_{T=-\infty}^{\infty} e^{-i\omega T} \text{Tr}(U^T) = \quad (2.75)$$

$$\sum_{m=-\infty}^{\infty} \sum_{i=0}^{N-1} \delta(\phi_i - \omega - 2\pi m) \quad (2.76)$$

where we have made use of the *Poisson identity*:

$$\sum_{n=-\infty}^{\infty} e^{2\pi i n x} = \sum_{m=-\infty}^{\infty} \delta(x - m) \quad (2.77)$$

an identity from the theory of Fourier transforms that is of singular importance, simplicity and power. If we multiply the above identity by a smooth function $f(x)$ and integrate we get the following *Poisson summation formula*:

$$\sum_{n=-\infty}^{\infty} \int_{n=-\infty}^{\infty} f(x) e^{2\pi i n x} dx = \sum_{m=-\infty}^{\infty} f(x). \quad (2.78)$$

Thus Fourier transforming the traces of the powers of the propagator will give us delta functions at the eigenangles.

Semiclassical theory then attempts to find $\text{Tr}(U^T)$ from purely classical quantities. The general structure of this trace formula is

$$\text{Tr}(U^T) \sim \sum_{\gamma(T)} A_{\gamma} \exp(2\pi i S_{\gamma}/\hbar) \quad (2.79)$$

where γ enumerates classical *periodic orbits* of period T , S_{γ} is the action of the periodic orbit, and A_{γ} is a weight that typically exponentially falls with the period T . This last statement may give rise to the expectation that the long orbits can be neglected, but remember that in chaotic systems there is an *exponential proliferation* of periodic orbits with period. Therefore this is a delicate problem that needs care and in fact while the trace of quantum maps on finite Hilbert spaces hardly poses a problem, whole of semiclassics is beset with convergence issues. There is also the question of *how long* the above approximation holds good, while a fair amount of work has gone into this it is again not very clear what exactly this time is and how it depends on the scaled Planck constant and the parameters of chaos. For instance one surprising result that has emerged is that *semiclassics can be more accurate for larger chaos!*

Semiclassics has been described as a determined usage of the stationary phase approximation. To give an idea of what goes on, we can make use of the quantum map machinery we have already discussed. As a fair warning this may be somewhat heavy on first reading, but this is really “semiclassics-lite”.

Consider the following map defined on the unit torus:

$$\begin{aligned} q_{j+1} &= q_j + p_j - l_j \\ p_{j+1} &= p_j - V'(q_{j+1}) - m_j, \end{aligned} \quad (2.80)$$

where $V(q)$ is the periodic “kicking” potential with unit periodicity, the prime indicates derivative, and the integers m_j and l_j are such that the map is restricted to the unit torus (winding numbers). They are the “modulo one” operations. As was discussed earlier the above map can be derived from a time

dependent Hamiltonian system. Also there exists a generating function for the map on the torus given by

$$S(q_j, q_{j+1}; l_j, m_j) = \frac{1}{2}(q_{j+1} - q_j + l_j)^2 - V(q_{j+1}) - m_j q_{j+1} \quad (2.81)$$

from which the map can be derived as $p_j = -\partial S/\partial q_j$ and $p_{j+1} = \partial S/\partial q_{j+1}$. This is of the F_1 type we discussed earlier.

The quantum map corresponding to the Eqs.(26) is given by the finite dimensional unitary matrix

$$\langle n|U|n' \rangle = \frac{e^{-i\pi/4}}{\sqrt{N}} \exp\left(\frac{i\pi}{N}(n-n')^2 - 2\pi i N V\left(\frac{n}{N}\right)\right), \quad (2.82)$$

which generalizes the quantum standard map used before. This takes on the function of the propagator as it connects states after consecutive kicks. Here the representation is in the position basis and n and n' may take the integer values from 0 to $N-1$. N is itself the dimensionality of the Hilbert space and is also the inverse Planck constant, and is restricted to be even integers for preservation of toral boundary conditions. Semiclassics means the study of the unitary operator as $N \rightarrow \infty$.

The object of primary interest, the trace of the powers of the propagator, from which the spectrum may be derived by a Fourier transform can be written as

$$\text{Tr}(U^T) = \frac{e^{-i\pi T/4}}{N^{T/2}} \sum_{n_i=0}^{N-1} \exp\left(\frac{2\pi i}{N} \sum_{j=1}^T \left(n_j^2 - n_j n_{j+1} - N^2 V\left(\frac{n_j}{N}\right)\right)\right), \quad (2.83)$$

with

$$n_{T+1} = n_1.$$

It is implied in the above that the outer sum is over the T variables n_i , $i = 1, 2, \dots, T$. Using the Poisson summation formula we can rewrite the above as

$$\begin{aligned} \text{Tr}(U^T) &= e^{-i\pi T/4} N^{T/2} \sum_{k_i=-\infty}^{\infty} \int_{-\epsilon}^{1-\epsilon} dx_1 \dots dx_T \\ &\exp\left(2\pi i N \sum_{j=1}^T (k_j x_j + x_j^2 - x_j x_{j+1} - V(x_j))\right), \end{aligned} \quad (2.84)$$

with

$$x_{T+1} = x_1, \text{ and } k_{T+1} = k_1.$$

The stationary phase approximation, assuming that N is large, gives the following T conditions

$$x_{j+1} = 2x_j - x_{j-1} - V'(x_j) + k_j; \quad j = 1, \dots, T, \quad x_0 = x_T, \quad x_1 = x_{T+1}, \quad (2.85)$$

with the further condition that

$$0 \leq x_j < 1.$$

These are precisely the equations that determine the period T orbits of the map. The integers k_j are related to the integers l_j and m_j of Eqs. (2.80) by the relation $k_j = l_{j-1} - l_j - m_{j-1}$. With the assumption that they uniquely determine a periodic orbit of period an integer fraction of T , we restrict the infinite sum to only those that relate to such a periodic orbit labeled below by γ . This is the first approximation and the second one is that we will extend the ranges of integration to the whole real

line. These approximations together are exact in the case of the quantum cat maps, which we have not discussed here, and the third related approximation is that we Taylor expand the potential about the periodic orbits retaining up to the quadratic terms. This approximation is unnecessary for the piecewise linear maps, but is necessary in general.

Therefore we define new variables y_j such that $x_j = q_j + y_j$ and q_j is the central periodic orbit.

$$\text{Tr}(U^T) \sim e^{-i\pi T/4} N^{T/2} \sum_{\gamma} \exp \left(2\pi i N \sum_{j=1}^T (-q_j q_{j+1} + q_j^2 + q_j k_j - V(q_j)) \right) \times \int_{-\infty}^{\infty} dy_1 \dots dy_T \exp \left(2\pi i N \sum_{j=1}^T (y_j^2 - y_j y_{j-1} - y_j^2 V''(q_j)/2) \right) \quad (2.86)$$

The sum

$$\sum_{j=1}^T (-q_j q_{j+1} + q_j^2 + q_j k_j - V(q_j)) \quad (2.87)$$

can be identified with the action of the periodic orbit, as one gets

$$S_{\gamma} = \sum_{j=1}^T (q_j^2 - q_j q_{j+1} - V(q_j) + q_j k_j + l_j^2/2), \quad (2.88)$$

We can neglect the term $l_j^2/2$, from the Lagrangian; this is legitimate as the action occurs as $e^{2\pi i NS}$, and since N is an even integer these terms do not matter.

The integral is evaluated by standard methods.

$$\int_{-\infty}^{\infty} d^T y \exp(i\pi N y^t A_{\gamma} y) = \frac{e^{i\pi T/4}}{N^{T/2}} \frac{e^{-i\pi \nu_{\gamma}/2}}{\sqrt{|\text{Det}(A_{\gamma})|}}. \quad (2.89)$$

Here y denotes the T component vector $\{y_j\}$ and y^t is its transpose. The real symmetric matrix A_{γ} is given by

$$A_{\gamma} = \begin{pmatrix} 2 - V''(q_1) & -1 & 0 & \dots & \dots & -1 \\ -1 & 2 - V''(q_2) & -1 & 0 & \dots & 0 \\ \vdots & \vdots & \vdots & \vdots & \vdots & \vdots \\ \vdots & \vdots & \vdots & \vdots & \vdots & \vdots \\ \vdots & \vdots & \vdots & \vdots & \vdots & \vdots \\ -1 & 0 & \dots & \dots & -1 & 2 - V''(q_T) \end{pmatrix}. \quad (2.90)$$

ν_{γ} is a “Maslov like” index, and is the number of negative eigenvalues of the matrix A_{γ} .

The nontrivial problem of evaluating the determinant is already solved and the results are known. The determinant can be related to the stability of the periodic orbit. If the residue of the periodic orbit, which is simply related to the trace of the stability matrix, is R_{γ} , then $R_{\gamma} = -\frac{1}{4}\text{Det}(A_{\gamma})$. or if we denote the stability matrix eigenvalues by λ_+^{γ} and λ_-^{γ} , $\text{Det}(A_{\gamma}) = \lambda_+^{\gamma} + \lambda_-^{\gamma} - 2$.

Thus finally we can write the asymptotic periodic orbit sum, or the trace formula, for the toral maps as

$$\text{Tr}(U^T) \sim \sum_{\gamma} \frac{\exp(2\pi i NS_{\gamma} - i\pi \nu_{\gamma}/2)}{\sqrt{|\lambda_+^{\gamma T} + \lambda_-^{\gamma T} - 2|}}. \quad (2.91)$$

The sum is over periodic orbits whose periods are integer fractions of T are labeled by γ . This is of the canonical Gutzwiller-Tabor form having in the exponent the *action* of the period T orbits, and the prefactor explicitly depending on the *stability* of these orbits. The piecewise linear maps such as the baker map, or the sawtooth map are such that the Maslov like phases are zero and the only type of periodic orbits are those of the direct hyperbolic kind. With this formula we can study the vast class of *mixed* systems, such as the well known standard map. It is then of interest to ask questions such as how long the semiclassical approximations are valid in such systems which one knows are generic. Not much is known on these issues due to difficulty of finding *classical* orbits.

A careful application of the above formula in the case of the standard map, and for the simplest possible trace, the time 1 trace, yields the following:

$$\text{Tr}(U) = \frac{e^{-i\pi/4}}{\sqrt{N}} \sum_{n=0}^{N-1} \exp(-ikN \cos(2\pi n/N)) \sim \quad (2.92)$$

$$\frac{e^{-i\pi/4}}{\sqrt{2\pi}} \left[\frac{2 \sin(Nk + \pi/4)}{\sqrt{k}} + \sum_{l=1}^{[k]} \frac{4 \sin(\theta_N(l) + \pi/4)}{(k^2 - l^2)^{1/4}} \right], \quad (2.93)$$

where

$$\theta_N(l) = N(\sqrt{k^2 - l^2} + l \arcsin(l/k)). \quad (2.94)$$

We have defined $k \equiv K/(2\pi)$, taken all quantum boundary conditions to be 0, and $[]$ denotes the integer value function. Notice how the quantum trace involves a sum containing N terms, which in the classical limit has infinite number of terms, while the semiclassical approximation has only $[k]$ terms, depending on the chaos parameter in the system! The sum is over all the fixed points of the standard map, there are $[k]$ of them. Thus semiclassics exposes a *duality* between classical periodic orbits and quantum traces, a duality that is deep and goes into modern areas of mathematical research.

Problem.

Verify if the semiclassical approximation for the trace of the standard map propagator, Eq. (2.93) is correct. Write a program that will do both the sums in this approximation, and evaluate the goodness of the approximation as a function k and N .

Semiclassical formulae such as these are an important analytical tool in understanding quantum chaotic systems. Poincaré had predicted that periodic orbits would be the way to penetrate the fortress of dynamics, and this has been borne out as the truth in the case of semiclassics.ev

Chapter 3

Random Matrix Theory and applications to quantum chaos

3.1 Introduction

The statistical aspects of quantum chaos is well described by random matrix theory (RMT), and is widely used in many areas from nuclear to mesoscopic, quantum information, high energy and field theory to condensed matter physics. These days RMT is being used in widely different areas such as time series analysis of EEG data, analysis of weather patterns and study of fluid flows to economics and of course the financial market. Wigner (1950s) suggested that since complex many body Hamiltonians were hopelessly difficult to solve, we may as well assume that the Hamiltonian matrix (in a generic representation) is a random matrix, that is a matrix whose elements are drawn from a distribution at random. The model that is most often used is when the distribution is a Gaussian and the matrix elements are independently drawn. This leads to the Gaussian ensembles. There are some fundamental symmetries that systems may obey despite all the complexity and chaos. To begin with the matrices must be Hermitian. If there is time-reversal (TR) symmetry this implies that given any arbitrary basis, we can find a related basis in which the Hamiltonian is real. Therefore TR symmetric Hamiltonians are generically real symmetric, while TR nonsymmetric Hamiltonians are in general complex.

Ensembles that are real symmetric and have Gaussian distributed entries constitute the Gaussian Orthogonal Ensemble, or GOE (if they satisfy some additional conditions to be discussed below and therefore the word “Orthogonal” should remain obscure for now). Similarly if they are complex Hermitian they are Gaussian Unitary Ensemble (GUE) We have also talked of unitary matrices, maps rather than Hamiltonians. Therefore the appropriate ensembles are called circular, and Dyson developed these from the point of view of group theory.

The early motivation for RMT in physics was in analysing excited heavy nuclei resonances and this figure shows their spacing distribution between nearest levels after unfolding (as described in previous lecture).

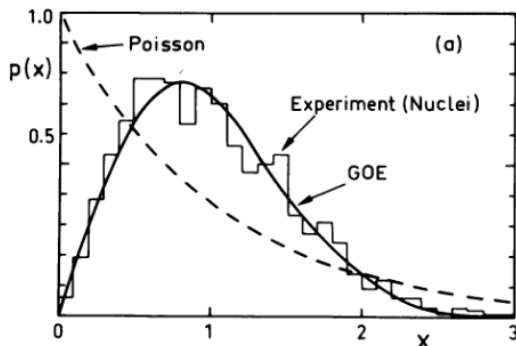


Figure from “Random-matrix physics: spectrum and strength fluctuations”, Brody, Flores, French, Mello, Pandey, Wong, Rev. Mod. Phys. (1983). 1726 level spacings from ^{239}U and other nuclei (Nuclear Data Ensemble) have been **unfolded** so that mean spacing is 1. The agreement of the GOE spacing distribution with the nuclear data is good.

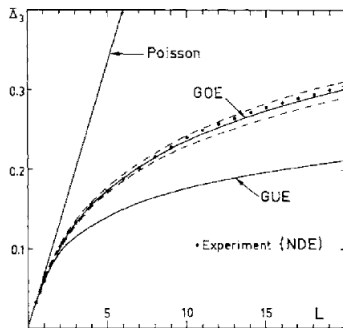


FIG. 9. The Δ_3 for the nuclear data ensemble (data points) and the GOE prediction (solid line). From Haq *et al.*, 1982.

The second figure shows what is called simply the Δ_3 statistics and measures rigidity of the spectrum (again to be discussed later). Agreement with nuclear data is once again quite clear.

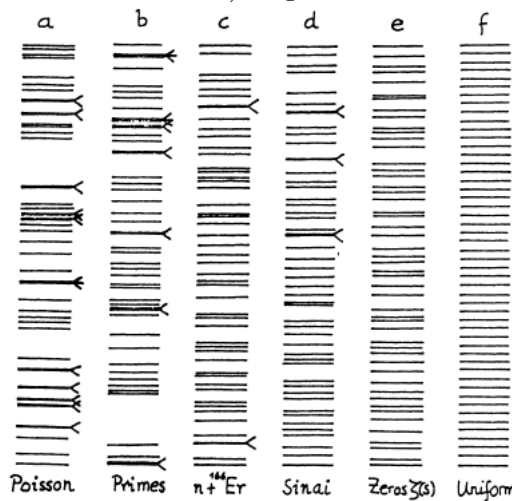


Figure 1.2. Some typical level sequences. From Bohigas and Giannoni (1984). (a) Random levels with no correlations, Poisson series. (b) Sequence of prime numbers. (c) Slow neutron resonance levels of the erbium 166 nucleus. (d) Possible energy levels of a particle free to move inside the area bounded by 1/8 of a square and a circular arc whose center is the mid point of the square; i.e. the area specified by the inequalities, $y \geq 0$, $x \geq y$, $x \leq 1$, and $x^2 + y^2 \geq r$. (Sinai’s billiard table.) (e) The zeros of the Riemann zeta function on the line $\text{Re } z = 1/2$. (f) A sequence of equally spaced levels (Bohigas and Giannoni, 1984).

The third figure shows various “spectra” that includes heavy nuclear resonances, prime numbers, zeta function zeros, billiard eigenvalues and the harmonic oscillator. Also shown is the case of a random sequence, the Poisson. What one sees is a remarkable range of complexity. When two levels come close together it is indicated as with a $<$ symbol. These are nearly degenerate quantum levels, or in the case of primes they would be twin-primes. It is seen that a random sequence, the Poisson, has much more chance of near degeneracy, this looks like the case of the primes also. However this is greatly reduced in the case of the Sinai billiard and even more so in the case of the zeta zeros (none shown for the sequence). Also shown is the harmonic oscillator like, just equal spacing spectra. The Poisson case, with a large probability of near degeneracies is the case of **integrable systems**. While the Sinai billiard is like the TR symmetric GOE which shows level repulsion to some extent. The zeta zeros have even stronger level repulsion and belong to the TR violating GUE class. The Sinai billiard and the heavy nuclei spectrum look to be approximately in the same universality class.

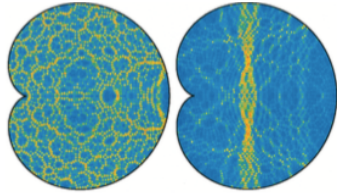


Fig. 1. Probability density of the 1,816th and 1,817th odd eigenstate.

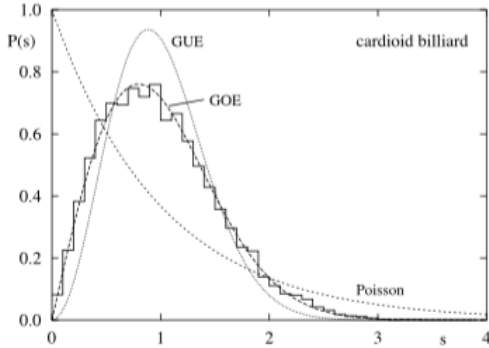


Fig. 2. Level spacing distribution for the energy spectrum of a quantum particle in the chaotic heart-shaped region of Fig. 1 vs. the level spacing distribution for Gaussian Unitary Ensemble, Gaussian Orthogonal Ensemble, and Poisson, respectively.

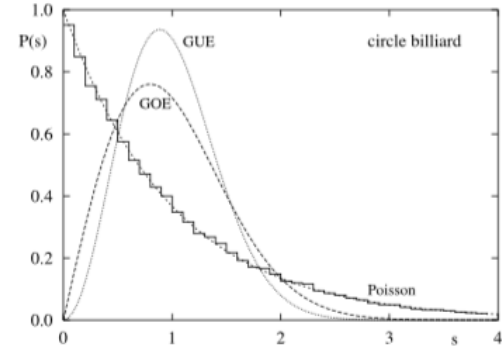
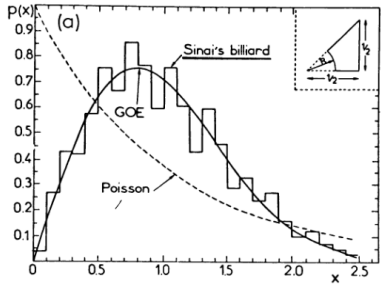


Fig. 3. Level spacing distribution for the energy spectrum of a quantum particle in a circular region vs. the level spacing distribution for Gaussian Unitary Ensemble, Gaussian Orthogonal Ensemble, and Poisson, respectively.

Shown in these figures are level spacing for the case of the cardioid billiard and the circular billiard, (after unfolding). The distribution of the spacings in the circular billiard is as if the levels are uncorrelated, and follows the exponential law e^{-s} , while the cardioid shows level repulsion, has vanishing probability of finding nearly degenerate levels. Recall that after unfolding the mean level spacing is 1, therefore small spacings implies that they are $\ll 1$. This data is from Backer and involves many more levels than the original computation in 1984 and published as “Characterization of Chaotic Quantum Spectra and Universality of Level Fluctuation Laws” by Bohigas, Giannoni, and Schmit (*Phys. Rev. Lett.* 52, 1 Published 2 January 1984). They studied the Sinai billiard and stated that “*It is found that the level fluctuations of the quantum Sinai’s billiard are consistent with the predictions of the Gaussian orthogonal ensemble of random matrices. This reinforces the belief that level fluctuation laws are universal.*” The statement that the spectral fluctuations of quantized chaotic systems have RMT fluctuations is known as the BGS conjecture, and it has been proved in parts by using semiclassical methods.



The above figure shows an inset of $1/8$ of the Sinai billiard. The problem would be solved as a free particle in this enclosure with appropriate boundary conditions (Dirichlet or Neumann) depending on the symmetry of the states. Due to the presence of reflection symmetries, there are different irreducible representations and the Hamiltonian block-diagonalizes in these sectors. **All RMT analysis must be done with spectra in the same symmetry class.** Mixing symmetry classes is like mixing spectra from two completely different systems and they will not be correlated and eventually lead to Poisson like behaviour. If you are expecting a GOE and find Poisson, it may be because all symmetries have not been identified and used.

3.2 Ensembles of matrices

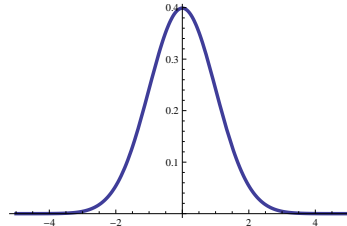
Consider the case of one continuous random variable:

$$\text{Prob}(a \leq x \leq b) = \int_a^b p(x) dx.$$

For example the Normal/Gaussian $N(0, \sigma^2)$:

$$p(x) = \frac{1}{\sqrt{2\pi}\sigma} \exp\left(-\frac{x^2}{2\sigma^2}\right),$$

shown below.



Let us attempt constructing “interesting” random matrix ensembles now. The simplest nontrivial case are 2×2 matrices, and the simplest among them are diagonal matrices.

Attempt-1

$$M = \begin{pmatrix} x & 0 \\ 0 & y \end{pmatrix}, \quad x, y \sim N(0, 1),$$

where $x \sim p(x)$ is to be read as random variable x has the density $p(x)$. The eigenvalues are simply x, y and therefore they are distributed as $N(0, 1)$, and spacing between them, $s = |x - y|$ is distributed as $\sim e^{-s^2/4}/(2\sqrt{\pi})$ (verify if correct). This shows that the “eigenvalues” will be highly likely to be close

to each other. However, the eigenvectors are $(0, 1)^T$ and $(1, 0)^T$, for *all* members of the ensemble. Does not sound so much like a random matrix ensemble. If a rotated basis is used the same matrix becomes:

$$\begin{aligned} M' &= \begin{pmatrix} \cos \theta & \sin \theta \\ -\sin \theta & \cos \theta \end{pmatrix} \begin{pmatrix} x & 0 \\ 0 & y \end{pmatrix} \begin{pmatrix} \cos \theta & -\sin \theta \\ \sin \theta & \cos \theta \end{pmatrix} \\ &= \begin{pmatrix} \cos^2 \theta x + \sin^2 \theta y & \sin \theta \cos \theta(-x + y) \\ \sin \theta \cos \theta(-x + y) & \sin^2 \theta x + \cos^2 \theta y \end{pmatrix}. \end{aligned}$$

Recall that if

$$X \sim N(0, \sigma_x^2), Y \sim N(0, \sigma_y^2), \text{ then } X \pm Y \sim N(0, \sigma_x^2 + \sigma_y^2),$$

and therefore the matrix in the rotated basis has elements with the following distributions:

$$x', y' \sim N(0, \cos^4 \theta \sigma_x^2 + \sin^4 \theta \sigma_y^2), \quad z' \sim N(0, \sin^2 \theta \cos^2 \theta (\sigma_x^2 + \sigma_y^2)).$$

There seems to be no way to get rid of the basis dependence with this model.

Attempt-2: A real symmetric ensemble

$$M = \begin{pmatrix} x & z \\ z & y \end{pmatrix}, \quad x \sim N(0, \sigma_x^2), y \sim N(0, \sigma_y^2), z \sim N(0, \sigma_z^2)$$

In a rotated basis:

$$\begin{aligned} M' &= \begin{pmatrix} x' & z' \\ z' & y' \end{pmatrix} = \begin{pmatrix} \cos^2 \theta x + \sin 2\theta z + \sin^2 \theta y & \frac{1}{2} \sin 2\theta(-x + y) + \cos 2\theta z \\ \frac{1}{2} \sin 2\theta(-x + y) + \cos 2\theta z & \sin^2 \theta x - \sin 2\theta z + \cos^2 \theta y \end{pmatrix} \\ x' &\sim N(0, \cos^4 \theta \sigma_x^2 + 4 \sin^2 \theta \cos^2 \theta \sigma_z^2 + \sin^4 \theta \sigma_y^2) \\ y' &\sim N(0, \sin^4 \theta \sigma_x^2 + 4 \sin^2 \theta \cos^2 \theta \sigma_z^2 + \cos^4 \theta \sigma_y^2) \\ z' &\sim N\left(0, \frac{1}{4} \sin^2 2\theta (\sigma_x^2 + \sigma_y^2) + \cos^2 2\theta \sigma_z^2\right) \end{aligned}$$

It is easy then to see that if $\sigma_x^2 = \sigma_y^2 = 2\sigma_z^2 = \sigma^2$ then $x' \sim N(0, \sigma^2)$, $y' \sim N(0, \sigma^2)$, and $z'' \sim N(0, \sigma^2/2)$, independent of θ . Thus in *all* bases the distribution of matrix elements is the same.

3.2.1 The Gaussian Orthogonal Ensemble

Again let x, y, z be real.

$$M = \begin{pmatrix} x & z \\ z & y \end{pmatrix}. \quad x \sim N(0, \sigma^2), y \sim N(0, \sigma^2), z \sim N(0, \sigma^2/2)$$

Joint Probability Distribution (JPDF) of matrix elements:

$$\begin{aligned} P(x, y, z) &= \exp\left(-\frac{1}{2\sigma^2}x^2\right) \exp\left(-\frac{1}{2\sigma^2}y^2\right) \exp\left(-\frac{1}{\sigma^2}z^2\right) \\ &= \exp\left(-\frac{1}{2\sigma^2}(x^2 + y^2 + 2z^2)\right) = \exp\left(-\frac{1}{2\sigma^2} \operatorname{tr} M^2\right) \end{aligned}$$

Probability to find the matrix in $dx dy dz = P(x, y, z) dx dy dz$.

$$M' = O M O^T, \quad O O^T = O^T O = I, \quad dx dy dz = dx' dy' dz'$$

The last is not obvious and needs to be shown, that is the Jacobian of the transformation between (x, y, z) and (x', y', z') is 1.

In general

$$P(M) dM = P'(M') dM'.$$

We have that the measure $dM = dM'$. an ensemble is **invariant** if $P(M) = P(M')$. Thus under the orthogonal group, the ensemble $P(M) = \exp(-\text{tr}M^2/2)$ is invariant as this is also $\exp(-\text{tr}M'^2/2)$. Notice that this is then like an equilibrium density in the space of matrices under conjugation by orthogonal matrices.

From matrix elements to spectra

One preferred basis for a **given** M : its **eigenbasis**. Diagonalize M : $M = O \Lambda O^T$. Jacobian from matrix elements to eigenvalues and eigenvectors: $(x, y, z) \mapsto (\lambda_1, \lambda_2, \theta)$

$$J = \begin{pmatrix} \cos^2 \theta & \sin^2 \theta & \sin 2\theta(\lambda_2 - \lambda_1) \\ -\frac{1}{2} \sin 2\theta & \frac{1}{2} \sin 2\theta & \cos 2\theta(\lambda_2 - \lambda_1) \\ \sin^2 \theta & \cos^2 \theta & \sin 2\theta(\lambda_1 - \lambda_2) \end{pmatrix}, \quad \det J = (\lambda_1 - \lambda_2)$$

$$P(M) dM = \exp\left(-\frac{1}{2\sigma^2}(\lambda_1^2 + \lambda_2^2)\right) |\lambda_1 - \lambda_2| d\lambda_1 d\lambda_2 d\theta. \quad (3.1)$$

JPDF of eigenvalues and distribution of eigenvectors:

$$P(\lambda_1, \lambda_2) = \frac{1}{Z_2} |\lambda_1 - \lambda_2| e^{-(\lambda_1^2 + \lambda_2^2)/(2\sigma^2)}, \quad P(\theta) = \frac{1}{2\pi} d\theta.$$

Gap or spacing between eigenvalues: The Wigner surmise

What is the distribution of the spacing $s = |\lambda_1 - \lambda_2|$?

$$p(s) = \int_{-\infty}^{\infty} d\lambda_1 \int_{-\infty}^{\infty} d\lambda_2 \delta[s - |\lambda_1 - \lambda_2|] P(\lambda_1, \lambda_2)$$

. Also requiring **both** $\langle 1 \rangle = 1$ and $\langle s \rangle = 1$ (mean level spacing is unity) fixes the scale σ and this gives the nearest-neighbor-spacing distribution (NNS):

$$p(s) = \frac{\pi}{2} s e^{-\pi s^2/4},$$

which is the famous Wigner surmise, as he found this and surmised that it is pretty much the same for the **nearest neighbour spacing distribution** even for large matrices. **Linear “level repulsion”**. **Potentially valid for time reversal symmetric systems**.

The $n \times n$ Gaussian Orthogonal Ensemble

Real symmetric matrices M with diagonal elements from $N(0, \sigma^2)$ and off-diagonal elements $N(0, \sigma^2/2)$: $P(M) = C \exp(-\text{tr}M^2/2)$, C being normalization constant.

How to generate it? Take A full of i.i.d. $N(0, \sigma^2)$ elements and construct $M = (A + A^T)/2$. A : **orthogonal/real Ginibre ensemble (1964)**. *Nonhermitian matrices*.

Exact JPDF of eigenvalues is known:

$$P(\lambda_1, \dots, \lambda_n) = \frac{1}{Z_n} e^{-\frac{1}{2} \sum_i \lambda_i^2} \prod_{i < j} |\lambda_i - \lambda_j|$$

The product term which is responsible for the correlations between the eigenvalues arises from the Jacobian of the transformation from matrix elements to eigenvalues-eigenvectors. Note that there are $n(n + 1)/2$ independent elements in M . There are n eigenvalues, and the diagonalizing matrix is orthogonal, such that $OO^T = I$, therefore these define $n(n + 1)/2$ constraints on the n^2 elements, leaving $n^2 - n(n + 1)/2$ independent elements in O . Thus the number of independent elements in the eigen(values and vectors) is $n + n^2 - n(n + 1)/2 = n(n + 1)/2$, which agrees with the number of independent elements in M . The product terms arises from a van der Monde determinant.

Wigner semicircle law $n \times n$ random matrix. How large can we expect the eigenvalues to be?

$$\text{tr}M^2 = \sum_i \lambda_i^2 = \sum_{i=1}^n \sum_{j=1}^n a_{ij}^2 \approx n^2 \sigma^2 / 2 \quad \text{thus typically } \lambda_i \sim \sqrt{n}\sigma$$

Density of states $D(\lambda)$: Number of eigenvalues between λ and $\lambda + d\lambda$ is $D(\lambda)d\lambda$. Let

$$x = \lambda / \sqrt{2n\sigma^2}, \quad \text{for large } n \quad D(x) = \frac{2}{\pi} \sqrt{1 - x^2}$$

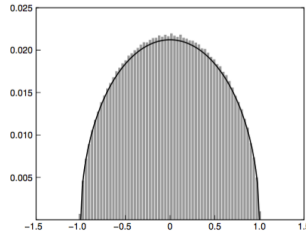


Figure 1.2 Distribution of eigenvalues: 500 Gaussian matrices (400 × 400)

3.2.2 Gaussian Unitary ensemble: GUE

$n \times n$ **Hermitian** matrices M whose real and imaginary parts are *i.i.d* normal distributed, such that

$$P(M) = \exp(-\text{tr}M^2/(2\sigma^2))$$

Invariant under **unitary transformations** $M' = UMU^\dagger$. This is known as the GUE.

Wigner surmise for NNS also follows from a 2×2 calculation:

$$p(s) = \frac{32}{\pi^2} s^2 \exp\left(-\frac{4}{\pi} s^2\right)$$

Note the quadratic level repulsion. Observed in time-reversal broken complex spectra and in Riemann zeta zeros! The JPDF of the eigenvalues is

$$P(\lambda_1, \dots, \lambda_n) = \frac{1}{Z_n} e^{-\frac{1}{2} \sum_i \lambda_i^2} \prod_{i < j} (\lambda_i - \lambda_j)^2,$$

the important difference being the quadratic term in the correlation which is the origin of the quadratic level repulsion.

Both the GOE and GUE jpdf can be written in a unified way as:

$$P_\beta(\lambda_1, \dots, \lambda_n) = \frac{1}{Z_n} e^{-\frac{\beta}{2} \sum_i \lambda_i^2} \prod_{i < j} |\lambda_i - \lambda_j|^\beta$$

Here $\beta = 1$ is GOE and $\beta = 2$ the GUE. Note that with this definition of the jpdf the GUE eigenvalues have to be scaled by $\sqrt{2}$ to get the earlier form, but they are equivalent as this affects only the normalization constant. The case $\beta = 4$ corresponds to the **Gaussian symplectic ensemble** consisting of quaternion matrices that are invariant under the symplectic group. Together, these three form the classic RMT ensembles and are called the Dyson three-fold way, and β are the Dyson indices.

General **invariant ensembles** are given by

$$P(H) \propto \exp(-\text{tr}V(H)),$$

where $V(H)$ is any smooth function. The JPDF of the eigenvalues follows immediately:

$$P(\lambda_1, \dots, \lambda_n) = \frac{1}{Z_n} e^{-\frac{1}{2} \sum_i V(\lambda_i)} \prod_{i < j} |\lambda_i - \lambda_j|^\beta$$

Theorem: Porter-Rosenzweig An invariant ensemble has *independent matrix elements* if and only if $V(H)$ is quadratic, that is the ensemble is Gaussian. Example of a “interacting model”

$$V(H) = \frac{1}{2} H^2 - \alpha H^4$$

Invariant, but not easy to construct the matrices themselves. Such ensembles called **Matrix Models** are studied in areas such as quantum gravity.

Wigner matrices are symmetric (or Hermitian) matrices with independent entries that are with some distribution with a finite second moment (not necessarily Gaussian). In this case the jpdf is very hard to find, and in general unknown. However it has been shown that for large n , the density of states is the Wigner semicircle. The Wigner semicircle is to random matrices, what the Gaussian distribution is to random numbers.

The circular ensembles are ensembles of **unitary** matrices. These are slightly harder to construct as the elements are correlated. The only constraint being that $\delta(UU^\dagger - I) = I_N$, where U is a $n \times n$ matrix, this forms the jpdf (unnormalized) of the matrix elements. (See article by F. Mezzadri in American Mathematical Notices, on Generating Random Matrices). They also come in 3 basic varieties of which the COE and CUE are widely applicable, for example to Floquet or quantum map propagators. Their fluctuation properties are for the most part identical to the GOE and GUE. The COE consists of **symmetric unitary** matrices invariant under the action $W^T UW$, where W is any unitary matrix and the CUE consists of unitary matrices that are invariant under the action $W_1 UW_2$ where W_1 and W_2 are any unitary matrix.

3.3 More on the nearest neighbor spacing and ratio of spacings

This is one of the earliest measures that was used and is quite simple. The question is how are the nearest neighbour energy differences distributed? Somewhat paradoxically, **if the system were integrable the NNS is Poisson distributed**, which will happen if the energy levels do not have any correlation between them. If the system is chaotic (in the classical limit) the distribution will be one of two

types depending of if there is TR symmetry or no TR symmetry. These are *universal* distributions, independent of the system and once full chaos has been achieved seemingly also indifferent to the degree of chaos. First we have to normalize the energy differences so that we can compare different spectra. To do this we normalize the levels so that the mean energy spacing is unity.

In the case of Hamiltonians we need to unfold the levels as described in the last chapter, fine $x_i = \overline{N(E_i)}$ from the “raw” levels E_i and find $s_i = x_{i+1} - x_i$. In the case of the unitary operators such as quantum maps, the mean spacing is simply $2\pi/N$ as the eigenangles are uniformly distributed over $[0, 2\pi)$. Therefore define

$$s_i = \frac{N}{2\pi}(\theta_i - \theta_{i-1}), \quad (3.2)$$

and consider the set of normalized spacings $\{s_i, i = 1, \dots, N-1\}$. If these are distributed according to the function $P(s)$, then the following holds almost always:

$$P(s) = \begin{cases} \exp(-s) & \text{Integrable.} \\ \frac{\pi}{2}s \exp(-\pi s^2/4) & \text{Chaotic. TR symmetric.} \\ \frac{32}{\pi^2}s^2 \exp(-4s^2/\pi) & \text{Chaotic. No TR symmetry.} \end{cases} \quad (3.3)$$

For mixed systems, distributions are found that are intermediate between the Poisson and the Wigner. Notice that small spacings are the rule in integrable systems, while for chaotic ones, the energy levels are very rarely found close together. The levels are said to *repel* each other in chaotic systems. Note that there is a linear repulsion for TR symmetric systems and a quadratic repulsion for non-TR symmetric ones.

More recently the ratio of spacings is finding favour as it does not need unfolding: define

$$r_i = \frac{E_{i+1} - E_i}{E_i - E_{i-1}}$$

where E_i are arranged in increasing order, and are not necessarily unfolded. Then the distribution of this and

$$\tilde{r}_i = \min \left(r_i, \frac{1}{r_i} \right)$$

are studied. It is possible to find the distribution of r_i from which that of \tilde{r}_i follows. Considerig just a 3-level system, using the jpdf as given above Atas et. al. (PRL, 2013) made a Wigner -like surmise that

$$P(r) = \frac{1}{Z_\beta} \frac{(r + r^2)^\beta}{(1 + r + r^2)^{1+(3/2)\beta}}. \quad (3.4)$$

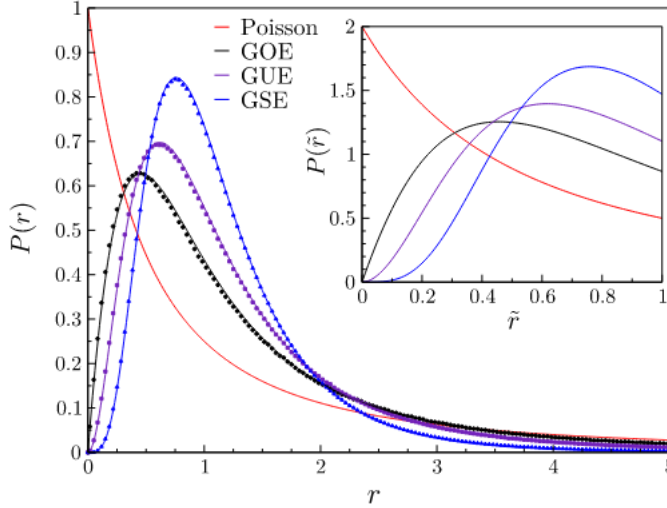


FIG. 1 (color online). Distribution of the ratio of consecutive level spacings $P(r)$ for Poisson and RMT ensembles: full lines are the surmise Eq. (7), points are numerical results obtained by diagonalizing matrices of size $N = 1000$ with Gaussian distributed entries, averaged over 10^5 histograms. Inset: the distribution $P(\tilde{r})$.

Exercise.

1. Diagonalizing the quantum baker map using any algorithm, find the eigenangles. Normalize them so that the mean spacing is unity. Verify if the angles are uniformly distributed. Find the spacing distribution. You may take $N = 100$ or above for somewhat decent statistics. It has been found that while there is level repulsion, the quantum baker map has number theoretic properties that are not understood and leads to deviations from RMT predicted distributions.
2. Do the same exercise for the quantum standard map on the torus. Notice how for small K , where it is nearly integrable, the NNS distribution will be Poissonian ($\exp(-s)$), while for $K \gg 5$, where complete classical chaos sets in the distribution will be RMT like. Show that if $\beta = 0$ the TR symmetric distribution is obtained, while if $\beta \neq 0$, the non-TR distribution is obtained. This shows how the phases may be used to make or break important symmetries that affect the spectrum dramatically. In fact this is a way in which one detect very weak TR violating effects in nuclear physics!

3.4 Eigenfunctions of random matrices

Compared to eigenvalues, the eigenvectors are very simple: they are uniformly distributed. For invariant ensembles, that we are considering, their dependence is only from the Jacobian, for $n = 2$ GOE for example, as can be seen from Eq. (3.1) for $n = 2$ this measure is $d\theta/(2\pi)$, uniform on the circle.

3.4.1 GOE eigenvectors

Let $|\psi\rangle$ be an eigenvector of a GOE matrix. In some orthonormal fixed bases $|j\rangle$, the components of $|\psi\rangle$ are $x_j = \langle j|\psi\rangle$. Then the jpdf of these components are uniform on the “normalization sphere”,

$$P(x_1, \dots, x_n) = C_n \delta \left(1 - \sum_{j=1}^n x_j^2 \right), \quad (3.5)$$

where C_n is the normalization constant.

A useful integral:

$$f(t) = \int_{-\infty}^{\infty} \delta \left(t - \sum_{j=1}^m x_j^2 \right) dx_1 \cdots dx_m = \frac{\pi^{m/2}}{\Gamma(m/2)} t^{(m/2)-1}. \quad (3.6)$$

Proof: Take the Laplace transform

$$\int_0^{\infty} e^{-ts} f(t) dt = \int_{-\infty}^{\infty} e^{-s \sum_{j=1}^m x_j^2} dx_1 \cdots dx_m = \frac{\pi^{m/2}}{s^{m/2}}. \quad (3.7)$$

The Laplace inverse

$$\mathcal{L}^{-1} \frac{1}{s^{\nu}} = \frac{t^{\nu-1}}{\Gamma(\nu)}, \quad (3.8)$$

which simply follows from

$$\int_0^{\infty} e^{-ts} t^{\nu-1} dt = \frac{\Gamma(\nu)}{s^{\nu}}. \quad (3.9)$$

Therefore

$$f(t) = \pi^{m/2} \mathcal{L}^{-1} \frac{1}{s^{m/2}} = \frac{\pi^{m/2}}{\Gamma(m/2)} t^{m/2-1}, \quad (3.10)$$

as stated.

The normalization C_n can be got by substituting $t = 1$, and we get

$$C_n = \frac{\Gamma(n/2)}{\pi^{n/2}}. \quad (3.11)$$

Also, the marginals can now be found:

$$\begin{aligned} P_k(x_1, \dots, x_k) &= C_n \int_{-\infty}^{\infty} \left(1 - \sum_{j=1}^k x_j^2 - \sum_{j=k+1}^n x_j^2 \right) dx_{k+1} \cdots dx_n. \\ &\quad \frac{\Gamma(n/2)}{\pi^{n/2}} \frac{\pi^{(n-k)/2}}{\Gamma((n-k)/2)} \left(1 - \sum_{j=1}^k x_j^2 \right)^{(n-k-2)/2}, \end{aligned} \quad (3.12)$$

is the jpdf of $k < n$ components. In particular the distribution of a single component is got with $k = 1$ and is

$$P_1(x) = \frac{\Gamma(n/2)}{\sqrt{\pi} \Gamma((n-1)/2)} (1-x^2)^{(n-3)/2}. \quad (3.13)$$

Exercise: Plot $P_1(x)$ starting with $n = 2$ and going on to $n = 10$. Now normalization is

$$\sum_{j=1}^n x_i^2 = 1, \text{ which implies that } \langle x_i^2 \rangle = 1/n, \quad (3.14)$$

which follows as all the components are statistically identical and $\langle \cdot \rangle$ is the ensemble average. Therefore $x_j^2 n \sim 1$ and this implies that

$$P_1(x) = \frac{\Gamma(n/2)}{\sqrt{\pi}\Gamma((n-1)/2)} \left(1 - \frac{2nx^2}{2n}\right)^{(n-3)/2}, \quad (3.15)$$

and in the large n limit this is

$$P_1(x) = \sqrt{\frac{n}{2\pi}} \exp(-nx^2/2), \quad (3.16)$$

Thus random states are such that the amplitudes are zero centered normal distribution with variance $1/n$. If the intensities were normalized as $\tilde{x}^2 = nx_j^2$, then $\tilde{x} \sim N(0, 1)$ for large n .

Exercise: Find the distribution of the intensities $t_j = x_j^2$, referred to as the Thomas-Porter distribution.

Participation ratio: The quantity $IPR = \sum_j x_j^4$ is the inverse participation ratio and is a measure of localization, the smaller it is the smaller is the localization. Participation ratio is $1/IPR$ and lies between 1 (extremely localized, only one component is nonzero, to N to when all components are of equal magnitude (signs can differ) and therefore state is “delocalized”).

$$\langle IPR \rangle = n \langle x^4 \rangle = n \int_{-\infty}^{\infty} x^4 P_1(x) dx = 3/n. \quad (3.17)$$

We can expect the average participation ratio to be $n/3$. This says that for time-reversal symmetric random states (as eigenvector of random matrices are referred to), about 1/3rd of the components are significant. While we have used the large n approximation, exact averages can also be easily found.

3.4.2 GUE eigenvectors

In this case the eigenvectors have complex coefficients, $z_j = x_j + iy_j$. The distribution of z_j is

$$P(z_1, \dots, z_n) = \frac{(n-1)!}{\pi^n} \delta \left(1 - \sum_{j=1}^n |z_j|^2 \right). \quad (3.18)$$

The real and imaginary parts are distributed uniformly on the $2n - 1$ -dimensional sphere, while the intensities $t_i = x_i^2 + y_i^2$ are uniform on the simplex $\sum_i t_i = 1$, $t_i \geq 0$:

$$P(t_1, \dots, t_n) = (n-1)! \delta \left(1 - \sum_{j=1}^n t_j \right). \quad (3.19)$$

The jpdf of $k < n$ intensities is

$$P(t_1, \dots, t_k) = \frac{\Gamma(n)}{\Gamma(n-k)} \left(1 - \sum_{j=1}^k t_j \right)^{n-k-1}. \quad (3.20)$$

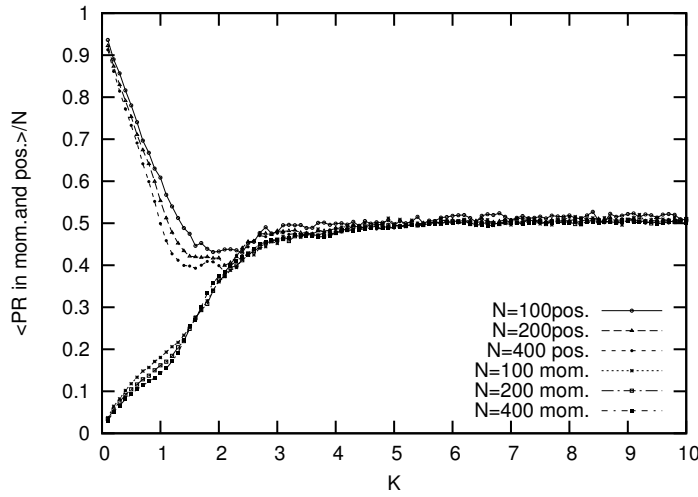


Figure 3.1: Average participation ratio for the quantum standard map eigenfunctions, calculated in both the position and momentum basis, at different N values as K is varied. We see that when K is small the states are localized in momentum and extended in position space, but as K is increased they come together to $N/2$, the GUE value. The phases have been chosen to break time-reversal symmetry.

and the single intensity distribution is

$$P_1(t) = (n-1)(1-t)^{n-2} = (n-1) \left(1 - \frac{nt}{n}\right)^{n-2} \rightarrow n \exp(-nt). \quad (3.21)$$

If one rescales $\tilde{t} = nt$, then $\tilde{t} \sim \exp(-\tilde{t})$, that is the intensities are exponentially distributed with a mean $1/n$.

The **inverse participation ratio** is given by

$$\langle IPR \rangle = \left\langle \sum_{j=1}^n t_j^2 \right\rangle = n \int_0^\infty t^2 n \exp(-nt) dt = 2/n, \quad (3.22)$$

and hence the participation ration is $n/2$. Thus we can expect for complex random states that about one-half of the components are significant, and hence **TR breaking systems tend to delocalize more**.

3.5 Trace constrained Wishart matrices: Entanglement

These ensembles describe reduced density matrices of random pure states, and hence useful for description of entanglement. Let $|\Phi\rangle$ be any bipartite pure state of the tensor product space $\mathcal{H}_1 \otimes \mathcal{H}_2$. It can be represented as

$$|\Phi\rangle = \sum_{i=1}^{n_1} \sum_{j=1}^{n_2} a_{ij} |ij\rangle, \quad (3.23)$$

where $\{|i\rangle\}, \{|j\rangle\}$ are any mutually orthonormal basis in their respective subspaces \mathcal{H}_1 and \mathcal{H}_2 . Let $n_1 = \dim \mathcal{H}_1 \leq n_2 = \dim \mathcal{H}_2$.

The *reduced density matrices*

$$\rho_1 = \text{tr}_2 (|\Phi\rangle\langle\Phi|), \quad \rho_2 = \text{tr}_1 (|\Phi\rangle\langle\Phi|), \quad (3.24)$$

obtained after partially tracing the other subsystem is the state accessible to either 1 or 2 respectively. They can be written in terms of the matrix A whose elements are the coefficients a_{ij} of the state as $\rho_1 = AA^\dagger$ and $\rho_2 = (A^\dagger A)^T$ (where A^T is the transpose of A). These are positive semi-definite matrices, and let their eigenvalue equations be $\rho_1|\phi_{1j}\rangle = \lambda_j|\phi_{1j}\rangle$ and $\rho_2|\phi_{2j}\rangle = \lambda_j|\phi_{2j}\rangle$, with non-vanishing eigenvalues indexed by $1 \leq j \leq n_1$. The (*Schmidt*) eigenvalues $\{\lambda_j\}$ of ρ_1 and ρ_2 are identical, except the larger subsystem (2) is additionally padded with $n_2 - n_1$ zero eigenvalues. Additionally, assume that the $\{\lambda_j\}$ are ordered such that $\lambda_1 \geq \dots \geq \lambda_{n_1}$.

The *Schmidt decomposition*

$$|\Phi\rangle = \sum_{j=1}^{n_1} \sqrt{\lambda_j} |\phi_{1j}\rangle |\phi_{2j}\rangle, \quad (3.25)$$

is the most compact form of writing the bipartite state $|\Phi\rangle$ in a product basis from orthonormal sets $\{|\phi_{1j}\rangle\}$ and $\{|\phi_{2j}\rangle\}$, and uses the eigenvalues λ_j and corresponding eigenvectors. By normalization of the state $|\Phi\rangle$ one has $\sum_{j=1}^{n_1} \lambda_j = 1$. The Schmidt decomposition follows from the singular value decomposition of a matrix whose entries are the coefficients of the state $|\Phi\rangle$ in any product basis. The state is unentangled if and only if $\lambda_1 = 1$ (and hence all other eigenvalues are 0), and the Schmidt decomposition gives the states of the individual subsystems. Otherwise $\lambda_2 > 0$ and the Schmidt decomposition consists of at least two terms. For maximally entangled states, $\lambda_j = 1/n_1$ for all j . The entanglement entropy in the state $|\Phi\rangle$ is the *von Neumann entropy* of the reduced density matrices,

$$S = -\text{tr}(\rho_1 \ln \rho_1) = -\text{tr}(\rho_2 \ln \rho_2) = -\sum_{i=1}^{n_1} \lambda_i \ln \lambda_i. \quad (3.26)$$

Thus if $S = 0$, then the state is unentangled, whereas a maximally entangled state has $S = \ln n_1$.

Now if a_{ij} is an eigenvector of a random matrix (from say GOE or GUE), what probability distribution does it impose on the Schmidt eigenvalues λ_i and hence the entanglement? What is the average value of the entanglement of random states? We know that a_{ij} is uniform on the normalization sphere. This can be arranged by simply choosing x_{ij} from a normal distribution, say $N(0, 1)$ and then normalizing. Thus the distribution of the matrix $[A_{ij}]$ is same as that if $[M_{ij}]/\sqrt{\text{tr}MM^\dagger}$ where M is an unstructured matrix with all elements iid $N(0, 1)$ numbers (“Ginibre ensemble”). Therefore the reduced density matrices are given by the ensemble of random matrices:

$$\rho = \frac{MM^\dagger}{\text{tr}MM^\dagger}. \quad (3.27)$$

Wishart started the study of Random matrices in the 1930's studying correlation matrices such as MM^T and the ensembles of relevance to entanglement in bipartite pure states are of such kind, except that their trace is constrained to unity due to state normalization. The jpdf of the λ_i , the square of the singular values of A are given by

$$P(\lambda_1, \lambda_2, \dots, \lambda_{n_1}) = B_{n_1, n_2} \delta \left(\sum_{i=1}^{n_1} \lambda_i - 1 \right) \prod_{i=1}^{n_1} \lambda_i^{\frac{\beta}{2}(n_2 - n_1 + 1) - 1} \prod_{j < k} |\lambda_j - \lambda_k|^\beta. \quad (3.28)$$

where $\beta = 1, 2$ corresponds to the real and complex entries of A and B_{n_1, n_2} is the normalization constant that is known explicitly. Several spectral properties associated with the jpdf in Eq. (3.28), in particular for the complex $\beta = 2$ case, have been studied extensively in the literature.

The average entanglement of pure bipartite states is therefore

$$\langle S \rangle = \int_0^\infty \cdots \int_0^\infty \left(- \sum_j \lambda_j \ln \lambda_j \right) P(\lambda_1, \dots, \lambda_n) d\lambda_1 \cdots d\lambda_n. \quad (3.29)$$

Remarkably enough this is known exactly (meaning for any n_1 and n_2) for the case $\beta = 2$ of complex matrices M , that too via a simple formula:

$$\langle S \rangle = \sum_{k=n_2+1}^{n_1 n_2} \frac{1}{k} - \frac{n_1 - 1}{2n_2} \approx \ln n_1 - \frac{n_1}{2n_2}. \quad (3.30)$$

See D. Page (1993), S. Sen (1995) etc.. If $n_2 \gg n_1$ the smaller subsystem entropy is nearly maximal. If we think of the larger space as that of a “bath”, it implies that random states maximize their entropy.

3.5.1 The Marchenko-Pastur law

The density of the Schmidt eigenvalues is obtained by integrating out all variables except one. For large n_1 and n_2 , that is $1 \ll n_1 \leq n_2$ with fixed ratio $Q = n_2/n_1 \geq 1$, the limit of the density of the scaled eigenvalues,

$$\tilde{\lambda}_i = \lambda_i n_1$$

is given by the Marchenko-Pastur distribution (1967):

$$\rho_{\text{MP}}^Q(x) = \frac{Q}{2\pi} \frac{\sqrt{(x_+ - x)(x - x_-)}}{x}, \quad x_- \leq x \leq x_+, \quad (3.31)$$

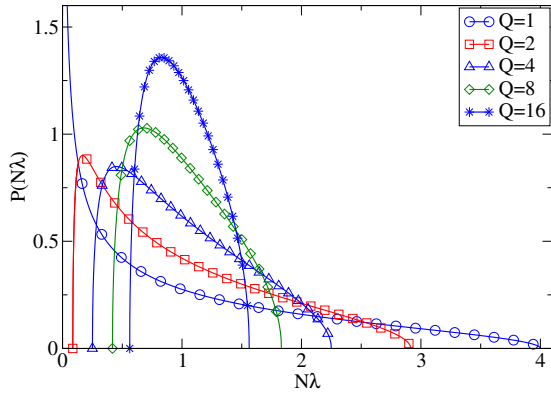
and 0 otherwise. The distribution is in the finite support $[x_-, x_+]$ where

$$x_\pm = 1 + \frac{1}{Q} \pm \frac{2}{\sqrt{Q}}. \quad (3.32)$$

The special case $Q = 1$ is worth mentioning separately:

$$\rho_{\text{MP}}(x) = \frac{1}{2\pi} \sqrt{\frac{4-x}{x}}, \quad 0 \leq x \leq 4, \quad (3.33)$$

and 0 otherwise. Thus in this case there is a divergence at the origin. The MP law and the Wigner semicircle law are closely allied, and the MP is a universal distribution for ensembles of correlation matrices, irrespective of the exact distribution of matrix elements as long as it has a finite second moment. See figure below for the MP law, where $x = N\lambda = n_1\lambda$.



3.6 Applications to Quantum chaos and thermalization

Applications are very many and we have already stated some to the eigenvalues and eigenvectors of the quantum spectra. We now turn to some applications to the issues of entanglement that also lies at the heart of thermalization. That chaos and non-integrability aid thermalization is also due to the fact that they abet entanglement growth.